Design of Low-Complexity Detection based on Matched-Filter for Coded MIMO Systems

符号化MIMOシステムにおけるMatched-Filterに基づく低演算信号検出法の設計

Yuto Hama

Supervisor: Prof. Hideki Ochiai

Department of Electronic and Engineering
Graduate School of Engineering

Yokohama National University

A dissertation for the degree of
Doctor of Philosophy

Date of Submission: March 2022

YNU 横浜国立大学
YOKOHAMA National University

Abstract

In order to deal with the increasing demand for wireless networks, diverse requirements will be defined for future standards such as the sixth generation mobile communications standard (6G). Focusing on applications for low-cost devices represented by Internet-of-Things (IoT), there are severe limitations on signal processing and power consumption. Thus, physical layer techniques for future cellular networks should be designed by taking these hardware limitations into account.

Multiple-input multiple-output (MIMO) systems have been getting much attention for the last several decades due to their attractive potential for performance enhancement, and several transmission schemes have been investigated in MIMO systems. Among them, in this dissertation, we focus on two MIMO transmission schemes, namely spatial multiplexing and spatial modulation, due to their potential for spectral efficiency enhancement as the number of antennas increases. These approaches require no channel state information at the transmitter side, but inter-channel interference (ICI) is not avoidable at the receiver. Therefore, the receiver needs to employ MIMO signal detection to separate the interfering transmit symbols. However, it generally requires high computational complexity with the increase in the number of antennas. Consequently, it may lead to high latency and high power consumption, which is not acceptable for low-cost devices as in IoT networks.

Motivated by the above background, we focus on a matched-filter (MF) detector known as the lowest complexity MIMO detector. In this dissertation, we first derive the statistical property of MF detector through exact mathematical analysis over Rayleigh fading channel. Based on this property, we apply MF detector to coded MIMO spatial multiplexing and spatial modulation systems. For spatial multiplexing, we propose a new interference cancellation (IC) approach so as to improve the error rate performance, developed as MF detector with QIC (MF-QIC) together with design criteria for polar codes. The simulation results demonstrate that MF-QIC outperforms other conventional signal detectors with the presence of channel estimation error. For spatial modulation, we apply MF detector as a sub-optimal detection by introducing an appropriate scaling, referred to as scaling MF detector. We also optimize the decoding metric for coded spatial modulation based on the derived statistical property for MF detector.

Acknowledgments

First of all, I would like to express my sincere appreciation to my supervisor, Prof. Hideki Ochiai, for his thoughtful supervision and for giving me the supreme hobby, which we call research. For seven years after laboratory assignment in my fourth year of undergraduate studies, he gave me a lot of thoughtful and encouraging comments, without which I would not have been able to succeed in my doctoral degree. I can say with confidence that it was right to choose him as my supervisor.

I would also like to appreciate to Prof. Tomoki Hamagami, Prof. Koichi Ichige, Prof. Chika Sugimoto, and Prof. Naoki Ishikawa. They gave me a lot of observant and helpful comments that enabled me to improve this dissertation.

I also wish to thank the past and current members of Ochiai laboratory. Especially, I would like to my grateful gratitude to Yuta Hori, Toshiki Matsumine, Shuntaro Suzuki, Yuki Matsumoto, and Junya Watanabe for their sincere help in research as well as in private.

I sincerely appreciate the financial support provided by Japan Society for the Promotion of Science (JSPS).

Last but not least, I'm eternally grateful to my family for their continuous support and tolerance throughout my life. If I could have another life, I would choose the same parents and little brother.

Yuto Hama

Contents

List of Figures

List of Tables

Chapter 1

Introduction

1.1 Background and Motivation

Massive number of diverse devices attempt to connect to wireless networks, and the demand for wireless communication is increasing day by day. Therefore, recent and future mobile standards need to satisfy several directional requirements [1]. Specifically, as an example in the fifth generation mobile communications standard (5G), the system requirements are specified in three categories defined as enhanced mobile broadband (eMBB), ultra reliable low latency communications (URLLC), and massive machine type communications (mMTC) [2]. For future mobile communications such as the sixth generation (6G) [3], it will be extended in a way that integrates these conditions represented by ultra-mMTC (umMTC) and massive URLLC (mURLLC) [4, 5]. Considering the background that the main focus until the fourth generation (4G) has been to enhance the data rate corresponding to eMBB as in 5G, physical layer techniques should be *redesigned* optimized for never-before-seen applications in future wireless communications. Among them, the acceleration of Internet-of-Things (IoT) is almost certain, and a massive number of low-cost devices attempt to communicate through wireless networks with severely limited computational resources and power consumption [6]. Based on this background, the main aim of this dissertation is to develop a new low-complexity physical layer technology with high power efficiency that simultaneously accommodates massive devices. In pursuing this end, this dissertation mainly investigates two essential technologies, multiple-input multiple-output (MIMO) [7] and channel coding [8], as described in the following.

Channel Coding

In wireless networks, channel coding performed by the error correcting codes is an essential technology to improve the resulting error rate performances with the aim of getting closer to Shannon capacity [9]. It is known as the theoretical achievable spectral efficiency over AWGN

channels, and it is expressed as

$$C = B \log_2 (1 + \text{SNR}) , \tag{1.1}$$

where B represents a channel bandwidth, and SNR is signal-to-noise ratio (SNR) at the receiver. In general, SNR can be improved by the increase of transmission power. However, its limitation is specified by 3GPP as well as the laws of each country according to the guideline for human protection. Thus, there is a severe restriction on the capacity improvement by SNR. In contrast, the channel bandwidth B can also contribute the capacity enhancement linearly as shown in (1.1). In practice, 5G, the most recent mobile standard, adopts significant broadband communication up to 800 MHz at millimeter wave (mmW), whereas that in LTE is up to 20 MHz. As a result, 5G has achieved a dramatic increase in terms of data rate compared to LTE. However, in order to ensure such broadband frequency resources, it has no other choice to use high frequency bands that have never been adopted in the past cellular networks due to extremely severe propagation loss. Based on the above observation, further investigation of channel coding so as to achieve Shannon capacity is still one of the most important challenges even toward future wireless communications [8].

In this work, we address three error correcting codes known to be approaching Shannon limit listed as follows:

- **Turbo codes** have been proposed by Berrou et al. in 1993 [10], which is known as the first capacity approaching error correcting codes. They are composed of two recursive convolutional codes (RCCs) which are parallel concatenated via an interleaver. The turbo decoder generally employs soft-input soft-output (SISO) decoding corresponding to each RCC based on Bahl, Cocke, Jelinek, and Raviv (BCJR) algorithm [11]. Its output in terms of extrinsic information is exchanged by iterative decoding process between two SISO decoders. Turbo codes have been adopted a lot of wireless communication standards such as 3G and LTE.

- **Low-density parity-check (LDPC) codes** were introduced by Gallarger in 1961 [12], and refound after a few decades [13] according to the development of computing potential. Their sparse parity check matrix enables the practical implementation based on the message passing algorithm. Furthermore, LDPC codes designed with density evolution have a potential to achieve within 0.0045 dB from Shannon limit [14]. Thus, the recent standards adopt LDPC codes such as data channel in 5G.

- **Polar codes** were recently discovered by Arikan in 2008 [15]. It has been theoretically

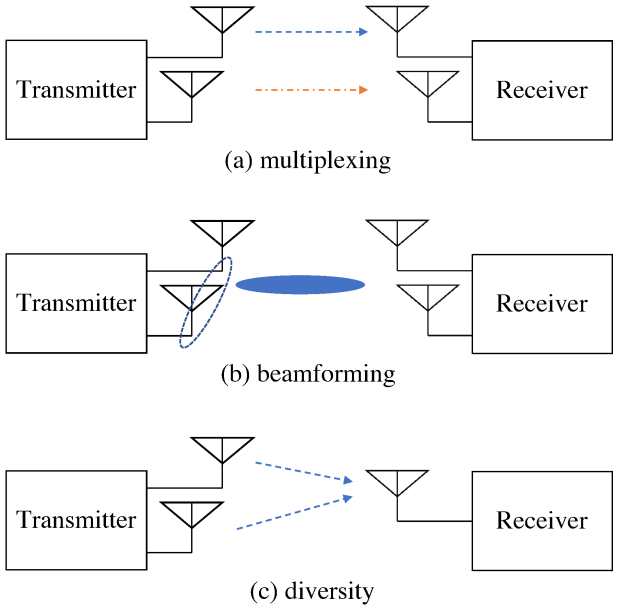

Figure 1.1: The achievable gain by multiple-antenna transmission.

demonstrated that they can achieve the capacity limit over symmetric binary-input discrete memoryless channels with practical computational resources. Polar codes are constructed based on channel polarization principle, but its optimal design for well-known fading channel model is still challenging as well as the practical propagation environment. Nevertheless, their performance with short block length is known to be superior to that of turbo and LDPC codes. Thus, polar codes have been adopted in control channel in 5G.

Multiple-Input Multiple-Output (MIMO)

In order to enhance the spectral efficiency as well as energy efficiency, multiple-antenna technique named multiple-input multiple-output (MIMO) is adopted in recent wireless standards such as LTE and Wi-Fi. Furthermore, MIMO becomes *de facto* standard since system configuration in 5G is established on the premise of MIMO. There are a variety of transmission schemes in MIMO systems, and each of them can provide different gains. In 5G as an example, mainly three transmission schemes are supported for point-to-point communication as illustrated in Fig. 1.1. Note that these techniques can be also applied in combination. Beamforming is one of the essential techniques in 5G, and it improves the signal-to-noise power ratio (SNR) by the control of phase shifter at the multiple antennas. As a result, the enhancement on power efficiency is expected by beamforming, and its gain is also called beamforming or array gain. Espe-

cially for mmW communications, beamforming by massive transmit antennas, namely massive MIMO [16, 17], is necessary at the base station (BS) to provide sufficient coverage due to high attenuation by large pathloss with respect to the distance. However, in general, it requires the channel information at the transmitter in some way such as the channel state information (CSI), the directions-of-departure (DoD), or Directions-of-Arrival (DoA). Spatial diversity approach is employed so as to reduce the effect of power attenuation due to fading. A few schemes have been investigated in the literature, and among them, space-time block code (STBC) [18] and space-time trellis code (STTC) [19] are well-known approaches, since they can be implemented simply but achieve good performances. However, the practical diversity technique limits the improvement in terms of system capacity. Spatial multiplexing represented by Bell Labs Layered Space-Time (BLAST) [20, 21] is a MIMO technique to improve the spectral efficiency without any band expansion by the parallel transmission of the different information sequence from different antennas. Furthermore, the previous work revealed that the capacity improves linearly with the number of antennas over ideal uncorrelated fading channels [22]. Therefore, compared with the other transmission schemes described above, we may conclude that multiplexing gain is the most attractive in MIMO systems. The main drawback in spatial multiplexing is higher complexity for signal detection at the receiver compared to other schemes. Since the computational complexity depends on the number of antennas, the complexity increases corresponding to the achievable spectral efficiency. In other words, there is a tradeoff between the spectral efficiency enhancement and the computational complexity for signal detection. In order to address this issue, a new transmission approach named spatial modulation was proposed in [23], which conveys information sequence on the antenna index in addition to the conventional constellation-based modulation transmitted by only one active antenna. The sparseness of the transmission symbol in spatial modulation contributes the complexity reduction, which is a challenging issue in spatial multiplexing. Furthermore, it is known that the minimum Euclidean distance (MED) can be increased compared with the same spectral efficiency [24]. In addition, its extension was proposed in terms of generalized spatial modulation (GSM) [25], where the multiple antennas are activated.

1.2 Coded MIMO System Model

Motivated by the above observations, we focus on coded MIMO spatial multiplexing and spatial modulation systems throughout this dissertation shown in Fig. 1.2, where the detailed description is given in the following.

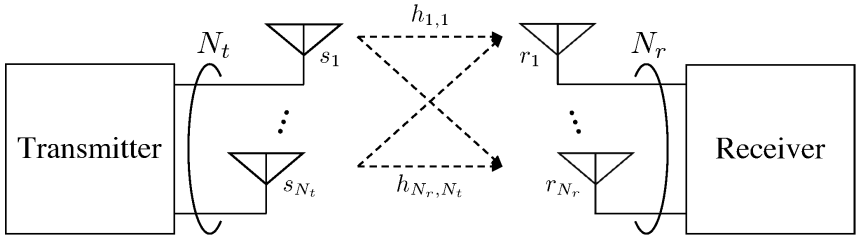

Figure 1.2: General MIMO transmission model with N_t transmit and N_t receive antennas.

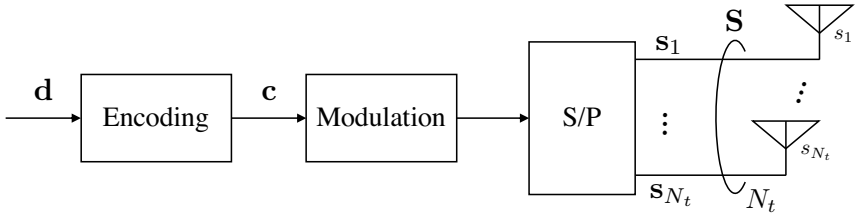

(a) single user

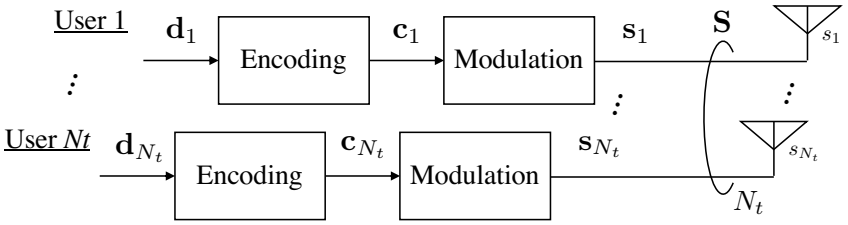

(b) multiple user

Figure 1.3: Coded modulation schemes for MIMO systems.

1.2.1 Channel Coding Principle

In this dissertation, we consider two coded modulation schemes for MIMO systems as shown in Fig. 1.3.

For a single user scenario, channel coding is performed before antenna mapping shown in Fig. 1.3(a), and thus, the generated codewords are mapped to and transmitted from all the transmit antennas. Let $\mathbf{c}$ denote the information bit sequence. It is encoded by a binary code $\mathcal{C}$ with rate R_c from a binary information sequence denoted by $\mathbf{d}$. A vector of $m = \log_2 M$ elements of $\mathbf{c}$ forms one transmitted symbol with M-PSK or M-QAM constellations. Finally, the modulated symbol sequence is mapped into and transmitted from all the transmit antennas. It leads to that the spatial diversity gain can be obtained with the number of transmit antennas even if the channel is static over each codeword transmission.

In the case of multiple user transmission, we assume that each user has a single antenna, and channel coding and modulation are performed at each transmit antennas. Let $\mathbf{c}_k$ denote the information bit sequence for the kth user. Similar to the single user case, it is encoded by a binary code $\mathcal{C}$ with rate R_c from a binary information sequence denoted by $\mathbf{d}_k$ corresponding to the kth user. Finally, the modulated symbol sequence $\mathbf{s}_k$ is generated from the codeword sequence $\mathbf{c}$ and transmitted from the kth user (or the kth transmit antennas). In this case, the codeword corresponding to each user can not obtain the spatial diversity gain over flat fading channels since each codeword is received through the same channel.

1.2.2 Symbol Representation of General MIMO Transmission

Let N_t and N_r denote the number of transmit and receive antennas, respectively. The lth transmitted symbol from the kth antenna represented by $s_k^{(l)}$ is modulated by M-PSK or M-QAM, where M is modulation order. Assuming that the transmit symbol of the sequence length L is transmitted from all the kth transmit antenna, it is denoted by $\mathbf{s}_k = \left(s_k^{(1)}, s_k^{(2)}, \cdots, s_k^{(l)}, \cdots, s_k^{(L)}\right) \in \mathcal{X}^L$, where $\mathcal{X}$ represents a set of constellation points. The overall transmit symbol is given by

$$\begin{aligned}\mathbf{S} &= \left(\mathbf{s}_1 \cdots \mathbf{s}_k \cdots \mathbf{s}_{N_t}\right)^T = \left(\mathbf{s}^{(1)} \cdots \mathbf{s}^{(l)} \cdots \mathbf{s}^{(L)}\right) \\ &= \begin{bmatrix} s_1^{(1)} & \cdots & s_1^{(l)} & \cdots & s_1^{(L)} \\ \vdots & \ddots & \vdots & \ddots & \vdots \\ s_k^{(1)} & \cdots & s_k^{(l)} & \cdots & s_k^{(L)} \\ \vdots & \ddots & \vdots & \ddots & \vdots \\ s_{N_t}^{(1)} & \cdots & s_{N_t}^{(l)} & \cdots & s_{N_t}^{(L)} \end{bmatrix},\end{aligned} \tag{1.2}$$

where the lth transmit symbol from all the transmit antenna is represented by $\mathbf{s}^{(l)}$. Similarly, the received symbol is defined as

$$\begin{aligned}\mathbf{R} &= \left(\mathbf{r}_1 \cdots \mathbf{r}_k \cdots \mathbf{r}_{N_r}\right)^T = \left(\mathbf{r}^{(1)} \cdots \mathbf{r}^{(l)} \cdots \mathbf{r}^{(L)}\right) \\ &= \begin{bmatrix} r_1^{(1)} & \cdots & r_1^{(l)} & \cdots & r_1^{(L)} \\ \vdots & \ddots & \vdots & \ddots & \vdots \\ r_k^{(1)} & \cdots & r_k^{(l)} & \cdots & r_k^{(L)} \\ \vdots & \ddots & \vdots & \ddots & \vdots \\ r_{N_r}^{(1)} & \cdots & r_{N_r}^{(l)} & \cdots & r_{N_r}^{(L)} \end{bmatrix},\end{aligned} \tag{1.3}$$

where $\mathbf{r}_k$ and $\mathbf{r}^{(l)}$ represent the received symbol at the kth antenna and the lth overall received symbol, respectively, in which r_k^l corresponds to the lth received symbol at the kth antenna. Based on the above definitions, the received symbol is expressed as

$$\mathbf{R} = \mathbf{HS} + \mathbf{N}, \tag{1.4}$$

where $\mathbf{H} = (\mathbf{h}_1\, \mathbf{h}_2\, \cdots\, \mathbf{h}_{N_t}) \in \mathbb{C}^{N_r \times N_t}$ denotes a complex channel matrix with each column vector $\mathbf{h}_k = (h_{1,k}, h_{2,k}, \cdots, h_{N_r,k})$ representing the channel corresponding to the kth transmit antenna, and $\mathbf{N}\left(\mathbf{n}^{(1)}\, \mathbf{n}^{(2)}\, \cdots\, \mathbf{n}^{(L)}\right) \in \mathbb{C}^{N_r \times N_s}$ is an additive white Gaussian noise (AWGN) matrix with each entry follows independent and identically distributed (i.i.d.) circularly symmetric complex Gaussian distribution with zero mean and variance $\sigma_n^2 = N_0$ per complex dimension, i.e., $n_i^{(l)} \sim \mathcal{CN}(0, N_0)$. Throughout this dissertation, we assume that the channel is modeled as uncorrelated Rayleigh fading such that each element of the channel matrix $\mathbf{H}$ is an i.i.d. circularly symmetric complex Gaussian random variable with $\mathcal{CN}(0, 1)$.

Finally, MIMO detector estimates the original transmitted symbol $\mathbf{S}$ from the received symbol $\mathbf{R}$ based on the prior information of the channel matrix $\mathbf{H}$. The detail of specific detection algorithm is described in Chapter 1.3.

1.2.3 Spatial Multiplexing and Spatial Modulation

The transmit symbol $\mathbf{S}$ given by (1.2) depends on which transmission scheme is employed at the transmitter as described in Chapter 1.1. Throughout this work, we focus on spatial multiplexing and spatial modulation as MIMO transmission schemes. Here, we introduce the general system model as a framework of *generalized spatial modulation (GSM)* [25], since spatial multiplexing and spatial modulation can be regarded as special cases of GSM as shown in Fig. 1.4. Note that the detailed notations for each scheme are given in each section. Let N_a denote the number of active antennas, which means that only N_a antennas transmit the modulated symbols at each symbol period indicated by l. In other words, $(N_t - N_a)$ antennas do not transmit any symbols (or transmit null constellation points) and work as inactive antennas. In GSM systems, in addition to the conventional transmission of modulated signals by M-PSK or M-QAM, information bits are also allocated for the combination that selects N_a antennas from all the N_t antennas. Thus, the resulting transmission rate (or spectral efficiency) is expressed as

$$\eta_{\text{GSM}} = \log_2 \left\lfloor \binom{N_t}{N_a} \right\rfloor + N_a \log_2 M. \tag{1.5}$$

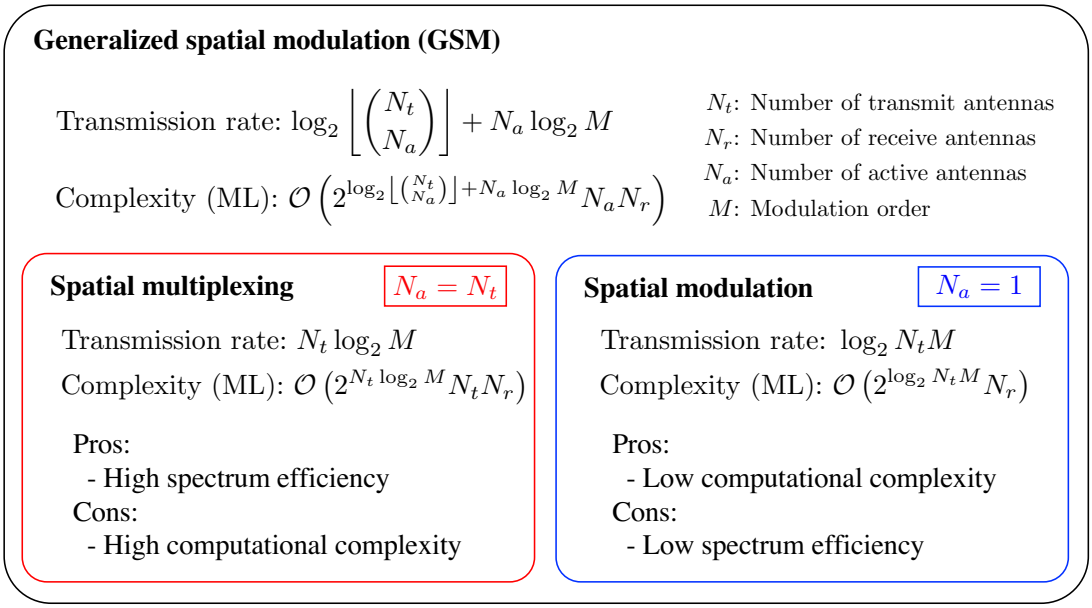

Figure 1.4: Generalized MIMO transmission schemes considered in this dissertation.

Since the number of candidates of the transmitted symbol also corresponds to η_{GSM}, the computational complexity order of GSM for MLD given by (1.9) is derived as $\mathcal{O}\left(2^{\eta_{\text{GSM}}} N_a N_r\right)$.

Spatial Multiplexing

Spatial multiplexing corresponds to the case with $N_a = N_t$ in GSM. Thus, all the transmit antennas carry the conventional M-PSK of M-QAM constellation points. From (1.5), the transmission rate of spatial multiplexing is expressed as

$$\eta_{\text{SMX}} = N_t \log_2 M. \tag{1.6}$$

It is observed from (1.6) that the maximum spectral efficiency increases linearly as the number of transmit antennas increases. In practice, previous studies have shown that the capacity in spatial multiplexing systems increases in proportion to the number of antennas over uncorrelated Rayleigh fading channels [22]. Therefore, spatial multiplexing has been getting much attention recently and adopted in several wireless communication standards such as Wi-Fi, LTE, and 5G.

Against this attractive advantage, a few critical issues are also known and widely studied. Among them, channel correlation and computational complexity for MIMO detection are extremely serious concerns for practical implementation. The former is the performance degradation due to channel correlation between the transmitter and receiver. The achievable data rate

depends on the rank of the channel matrix $\mathbf{H}$, but full rank can be obtained only by an ideal uncorrelated channel. In practical environments, since the propagation path may not be sufficient for the number of antennas, the achievable capacity is exceeded. To deal with this issue, the concept of cell-free MIMO has been proposed and well investigated most recently [26, 27], where it can manage the channel correlation by introducing distributed antennas. On the other hand, the computational complexity for signal detection in spatial multiplexing systems is a crucial problem that needs to be addressed. In fact, MLD requires high complexity order of $\mathcal{O}\left(2^{N_t} M N_t N_r\right)$, and grows exponentially with the number of transmit antennas (or transmission rate) [28, 29]. Therefore, a drastic approach to reduce the computational complexity of MIMO detector has not yet been established. Motivated by this background, we focus on MF detector and propose a new coded modulation approach combined with interference cancellation (IC) technique in Chapter 3.

Spatial Modulation

In order to cope with high complexity of spatial multiplexing, spatial modulation is also a valid approach. Spatial modulation corresponds to the case with $N_a = 1$ for GSM [23], and its transmission rate is given by

$$\eta_{\text{SM}} = \log_2 \left(N_t M\right). \tag{1.7}$$

Compared to the spectral efficiency of spatial multiplexing, which increases linearly, that of spatial modulation increases logarithmically with the number of antennas. In contrast, the complexity order for MLD of spatial modulation is much lower than that of spatial multiplexing and given by $\mathcal{O}\left(M N_t N_r\right)$. Furthermore, it is known that MED of spatial modulation can be reduced compared to spatial multiplexing with the same transmission rate in some cases. As an example with $N_t = 4$ and the transmission rate $\eta_{\text{SMX}} = \eta_{\text{SM}} = 2$, MED of spatial modulation can achieve 2 by QPSK signaling, whereas that of spatial multiplexing is 1 with BPSK signaling. Thus, spatial modulation has the potential to achieve better performance even with lower detection complexity. As the main drawback, the compatibility with conventional binary error correcting codes is poor, and the applicable signal detector is limited to the optimal-based approaches such as MLD and sphere decoding [30]. In order to tackle this problem, we derive the optimal design of sub-optimal detection based on MF detector for spatial modulation in Chapter 4.

1.3 MIMO Detection

Focusing on the lth transmitted symbol, (1.4) can be derived in the vector form as

$$\mathbf{r}^{(l)} = \mathbf{H}\mathbf{s}^{(l)} + \mathbf{n}^{(l)}. \tag{1.8}$$

At the receiver, the original transmitted vector $\mathbf{s}^{(l)}$ is estimated as $\hat{\mathbf{s}}^{(l)}$ by MIMO detector.

Maximum Likelihood Detector

The optimal approach is known as maximum likelihood detection (MLD), and it is performed as

$$\hat{\mathbf{s}}^{(l)} = \min_{\mathbf{s}} \left\| \mathbf{r}^{(l)} - \mathbf{H}\mathbf{s}^{(l)} \right\|^2. \tag{1.9}$$

However, its computational complexity grows exponentially with the number of transmit antennas as well as bit per symbol for modulation scheme $m = \log_2 M$. So as to reduce the complexity of MLD, several reduced-complexity versions have been proposed such as tree-search-based detectors [31, 32]. Nevertheless, their worst complexity order would be the same as that of MLD.

Linear Detector

Based on the above observation, the practical systems employ a low-complexity linear detection. The general operation of the linear detectors is calculating the soft-output estimated vector $\hat{\mathbf{s}}^{(l)}$ by simple linear transform as

$$\hat{\mathbf{s}}^{(l)} = \mathbf{W}^{\mathrm{H}}\hat{\mathbf{r}}^{(l)}, \tag{1.10}$$

where $\mathbf{X}^{\mathrm{H}}$ is the Hermitian transpose of a matrix $\mathbf{X}$, and $\mathbf{W} = (\mathbf{w}_1\, \mathbf{w}_2 \cdots \mathbf{w}_k \cdots \mathbf{w}_{N_t}) \in \mathbb{C}^{N_r \times N_t}$ represents the weight matrix of each linear detector, in which the kth vector $\mathbf{w}_k$ represents the weight vector corresponding to the kth transmit antenna. A simple solution is to use the inverse of the channel matrix $\mathbf{H}$ for the weight matrix in (1.10). This approach is known as zero-forcing (ZF), which maximizes the signal-to-interference ratio (SIR). Its weight matrix is given by

$$\mathbf{W}^{\mathrm{H}} = \left(\mathbf{H}^{\mathrm{H}}\mathbf{H}\right)^{-1}\mathbf{H}^{\mathrm{H}}. \tag{1.11}$$

However, ZF detector causes noise power augmentation. Thus, the linear detection based on minimum mean-square error (MMSE) is introduced, where it takes both the interference and noise into account. As a result, MMSE detector achieves a better performance than ZF especially compared in the low SNR region. The weight matrix of MMSE detector is expressed as

$$\mathbf{W}^{\mathrm{H}} = \left(\mathbf{H}^{\mathrm{H}}\mathbf{H} + \frac{N_0}{N_t}\mathbf{I}_{N_t} \right)^{-1} \mathbf{H}^{\mathrm{H}}, \tag{1.12}$$

where $\mathbf{I}_{\mathrm{N}}$ denotes the identity matrix with size N. These linear detectors have been widely adopted due to their simple and unified signal processing independent of modulation schemes. However, their complexity order still grows cubicly with the number of antennas [33] due to the requirement of matrix inversion.

1.3.1 Matched-Filter Detector

Therefore, we focus on a matched-filter (MF) detector, also known as maximum ratio combining (MRC) [34–36][1] since it has been regarded as the lowest complexity detection among all MIMO detectors [37]. MF detector is also categorized into linear detection and maximizes the output SNR.

In what follows, we first derive the weight matrix of MF detector based on the SNR maximization criteria. From (1.10), the kth output is expressed as

$$\hat{s}_k = \mathbf{w}_k^{\mathrm{H}}\mathbf{h}_k\mathbf{s}^{(l)} + \mathbf{w}_k^{\mathrm{H}}\mathbf{n}. \tag{1.13}$$

The signal power in (1.13) is given by

$$E\left\{ \left| \mathbf{w}_k^{\mathrm{H}}\mathbf{h}_k s_k^{(l)} \right|^2 \right\} = \left| \mathbf{w}_k^{\mathrm{H}}\mathbf{h}_k \right|^2 E_t \tag{1.14}$$

where E_s denotes the transmit power per transmit antenna. Likewise, the noise power is calculated by

$$\begin{aligned} E\left\{ \left| \mathbf{w}_k^{\mathrm{H}}\mathbf{n} \right|^2 \right\} &= E\left\{ \mathbf{w}_k^{\mathrm{H}}\mathbf{n} \left(\mathbf{w}_k^{\mathrm{H}}\mathbf{n} \right)^* \right\} = E\left\{ \mathbf{w}_k^{\mathrm{H}}\mathbf{n} \left(\mathbf{n}^T\mathbf{w}_k^* \right)^* \right\} \\ &= \mathbf{w}_k^{\mathrm{H}} E\left\{ \mathbf{n}\mathbf{n}^T \right\} \mathbf{w}_k = \mathbf{w}_k^{\mathrm{H}}\mathbf{w}_k N_0. \end{aligned} \tag{1.15}$$

[1]Note that MF can be also applied at the transmitter side, and in such a scenario, it is widely known as maximum ratio transmission (MRT) and conjugate beamforming (CB) especially in a framework of massive MIMO [16]. In this dissertation, we focus only on the case where MF is adopted at the receiver.

Thus, the SNR of the linear filter output is expressed as

$$\gamma_{\text{linear}} = \frac{\left|\mathbf{w}_k^{\mathrm{H}}\mathbf{h}_k\right|^2}{\mathbf{w}_k^{\mathrm{H}}\mathbf{w}_k} \cdot \frac{E_t}{N_0}, \tag{1.16}$$

From Cauchy-Schwartz inequality, the following expression holds for any vectors represented by $\mathbf{a}$ and $\mathbf{b}$:

$$\left|\mathbf{a}^{\mathrm{H}}\mathbf{b}\right|^2 \leq \mathbf{a}^{\mathrm{H}}\mathbf{a}\mathbf{b}^{\mathrm{H}}\mathbf{b}, \tag{1.17}$$

with equality if and only if $\mathbf{b} = c\mathbf{a}$ (c is an arbitrary constant). By substituting $\mathbf{a} = \mathbf{w}_k$ and $\mathbf{b} = \mathbf{h}_k$ into (1.17), the following formula holds:

$$\frac{\left|\mathbf{w}_k^{\mathrm{H}}\mathbf{h}_k\right|^2}{\mathbf{w}_k^{\mathrm{H}}\mathbf{w}_k} \tag{1.18}$$

Therefore, the SNR of the linear detector output in (1.16) is maximized with $\mathbf{w}_k^{\mathrm{H}} = c_k\mathbf{h}_k^{\mathrm{H}}$, where c_k is arbitrary constant for the kth linear detector output. Here, we simply consider the case with $c_k = 1$ for any transmit antenna index $k \in \{1, \cdots, N_t\}$. As a result, the kth weight vector of MF detector is given by

$$\mathbf{w}_k^{\mathrm{H}} = c_k\mathbf{h}_k^{\mathrm{H}} = \mathbf{h}_k^{\mathrm{H}}, \tag{1.19}$$

and we finally get the weight matrix of MF detector expressed as

$$\mathbf{W}^{\mathrm{H}} = \mathbf{C}\mathbf{H}^{\mathrm{H}} = \mathbf{H}^{\mathrm{H}}, \tag{1.20}$$

where $\mathbf{C} = \mathrm{diag}\left(c_1, c_2, \cdots, c_k, \cdots, c_{N_t}\right) \in \mathbb{C}^{N_t \times N_t}$ is a diagonal matrix in which the kth diagonal element corresponds to c_k. We note that the scaling by $\mathbf{C}$ does not affect the resulting performance for spatial multiplexing. In contrast, the optimal scaling parameter exists for spatial modulation. The details are described in Chapter 4.

It is obvious that MF detector does not require any calculation for the weight matrix generation, and this fact enables the lowest complexity detection only by the operation in (1.10). On the other hand, those of ZF and MMSE are given by (1.11) and (1.12). It includes the inverse matrix generation, and thus, ZF and MMSE require much more complexity than MF even though it is lower compared to MLD. In general, there is a tradeoff between the error rate performance and computational complexity for MIMO detectors, and various approaches have been proposed in

the literature. Therefore, the development of computationally efficient symbol detection schemes plays an important role.

1.4 Outline and Contributions

This dissertation is summarized as follows:

- In Chapter 2 titled as **"Performance Analysis of Matched-Filter Detector over Rayleigh Fading Channel"**, we analyze the statistical property of MF detector over uncorrelated Rayleigh fading channel. Throughout the mathematical analysis, we derive the exact distribution of the MF output in a closed-form formula. Based on that, we derive the uncoded BER expression for arbitrary PSK and QAM modulation. For coded MIMO systems, we present the optimal metric for channel decoder in terms of log-likelihood ratio and the mutual information.

- In Chapter 3 titled as **"Matched-Filter Detector with Quadrature Interference Cancellation for Uplink MIMO Spatial Multiplexing"**, we propose a new interference cancellation technique for uplink coded multi-user MIMO spatial multiplexing systems, namely quadrature interference cancellation (QIC). It is designed for MF detector based on the statistical property derived in Chapter 2. Since the concept of QIC is similar to multilevel coded modulation (MLD), the parameters associated with error correcting codes should be carefully addressed. Thus, we also provide the design criteria of code rate and construction by taking polar codes as an example. Furthermore, the approximated theoretical expression in terms of block error rate (BLER) performance is also developed. Numerical results demonstrate that our proposed polar-coded MF-QIC outperforms other conventional approaches even in the presence of channel estimation error.

- In Chapter 4 titled as **"Scaling Matched-Filter Detector for MIMO Spatial Modulation"**, we consider coded MIMO spatial modulation where MF detector is employed as sub-optimal detection. In order to apply MF detector to spatial modulation, we first introduce appropriate scaling. Unlike the optimal detection such as MLD, the log-likelihood ratio is not clear for the sub-optimal detection since its derivation is different from conventional spatial multiplexing. Therefore, based on the analytical results in Chapter 2, we derive the optimal metric of scaling MF detector for channel decoding.

- Chapter 5 concludes this dissertation.

Chapter 2

Performance Analysis of Matched-Filter Detector over Rayleigh Fading Channel

In this chapter, we exactly analize the statistical property of MF detector over uncorrelated Rayleigh fading channels.

Published as:

Y. Hama and H. Ochiai, "Performance Analysis of Matched-Filter Detector for MIMO Spatial Multiplexing over Rayleigh Fading Channels with Imperfect Channel Estimaiton, " *IEEE Trans. on Commun.,* vol. 67, no. 4, pp. 3220-3233, May. 2019.

2.1 Introduction

Massive MIMO or a large scale MIMO, which involves a large number of antennas at the transmitter and/or receiver sides, has turned out to be promising in terms of its significantly high spectral efficiency and reliability at least from the theoretical viewpoint [16, 17, 38–40]. There are various approaches towards realization of MIMO systems, and spatial multiplexing is one of the promising approaches as the capacity increases linearly with the number of transmit antennas under the assumption of independent fading [7, 20, 21]. For the signal detection in spatial multiplexing systems, the MLD may be applicable to the systems with a few antennas, but not necessarily suitable for MIMO spatial multiplexing systems with much more antennas. Therefore, as the number of antennas increases, the conventional low-complexity linear detectors become a realistic option. There are several representative linear detectors well investigated in the literature. Among them, the zero-forcing (ZF) detector can maximize the signal-to-interference ratio (SIR), but it causes noise power augmentation. This problem is solved by the minimum mean-square error (MMSE) detector, where it considers both the interference and noise, leading to a better performance than the ZF detector especially in low signal-to-noise ratio (SNR) regime.

The above two linear detectors have been widely studied, but their complexity still grows with the cubic order of the number of antennas [33] due to the requirement of matrix inversion. On the other hand, another well known, even lower-complexity detector is the matched-filter (MF)

detector, also known as the maximum ratio combining (MRC) detector [34–37][1]. In fact, the MF detector has been regarded as the lowest computational complexity detector among all practical MIMO detectors studied in the literature [37], but at the cost of severe performance degradation. Since the matched filter operates such that the output SNR is maximized for each transmit antenna and thus does not take into account the interference caused by the symbols transmitted from the other antennas, its performance without channel coding is prohibitively poor in high SNR. Nevertheless, in the case of low SNR, recent studies demonstrate that near optimal performance can be achieved with the assistance of powerful channel coding, and this is especially the case when the number of antennas is large [42]. This fact has motivated us to study the fundamental performance limit of the MF detector in MIMO spatial multiplexing systems. Due to the central limit theorem, the performance of the MF detector can be easily analyzed in the framework of massive MIMO. However, invoking such an approximation generally requires the assumption of large antennas.

We note that the *exact* performance analysis for MIMO systems is still challenging, even for simple cases such as those over uncorrelated Rayleigh fading channels. The performances of linear detectors depend on the signal-to-interference-plus-noise ratio (SINR) [43], and the closed-form bit error rate (BER) expressions of the ZF detector are discussed in [44], where the error rate performance and outage probabilities of MMSE detector are also examined based on the high SNR approximation. In [45], based on the Gamma distribution approximation of the MMSE receiver output, the approximate BER expression is derived. In [46], on the other hand, the exact *instantaneous* BER (conditioned on a channel realization) is derived in a closed form for a general quadrature amplitude modulation (QAM) signaling under the framework of MMSE detection, but in practice, the *average* BER expression for a typical Rayleigh fading scenario would be desirable if it is expressed by a simple closed-form equation. Very recently, based on the assumption of large number of receive antennas, the distribution of the output of ZF detector and the resulting coded performance have been derived in [47].

Since the ZF detector is able to remove all the interfering symbols, its output contains only the two terms, i.e., signal and noise. On the other hand, the MF detector should take into account the correlation between the desired and interfering symbols. Therefore, the exact analysis of MF detector would be more complicated than that of ZF detectors. In [48], the outage probability of

[1] In the literature of MIMO-MRC systems, MRC detectors are linked with transmit beamforming assuming that channel knowledge is available at both the transmitter and receiver [41], in which case a single stream is transmitted over multiple transmit antennas. On the other hand, this chapter focuses on MIMO spatial multiplexing where each antenna transmits its own symbol and thus the transmitted symbols interfere with each other at the receiver, even with MRC detection. Thus, the theoretical framework of this chapter is significantly different from the conventional MIMO-MRC system.

the MF *precoder* is derived under the framework of downlink multi-user massive MIMO, which is shown to become accurate *with a large number of antennas*. The exact expression of the outage probability for MF precoder is also derived in the very recent work [49], but it involves an expression with an infinite summation. Therefore, the asymptotic forms are developed under the framework of massive MIMO systems.

To the best of the authors' knowledge, the exact and closed-form expressions for uncoded BER under the framework of MIMO spatial multiplexing with arbitrary numbers of transmit and receive antennas, even with simple uncorrelated Rayleigh fading channels, has not been well developed in the literature. Therefore, in this chapter, we study the *exact* performance of the MF detector *without any restrictions on the numbers of transmit and receive antennas*. To this end, we first derive the exact and closed-form probability distributions of the MF detector output. We then derive the closed-form BER expressions of uncoded MIMO systems with BPSK, QPSK, and square-type M-ary QAM signaling with arbitrary numbers of transmit and receive antennas. Our results can be seen as the MIMO generalization of the MRC detector over Rayleigh fading channels whose closed-form BER expressions are well known in the case of single-input multiple-output (SIMO) scenarios [50]. Furthermore, we derive an approximate cumulative distribution function (cdf) when the number of antennas becomes large. Using this result, we also derive the asymptotic BER expression for QAM. The developed result can also be used for the derivation of the optimal and closed-form log-likelihood ratio (LLR) expression with the MF detector in the case of coded MIMO systems. Furthermore, it enables us to calculate the mutual information which serves as the performance limit of the coded MIMO systems over ideally interleaved channels. The results are confirmed by Monte-Carlo simulations using a low-density parity-check (LDPC) code [12], justifying our findings in this chapter. We will also find that the optimal LLR expression based on the exact metric developed here matches with that based on the simple Gaussian distribution modeling, which may justify the use of simple Gaussian-based metric for coded MIMO systems with MF detector. Furthermore, considering the application of MF detector to a more practical scenario, we extend our exact analysis to the systems with imperfect channel estimation.

Our fundamental analytical framework will be built on single-user MIMO systems where both the transmitter and receiver can have an arbitrary number of antennas, but the derived analytical results as well as the insight gained may be applicable to the uplink of multi-user MIMO systems where hundreds of antennas are placed at the base station (BS). For such systems, the use of MF detector may substantially simplify the complexity overhead of the signal processing imposed for the BS. Our main objective is, through rigorous theoretical analysis, to elucidate

the conditions where the MF detector may be beneficial in terms of the number of antennas and channel SNR, for both uncoded and coded cases.

This chapter is organized as follows. In Section 3.2, we describe the system model adopted throughout this chapter. The exact analysis of the MF detector output is performed in Section 2.3. The closed-form BER expressions in the cases of uncoded BPSK, QPSK, and M-QAM are derived in Section 2.4. Section 2.5 is devoted to the development of the optimal metric for coded cases as well as the corresponding mutual information, where the simulation results that support the theoretical results are also provided. Our analysis is extended to the practical scenario with channel estimation error in Section 2.6. Finally, Section 4.6 concludes this chapter.

2.2 MIMO Spatial Multiplexing System

The general MIMO system model has been already introduced in Section 1.2. Here, we describe the detailed system model considerred in this chapter.

2.2.1 System and Channel Models

We consider a single-user $N_t \times N_r$ MIMO spatial multiplexing system, where N_t and N_r denote the numbers of antennas at the transmitter and receiver, respectively. We denote a set of the transmit symbols through N_t antennas by the column vector $\mathbf{s} = (s_1, s_2, \cdots, s_{N_t})^T \in \mathcal{X}^{N_t \times 1}$ where $\mathcal{X} \subset \mathbb{C}$ denotes a set of the constellation points to be transmitted from each antenna. Throughout this chapter, we focus on the lth transmit symbol through MIMO channel given by (1.8), and omit the symbol index l for simplicity. Thus, the received symbol vector $\mathbf{r} \in \mathbb{C}^{N_r \times 1}$ is expressed as

$$\mathbf{r} = \mathbf{H}\mathbf{s} + \mathbf{n}, \tag{2.1}$$

where $\mathbf{n} = (n_1, n_2, \cdots, n_{N_r})^T \in \mathbb{C}^{N_r \times 1}$ is an additive white Gaussian noise (AWGN) vector and $\mathbf{H} = (\mathbf{h}_1 \ \mathbf{h}_2 \ \cdots \ \mathbf{h}_{N_t}) \in \mathbb{C}^{N_r \times N_t}$ is a complex channel matrix. Each column vector $\mathbf{h}_k = (h_{1,k}, h_{2,k}, \cdots, h_{N_r,k})^T$ represents the channel corresponding to the kth transmit antenna with $k \in \{1, 2, \cdots, N_t\}$.

In order to analyze the performance in a mathematically rigorous manner, we further make the following basic assumptions throughout this chapter: Each element n_i of the noise vector $\mathbf{n}$ follows an independent and identically distributed (i.i.d.) circularly symmetric complex Gaussian random variable with zero mean and variance $\sigma_n^2 = N_0$ *per complex dimension*, i.e.,

$n_i \sim \mathcal{CN}(0, N_0)$. Also, the channel is modeled as uncorrelated Rayleigh fading such that each element of the channel matrix $\mathbf{H}$ is an i.i.d. circularly symmetric complex Gaussian random variable with zero mean and unit variance, i.e., $h_{i,k} \sim \mathcal{CN}(0, 1)$. Therefore, $E\left\{|h_{i,k}|^2\right\} = 1$ for any pair of $i \in \{1, 2, \cdots, N_r\}$ and $k \in \{1, 2, \cdots, N_t\}$, where $E\{\cdot\}$ denotes an expectation operation.

Finally, as is often the case with MIMO spatial multiplexing systems, we assume that the transmitter does not have the knowledge of channel state information (CSI) but the receiver has the perfect knowledge, i.e., $\mathbf{H}$ is available at the receiver side but not at the transmitter side. The assumption of perfect CSI at the receiver will be relaxed later in Section 2.6, where the effect of channel estimation errors is also analyzed.

2.2.2 Transmitter Model

Since the transmitter does not have any CSI, we assume that the transmit energy is distributed equally over the entire transmit antennas. In other words, each transmit antenna is assumed to generate a statistically independent symbol without any precoding and we denote the average symbol energy *per transmit antenna* by E_t. Let the kth transmit symbol be denoted by $s_k = x_k + jy_k$ where $x_k, y_k \in \mathbb{R}$. Then, in the case of BPSK, we set $y_k = 0$ and define $\mathcal{X} = \{-\sqrt{E_t}, \sqrt{E_t}\} \subset \mathbb{R}$. Likewise, for QPSK, both x_k and y_k are chosen from $\mathcal{X} = \{-\sqrt{E_t/2}, \sqrt{E_t/2}\}$. In the case of square-type M-ary QAM composed of two independent $\sqrt{M}$-pulse amplitude modulation (PAM) constellations, both x_k and y_k are chosen from $\mathcal{X} = \{-(\sqrt{M}-1)A, \cdots, -3A, -A, A, 3A, \cdots, (\sqrt{M}-1)A\}$ where $A = \sqrt{3E_t/2(M-1)}$.

Without loss of generality, the reduction of energy due to path loss and shadowing is normalized such that the average energy per transmit antenna is expressed in terms of the average energy of the received symbol E_s as $E_t = E_s/N_t$. (Or, in other words, E_t is the received symbol energy observed at each receive antenna normalized by the number of transmit antennas.) Furthermore, we define the parameter $\gamma_s = E_s/N_0$ which corresponds to the average SNR *per receive antenna*.

The SNR *per bit*, denoted by γ_b, is commonly defined as

$$\gamma_b \triangleq \frac{E_s}{mN_0} = \frac{\gamma_s}{m}, \tag{2.2}$$

where m is the number of bits per symbol (i.e., $m = 1$ for BPSK and $m = 2$ for QPSK), and thus

$$\frac{E_t}{N_0} = \frac{m}{N_t}\gamma_b = \frac{\gamma_s}{N_t}. \tag{2.3}$$

2.2.3 Receiver Model

The primary role of MIMO detector is to output the estimate $\hat{s}_k = \hat{x}_k + j\hat{y}_k$ corresponding to the transmitted symbol s_k, which can be further used by the soft-decision channel decoder in the case of coded systems.

Given $\mathbf{H}$ at the receiver, the general operation of the MIMO linear detector is to calculate the soft-output vector $\hat{\mathbf{s}} = (\hat{s}_1, \hat{s}_2, \cdots, \hat{s}_{N_t})^T \in \mathbb{C}^{N_t \times 1}$ by linear transformation:

$$\hat{\mathbf{s}} = \frac{1}{\sqrt{N_r}} \mathbf{W}^{\mathrm{H}} \mathbf{r}, \tag{2.4}$$

where $\mathbf{W} = (\mathbf{w}_1 \ \mathbf{w}_2 \ \cdots \ \mathbf{w}_{N_t}) \in \mathbb{C}^{N_r \times N_t}$ is the weight matrix and $\mathbf{X}^{\mathrm{H}}$ represents the Hermitian transpose of a matrix $\mathbf{X}$. Note that for analytical convenience and without loss of generality, we here introduced the scaling matrix $\mathbf{C} = \frac{1}{\sqrt{N_r}} \mathbf{I}_{N_t}$ so as to normalize the variance of the detector output throughout this chapter.

For the ZF detector, the weight matrix is given by the pseudo-inverse of the channel matrix [51]

$$\mathbf{W}^{\mathrm{H}} = \left(\mathbf{H}^{\mathrm{H}} \mathbf{H}\right)^{-1} \mathbf{H}^{\mathrm{H}}, \tag{2.5}$$

which requires the complexity order of $O(N_t^3)$ due to the inversion operation of $N_t \times N_t$ matrix in addition to matrix multiplication. On the other hand, for the MF detector, the weight matrix is simply chosen identical to the channel matrix, i.e.,

$$\mathbf{W}^{\mathrm{H}} = \mathbf{H}^{\mathrm{H}}, \tag{2.6}$$

or equivalently,

$$\mathbf{w}_k^{\mathrm{H}} = \mathbf{h}_k^{\mathrm{H}}. \tag{2.7}$$

Therefore, no matrix inversion is necessary, and thus the complexity order is dominated by matrix multiplication operation only, which grows linearly with N_r per each transmit antenna. The benefit of MF detector over the other detectors thus becomes significant especially when the number of the transmit antennas becomes large, as in the case of massive MIMO scenarios.

2.2.4 Remark

Our subsequent analysis is valid for any combination of antennas at the transmitter and receiver as long as the channels follow uncorrelated Rayleigh fading. However, the assumption of large antennas at both sides for point-to-point communications may not be realistic. In fact, our analytical model can be easily extended to the uplink of a single-cell multi-user MIMO system where most of the obtained results may be applicable. In such a system, each cell consists of a single BS with N_r receive antennas and N_t single-antenna users [39, 52]. In fact, our $N_t \times N_r$ MIMO model directly applies to the system if the power control of the users is appropriately performed such that the average SNR of all the users (antennas) is identical. Furthermore, the geometrical separation of users in the uplink justifies the use of uncorrelated fading model for each transmit antenna. Many recent theoretical studies on multi-user MIMO systems such as [38, 49, 53, 54] are based on such an ideal assumption, which we also follow in this chapter.

2.3 Exact Analysis of MIMO Systems with MF Detector Output

In this section, we derive the conditional probability density function (pdf) of the MF detector output for the system and channel models described in the previous section. The result will be utilized for performance studies of uncoded and coded MIMO spatial multiplexing systems in the subsequent sections.

2.3.1 A Probabilistic Model for Output of MF Detector

Let $\check{\mathbf{s}}_k \triangleq (s_1, s_2, \cdots, s_{k-1}, s_{k+1}, \cdots, s_{N_t})^T$ denote a vector of the transmit symbols where the symbol from the kth antenna is excluded. Let $\check{p}_k$ denote its square norm, i.e.,

$$\check{p}_k \triangleq \|\check{\mathbf{s}}_k\|^2. \tag{2.8}$$

Our main finding in this section is as follows.

Theorem 1. *The pdf of the real part of the MF output of the kth transmit antenna, $\hat{x}_k \triangleq \Re\{\hat{s}_k\}$,*

conditioned on its input $x_k \triangleq \Re\{s_k\}$ *and all the other transmit symbols* $\check{\mathbf{s}}_k$*, is expressed by*

$$p_{\hat{x}_k}(\hat{x}|x_k = x, \check{p}_k) = \frac{\sqrt{N_r}}{(N_r-1)!\sqrt{x^2+\check{p}_k+N_0}}\left[\frac{\check{p}_k+N_0}{2\left(x^2+\check{p}_k+N_0\right)}\right]^{N_r-1} e^{-\frac{2\sqrt{N_r}\left(\sqrt{x^2+\check{p}_k+N_0}|\hat{x}|-x\hat{x}\right)}{\check{p}_k+N_0}} \times \sum_{i=0}^{N_r-1}\frac{(N_r-1+i)!}{2^i\, i!\,(N_r-1-i)!}\left[\frac{2\sqrt{N_r\left(x^2+\check{p}_k+N_0\right)}\,|\hat{x}|}{\check{p}_k+N_0}\right]^{N_r-1-i}, \tag{2.9}$$

which is the pdf conditioned on $\check{p}_k$*. The corresponding pdf* $p_{\hat{y}_k}(\hat{y}|y_k = y, \check{p}_k)$ *for the imaginary part* $\hat{y}_k \triangleq \Im\{\hat{s}_k\}$ *is also given by* (2.9) *with* x *and* $\hat{x}$ *replaced by* y *and* $\hat{y}$*, respectively.*

Proof. We first identify that the pdf of the output $\hat{s}_k$ conditioned on s_k, $\check{p}_k$, and α_k is expressed by Gaussian distribution and then derive the desired distribution by averaging out the conditioning random variable α_k. An alternative approach by identifying the output as the quadratic form of real-valued Gaussian random variables is given in Section 2.6.2.

From (2.4), the kth estimated symbol $\hat{s}_k$ output from the corresponding MF detector is expressed as

$$\begin{aligned}\hat{s}_k &= \frac{1}{\sqrt{N_r}}\mathbf{w}_k^{\mathrm{H}}\mathbf{r} = \frac{1}{\sqrt{N_r}}\mathbf{w}_k^{\mathrm{H}}\left(\mathbf{h}_k s_k + \sum_{\ell=1,\ell\neq k}^{N_t}\mathbf{h}_\ell s_\ell + \mathbf{n}\right)\\ &= \frac{1}{\sqrt{N_r}}\sum_{i=1}^{N_r}|h_{i,k}|^2 s_k + \underbrace{\frac{1}{\sqrt{N_r}}\left\{\sum_{i=1}^{N_r}\sum_{\ell=1,\ell\neq k}^{N_t}h_{i,k}^* h_{i,\ell}s_\ell + \sum_{i=1}^{N_r}h_{i,k}^* n_i\right\}}_{\tilde{n}_k},\end{aligned} \tag{2.10}$$

where $\tilde{n}_k$ is the sum of the interference and noise terms.

$$\begin{aligned}p_{\hat{x}_k}\left(\hat{x}|x_k = \sqrt{E_t/m}\right) = &\frac{\sqrt{N_r}}{(N_r-1)!\sqrt{N_0\left[\{m\left(N_t-1\right)+1\}\gamma_b/N_t+1\right]}}\left[\frac{m(N_t-1)\gamma_b/N_t+1}{2\left[\{m\left(N_t-1\right)+1\}\gamma_b/N_t+1\right]}\right]^{N_r-1}\\ &\times e^{-\frac{2\sqrt{N_r}\left(\sqrt{\left[\{m(N_t-1)+1\}\gamma_b/N_t+1\right]}|\hat{x}|-\sqrt{\gamma_b/N_t}\hat{x}\right)}{\pi\sqrt{N_0}\{m(N_t-1)\gamma_b/N_t+1\}}}\\ &\times\sum_{i=0}^{N_r-1}\frac{(N_r-1+i)!}{2^i\, i!\,(N_r-1-i)!}\left[\frac{2\sqrt{N_r\left[\{m\left(N_t-1\right)+1\}\gamma_b/N_t+1\right]}\,|\hat{x}|}{\pi\sqrt{N_0}\left\{m(N_t-1)\gamma_b/N_t+1\right\}}\right]^{N_r-1-i}\end{aligned} \tag{2.11}$$

Let us now assume that the entries of the matrix $\mathbf{H}$ are i.i.d. random variables with $\mathcal{CN}(0,1)$ as defined in Section 2.2.1, except for the column vector $\mathbf{h}_k$ that corresponds to the kth transmit antenna, which is considered to be known at the detector. Furthermore, the column vector $\mathbf{s}$ is considered as fixed as well. Under this condition, it is easy to observe that the output $\hat{s}_k$ is a complex Gaussian random variable with mean given by

$$E\left\{\hat{s}_k \,|\, \mathbf{h}_k\right\} = \frac{1}{\sqrt{N_r}} \sum_{i=1}^{N_r} |h_{i,k}|^2 \, s_k = \sqrt{N_r}\alpha_k s_k, \tag{2.12}$$

where α_k can be seen as a signal attenuation factor expressed as

$$\alpha_k \triangleq \frac{1}{N_r} \sum_{i=1}^{N_r} |h_{i,k}|^2 = \frac{1}{N_r} \|\mathbf{h}_k\|^2 , \tag{2.13}$$

and variance given by

$$\begin{aligned}
\text{VAR}\left(\hat{s}_k \,|\, \mathbf{h}_k\right) &= E\left\{ |\tilde{n}_k|^2 \,\middle|\, \mathbf{h}_k \right\} \\
&= \frac{1}{N_r} \sum_{i=1}^{N_r} |h_{i,k}|^2 \sum_{\ell=1,\ell\neq k}^{N_t} E\left\{|h_{i,\ell}|^2\right\} |s_\ell|^2 + \frac{1}{N_r} \sum_{i=1}^{N_r} |h_{i,k}|^2 \, E\left\{|n_i|^2\right\} \\
&= \frac{1}{N_r} \|\mathbf{h}_k\|^2 \left\{ \sum_{\ell=1,\ell\neq k}^{N_t} |s_\ell|^2 + N_0 \right\} \\
&= \alpha_k \left(\|\check{\mathbf{s}}_k\|^2 + N_0 \right) = \alpha_k \left(\check{p}_k + N_0 \right),
\end{aligned} \tag{2.14}$$

which depends only on $\check{p}_k$ instead of $\check{\mathbf{s}}_k$. Note that α_k in (2.13) is normalized such that $E\left\{\alpha_k\right\} = 1$.

Therefore, conditioned on s_k, $\check{p}_k$, and α_k, the pdf of the output $\hat{s}_k$ is expressed as

$$p_{\hat{s}_k}\left(\hat{s}_k | s_k, \alpha_k, \check{p}_k\right) = \frac{1}{\pi\alpha_k\left(\check{p}_k + N_0\right)} e^{-\frac{\left|\hat{s}_k - \sqrt{N_r}\alpha_k s_k\right|^2}{\alpha_k\left(\check{p}_k + N_0\right)}}. \tag{2.15}$$

Consequently, the pdf for the real-valued random variable $\hat{x}_k = \Re\left\{\hat{s}_k\right\}$ is given by

$$p_{\hat{x}_k}\left(\hat{x}_k | x_k, \alpha_k, \check{p}_k\right) = \frac{1}{\sqrt{\pi\alpha_k\left(\check{p}_k + N_0\right)}} e^{-\frac{\left(\hat{x}_k - \sqrt{N_r}\alpha_k x_k\right)^2}{\alpha_k\left(\check{p}_k + N_0\right)}}. \tag{2.16}$$

Since $h_{i,k}$ follows $\mathcal{CN}(0,1)$ and i.i.d., the signal attenuation factor α_k defined in (2.13) is a

sum of the square of $2N_r$ i.i.d. real-valued zero-mean Gaussian random variables with the variance of each random variable given by $1/2N_r$. As a result, α_k follows a chi-square distribution with $2N_r$ degrees of freedom where its pdf is expressed as [50]

$$p_{\alpha_k}(\alpha) = \frac{N_r^{N_r} e^{-N_r\alpha}\alpha^{N_r-1}}{(N_r-1)!}. \tag{2.17}$$

The resulting pdf of (2.16) unconditioned on α_k is given by

$$\begin{aligned} p_{\hat{x}_k}\left(\hat{x}_k|x_k,\check{p}_k\right) &= \int_0^\infty p_{\alpha_k}\left(\alpha\right) p\left(\hat{x}_k|x_k,\alpha_k=\alpha,\check{p}_k\right) d\alpha \\ &= \frac{N_r^{N_r}}{(N_r-1)!} e^{2\sqrt{N_r}\frac{\hat{x}_k x_k}{\check{p}_k+N_0}} \frac{1}{\sqrt{\pi\left(\check{p}_k+N_0\right)}} \int_0^\infty \alpha^{N_r-\frac{3}{2}} e^{-\frac{\hat{x}_k^2}{\alpha(\check{p}_k+N_0)}-N_r\alpha\left(1+\frac{x_k^2}{\check{p}_k+N_0}\right)} d\alpha \\ &= \frac{N_r^{N_r}}{(N_r-1)!} e^{2\sqrt{N_r}\frac{\hat{x}_k x_k}{\check{p}_k+N_0}} \frac{1}{\sqrt{\pi\left(\check{p}_k+N_0\right)}} \\ &\quad \times 2\left(\frac{\hat{x}_k^2}{N_r\left(\check{p}_k+N_0+x_k^2\right)}\right)^{\frac{N_r}{2}-\frac{1}{4}} K_{N_r-\frac{1}{2}}\left(\frac{2\sqrt{N_r\hat{x}_k^2\left(\check{p}_k+N_0+x_k^2\right)}}{\check{p}_k+N_0}\right), \end{aligned} \tag{2.18}$$

where $K_\mu(z)$ is the modified Bessel function of the second kind. Using the following identity that holds for a positive integer n

$$K_{n+\frac{1}{2}}(z) = \sqrt{\frac{\pi}{2z}} e^{-z} \sum_{r=0}^{n} \frac{(n+r)!}{r!(n-r)!(2z)^r}, \tag{2.19}$$

and after some rearrangement, we obtain (2.9). The result for $\hat{y}_k = \Im\left\{\hat{s}_k\right\}$ follows in exactly the same manner. □

2.3.2 Expression for PSK Signaling or Large N_t

We now consider the cases when the signal is modulated by constant envelope (i.e., PSK) or the number of transmit antennas N_t is large. In the former case, we have $|s_\ell| = \sqrt{E_t}$ with probability 1 and thus $\check{p}_k = (N_t-1)E_t$. Similarly, if N_t is large such that the law of large numbers applies, we have

$$\check{p}_k = \sum_{\ell=1,\ell\neq k}^{N_t} |s_\ell|^2 \approx \sum_{\ell=1,\ell\neq k}^{N_t} E\left\{|s_\ell|^2\right\} = (N_t-1)E_t. \tag{2.20}$$

For example, in the case with BPSK and QPSK signaling, substituting (2.20) into (2.9) and

setting $x_k = \sqrt{E_t/m}$, where $m = 1$ for BPSK and $m = 2$ for QPSK, we obtain (2.11), shown at the top of this page.

2.3.3 Asymptotic Form for Large N_r

Note that the variance of α_k is given by

$$\text{VAR}\left(\alpha_k\right) = \frac{1}{N_r}, \tag{2.21}$$

which becomes 0 as N_r increases. Therefore, as the number of receive antennas increases, the attenuation factor approaches unity due to the law of large numbers since $E\left\{\alpha_k\right\} = 1$. Therefore, from (2.16), it can be approximated as

$$p_{\hat{x}_k}\left(\hat{x}_k | x_k, \check{p}_k\right) \approx \frac{1}{\sqrt{\pi\left(\check{p}_k + N_0\right)}} e^{-\frac{1}{\check{p}_k + N_0}\left(\hat{x}_k - \sqrt{N_r} x_k\right)^2}. \tag{2.22}$$

Furthermore, in the case of PSK signaling or large N_t cases such that (2.20) is valid, we obtain

$$p_{\hat{x}_k}\left(\hat{x}_k | x_k\right) \approx \frac{1}{\sqrt{\pi N_0\left\{m(N_t - 1)\gamma_b/N_t + 1\right\}}} e^{-\frac{1}{N_0\left\{m(N_t-1)\gamma_b/N_t+1\right\}}\left(\hat{x}_k - \sqrt{N_r} x_k\right)^2}, \tag{2.23}$$

which corresponds to the commonly used Gaussian approximation for MF output without conditioning on the input signaling.

2.3.4 Numerical Comparisons

We examine the exact theoretical distributions of the MF output developed in this section by comparing with those obtained based on Monte-Carlo simulations. The results are compared in Fig. 2.1 for the case of BPSK signaling with $E_s = 1$ and $\gamma_b = 0$ dB. The numbers of antennas are chosen as $2, 8$, and 32 with $N_t = N_r$. The pdf of MF output is calculated by the closed-form expression of (2.11). Both the results show perfect agreement, which justifies the accuracy of our derivation. The theoretical pdf based on the asymptotic form of (2.23), which is valid for any N_t in the case of PSK as long as N_r is large enough such that α_k can be modeled as constant, is also shown in Fig. 2.1, where, as expected, considerable discrepancy is observed when the number of antennas is small. In particular, while the asymptotic distribution follows Gaussian, the exact distribution in the case of $N_t = N_r = 2$ exhibits noticeable skewness and thus far from being Gaussian. With the increase of the number of receive antennas, however, all the distributions

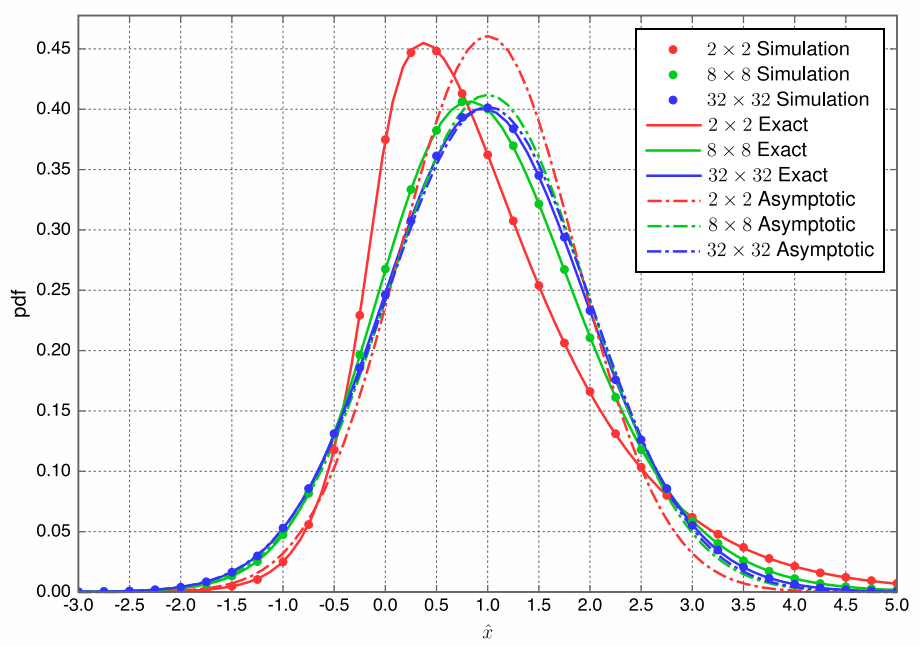

Figure 2.1: Comparison of the pdf of MF detector output calculated by the closed-form theoretical expressions (both exact and asymptotic) as well as Monte-Carlo simulations with BPSK signaling ($E_s = 1$ and $\gamma_b = 0$ dB).

may converge as expected.

We further investigate the difference between the exact expression (2.11) and its asymptotic form (2.23) by the Kullback-Leibler divergence (KLD). Let $p(x)$ and $q(x)$ denote the pdfs of the continuous random variables P and Q. The KLD is defined as

$$D_{\mathrm{KL}}\left(P \parallel Q\right) \triangleq \int_{-\infty}^{\infty} p(x) \log \frac{p(x)}{q(x)} dx. \tag{2.24}$$

The KLD is always non-negative and becomes 0 if and only if the two distributions are identical. Figure 2.2 shows the KLD with $p(x)$ given by the Gaussian approximation, i.e., (2.23), and $q(x)$ by the exact distribution, i.e., (2.11), when $N = N_t = N_r$ with several SNR values. We observe that as the number of antennas increases or SNR decreases, the KLD decreases as expected. As an example, the KLD of SNR -15 dB with $N = 10$ is almost the same as that of SNR 30 dB with $N \approx 30$. This behavior justifies that even if the number of antennas is not so large, the conventional Gaussian approximation becomes effective if the SNR is low.

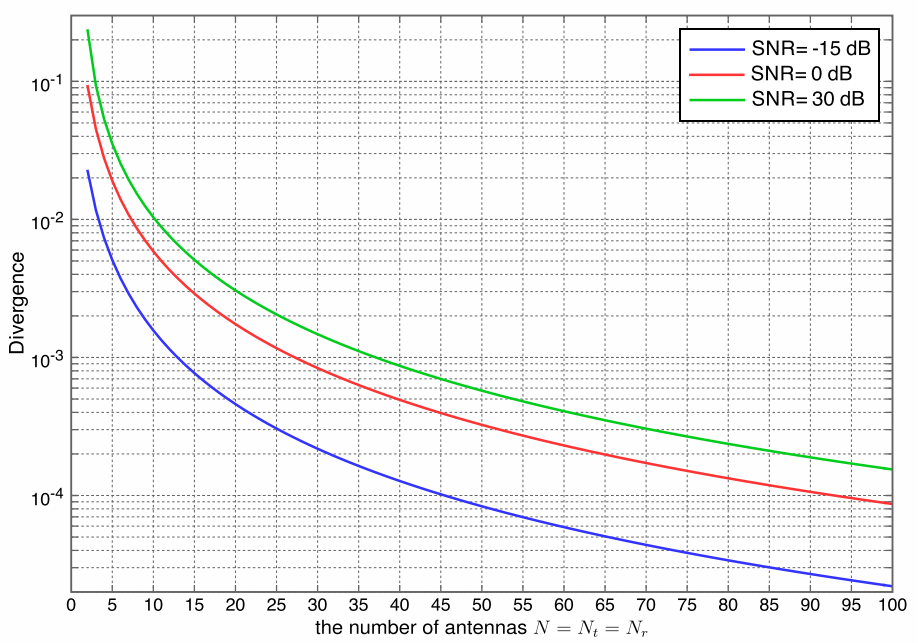

Figure 2.2: Comparison of the KLD between the pdf of MF detector output calculated by the exact closed-form theoretical expression and asymptotic expression with BPSK signaling. Note that the vertical axis is in logarithmic scale.

2.4 Exact BER Analysis

Based on the results developed in the previous section, in this section we derive the closed-form BER expressions in the case of BPSK, QPSK, and M-QAM signaling without any restrictions on the numbers of antennas N_t and N_r. It will be shown that the obtained results are the generalization of the well-known BER expressions developed for the receiver diversity with MRC over Rayleigh fading channels.

2.4.1 Cumulative Distribution Function of MF Output

The conditional cumulative distribution function (cdf) of MF output $\hat{x}_k$ is expressed as

$$\begin{aligned} F_{\hat{x}_k}\left(X|x_k = x, \check{p}_k\right) &\triangleq \Pr\left(\hat{x}_k < X \mid x_k = x, \check{p}_k\right) \\ &= \int_{-\infty}^{X} p_{\hat{x}_k}\left(\hat{x}|x_k = x, \check{p}_k\right) d\hat{x}. \end{aligned} \tag{2.25}$$

By substituting (2.9) into (2.25) and performing integration, we have

$$
\begin{aligned}
&F_{\hat{x}_k}\left(X|x_k=x,\check{p}_k\right)= \\
&\begin{cases}
\left(\dfrac{1}{2}-\dfrac{x}{2\sqrt{x^2+\check{p}_k+N_0}}\right)^{N_r} e^{\frac{2\sqrt{N_r}X}{\sqrt{x^2+\check{p}_k+N_0}-x}} \\
\quad\times\displaystyle\sum_{i=0}^{N_r-1}\binom{N_r-1+i}{i}\left(\frac{1}{2}+\frac{x}{2\sqrt{x^2+\check{p}_k+N_0}}\right)^{i} \\
\quad\times\displaystyle\sum_{l=0}^{N_r-i-1}\frac{1}{l!}\left(\frac{-2\sqrt{N_r}X}{\sqrt{x^2+\check{p}_k+N_0}-x}\right)^{l}, \quad \text{for } X\le 0, \\
1-\left(\dfrac{1}{2}+\dfrac{x}{2\sqrt{x^2+\check{p}_k+N_0}}\right)^{N_r} e^{\frac{-2\sqrt{N_r}X}{\sqrt{x^2+\check{p}_k+N_0}+x}} \\
\quad\times\displaystyle\sum_{i=0}^{N_r-1}\binom{N_r-1+i}{i}\left(\frac{1}{2}-\frac{x}{2\sqrt{x^2+\check{p}_k+N_0}}\right)^{i} \\
\quad\times\displaystyle\sum_{l=0}^{N_r-i-1}\frac{1}{l!}\left(\frac{2\sqrt{N_r}X}{\sqrt{x^2+\check{p}_k+N_0}+x}\right)^{l}, \quad \text{for } X>0.
\end{cases}
\end{aligned}
\tag{2.26}
$$

2.4.2 BER Expressions for BPSK and QPSK Signaling

The exact BER performance in the case of BPSK and QPSK signaling with Gray mapping can be calculated by way of the cdf of (2.26) with (2.20) and $x=\sqrt{E_t/m}$ as

$$
\begin{aligned}
P_b &= \Pr\left(\hat{x}_k<0\,|\,x_k=\sqrt{E_t/m},\,\check{p}_k=(N_t-1)\,E_t\right) \\
&= F_{\hat{x}_k}\left(0\,|\,x_k=\sqrt{E_t/m},\,\check{p}_k=(N_t-1)\,E_t\right) \\
&= \left(\frac{1}{2}-\frac{\sqrt{E_t/m}}{2\sqrt{\left(N_t-1+\frac{1}{m}\right)E_t+N_0}}\right)^{N_r} \\
&\quad\times\sum_{i=0}^{N_r-1}\binom{N_r-1+i}{i}\left(\frac{1}{2}+\frac{\sqrt{E_t/m}}{2\sqrt{\left(N_t-1+\frac{1}{m}\right)E_t+N_0}}\right)^{i}.
\end{aligned}
\tag{2.27}
$$

By substituting E_t of (2.3) into the above expression, the resulting BER of MF detector can

be expressed in terms of γ_b for BPSK as

$$P_b = \left(\frac{1-\mu}{2}\right)^{N_r} \sum_{i=0}^{N_r-1} \binom{N_r-1+i}{i} \left(\frac{1+\mu}{2}\right)^{i}, \tag{2.28}$$

where the SNR parameter $\mu \in (0,1)$ is expressed as

$$\mu_{\text{MF,BPSK}} = \sqrt{\frac{\gamma_b/N_t}{\gamma_b+1}} = \frac{1}{\sqrt{N_t + \frac{N_t}{\gamma_b}}}. \tag{2.29}$$

Note that the expression (2.28) agrees with the well-known BER expression for BPSK with MRC using N_r receive antennas over Rayleigh fading channel (i.e., [50, Eq. (13.4-15)]), and the only difference is that now the parameter $\mu \in (0,1)$ is a function of N_t given by (2.29). Therefore, the above result can be seen as a generalization of the SIMO MRC detector to MIMO spatial multiplexing with N_t transmit antennas. Furthermore, for a given N_r, the BER of (2.28) approaches 0 as μ approaches 1. Therefore, achieving higher μ for a given value of γ_b will be desirable in terms of the resulting BER. However, from (2.29) we observe that $\mu \to 1/\sqrt{N_t}$ as $\gamma_b \to \infty$, and thus as N_t increases, μ monotonically decreases, which confirms that increasing N_t should monotonically increase the achievable BER in the case of MIMO MF detection.

Likewise, for QPSK we have the same form as (2.28) but now μ is expressed as

$$\mu_{\text{MF,QPSK}} = \sqrt{\frac{\gamma_b/N_t}{(2-1/N_t)\,\gamma_b+1}} = \frac{1}{\sqrt{(2N_t-1) + \frac{N_t}{\gamma_b}}}. \tag{2.30}$$

Comparing (2.30) with (2.29), we observe that as γ_b increases, the parameter μ of QPSK approaches $1/\sqrt{2N_t-1}$, instead of the BPSK limit $1/\sqrt{N_t}$. (Both expressions agree if and only if $N_t = 1$.) This is due to the fact that in the case of MF detector, upon detecting the real part of QPSK symbols, not only the real part but also the imaginary part of the QPSK symbols transmitted from the other (N_t-1) antennas will be observed as interference at the receiver. This also explains that in the case of MIMO spatial multiplexing systems, the interference of QPSK should be greater than that of BPSK by a factor of about 3 dB.

It can be seen that when γ_b goes to infinity, we have the lower limit of BER for BPSK as

$$\begin{aligned}\bar{P}_b &\triangleq \lim_{\gamma_b \to \infty} P_b \\ &= \frac{1}{2^{N_r}} \left(1 - \frac{1}{\sqrt{N_t}}\right)^{N_r} \sum_{i=0}^{N_r-1} \binom{N_r - 1 + i}{i} \frac{1}{2^i} \left(1 + \frac{1}{\sqrt{N_t}}\right)^i. \end{aligned} \tag{2.31}$$

From (2.31), we observe that increasing N_r helps reducing the BER limit $\bar{P}_b$ but increasing N_t leads to increasing $\bar{P}_b$ in return for higher bit rate or spectral efficiency.

2.4.3 Comparison with ZF Detector

ZF and MMSE are the two well-studied linear detectors. To the best of our knowledge, the exact closed-form expression for the BER of MMSE detector has not been derived, even in the simple i.i.d. Rayleigh fading channels with perfect CSI. On the other hand, by the fact that SNR of the ZF detector output follows a chi-square distribution with $2(N_r - N_t + 1)$ degrees of freedom [44], the closed-form expression in the case of ZF detector with the same ideal assumptions given the condition $N_r \geq N_t$ can be derived as [44, 51][2]

$$P_b = \left(\frac{1-\nu}{2}\right)^{N_r - N_t + 1} \sum_{i=0}^{N_r - N_t} \binom{N_r - 1 + i}{i} \left(\frac{1+\nu}{2}\right)^i, \tag{2.32}$$

where ν for both BPSK and QPSK signaling (with Gray mapping) is given by

$$\nu_{\text{ZF}} = \sqrt{\frac{\gamma_b/N_t}{\gamma_b/N_t + 1}} = \frac{1}{\sqrt{1 + \frac{N_t}{\gamma_b}}}. \tag{2.33}$$

The BER expression of MF in (2.28) and that of ZF in (2.32) have the first product term $\frac{1-\mu}{2}$ in common, and if the parameters μ of (2.29), (2.30) or ν of (2.33) approach 1, the bit error rate approaches 0. Therefore, the comparison of the first product term together with the SNR parameters provides us the following insight:

1) For low SNR case, i.e., $\gamma_b \to 0$, both the parameters μ of MF and ν of ZF approach zero, but the first product in the case of MF decreases with its exponent N_r, whereas that of ZF decreases with $N_r - N_t + 1$. In other words, the observable diversity order of MF is N_r,

[2]The bit error rate expression shown in [44] is slightly different from (2.32). We have confirmed that our expression derived here is the correct version.

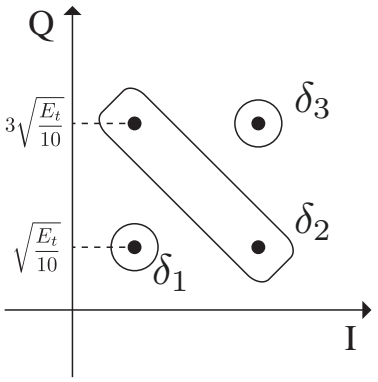

Figure 2.3: The constellation points of 16-QAM signaling within one quadrant.

whereas that of ZF is $N_r - N_t + 1$. Therefore, in the case of MF, increase of the transmit antennas N_t does not affect the BER in low SNR, whereas it increases the BER when ZF is employed.

2) For high SNR case, i.e., $\gamma_b \to \infty$, the parameters μ of MF do not approach 1 when $N_t > 1$, whereas ν of ZF approaches 1 irrespective of the value N_t. This explains the error floor effect of the MF detector when $N_t > 1$.

3) In the case of high SNR, the increase of constellation sizes from BPSK to QPSK may degrade the performance of MF significantly, whereas the performance remains the same for ZF.

2.4.4 Exact BER Expression for M-QAM Signaling

The conditional cdf of MF output (2.26) can also be used for the derivation of the exact BER performance for uncoded high-order square-type QAM. We consider the M-QAM formed by two $\sqrt{M}$-PAM constellations as described in Section 2.2.2. Instead of a conventional derivation approach which first identifies the symbol error rate and then associates the symbol error event with bit error events, we directly develop the probability of the bit error events. In general, the BER conditioned on $\check{p}_k$ can be expressed as a linear combination of the conditional cdf:

$$P_b\left(\check{p}_k\right) = a_0 + \sum_{n=1}^{L} a_n F_{\hat{x}_k}\left(c_n \,|\, x_k = b_n, \check{p}_k\right), \tag{2.34}$$

for some constants $a_n, b_n, c_n \in \mathbb{R}$ and $L \in \mathbb{Z}$ that depend on the constellation and bit mapping. For example, in the case of $M = 16$ with Gray mapping, the BER conditioned on $\check{p}_k$ can be

expressed through direct calculation as

$$\begin{aligned} P_b\left(\check{p}_k\right) = \frac{1}{4}\big[1 &+ F_{\hat{x}_k}\left(0 \,|\, x_k = 3A, \check{p}_k\right) + F_{\hat{x}_k}\left(0 \,|\, x_k = A, \check{p}_k\right) \\ &+ F_{\hat{x}_k}\left(\kappa \,|\, x_k = 3A, \check{p}_k\right) - F_{\hat{x}_k}\left(-\kappa A \,|\, x_k = 3A, \check{p}_k\right) \\ &+ F_{\hat{x}_k}\left(-\kappa A \,|\, x_k = A, \check{p}_k\right) - F_{\hat{x}_k}\left(\kappa A \,|\, x_k = A, \check{p}_k\right)\big], \end{aligned} \tag{2.35}$$

with $A = \sqrt{E_t/10}$ and $\kappa = 2\sqrt{N_r}$.

The unconditioned BER is given by

$$P_b = \sum_{\delta \in \mathcal{D}} P_{\check{p}_k}(\delta) P_b\left(\check{p}_k = \delta\right), \tag{2.36}$$

where $P_{\check{p}_k}(\delta)$ is the probability mass function (pmf) of $\check{p}_k$ and $\mathcal{D}$ is the set of all possible values of δ that $\check{p}_k$ can take. It is expressed by $(N_t - 1)$-fold convolution:

$$P_{\check{p}_k}(\delta) = \underbrace{P_{|s_\ell|^2}(\delta) * \cdots * P_{|s_\ell|^2}(\delta)}_{N_t - 1}, \tag{2.37}$$

where $P_{|s_\ell|^2}(\delta)$ is the pmf of the square magnitude of M-QAM symbols. For example, in the case of 16-QAM, by letting δ_1, δ_2, and δ_3 denote the three possible values of the square magnitude of 16-QAM $|s_\ell|^2$ as shown in Fig. 2.3, the resulting pmf is given by

$$P_{|s_\ell|^2}(\delta) = \begin{cases} \frac{1}{4}, & \delta = \delta_1, \\ \frac{1}{2}, & \delta = \delta_2, \\ \frac{1}{4}, & \delta = \delta_3. \end{cases}$$

In the case of $N_t = 4$, the corresponding distribution is listed in Table 2.1.

By substituting (2.37) into (2.36), we can derive the exact BER expressions for M-QAM that do not require any numerical integration.

2.4.5 Asymptotic BER Expression for QAM

The exact analysis for QAM cases requires calculation of the pmf for $\check{p}_k$ based on (2.37), which generally requires high computational effort. On the other hand, if the number of transmit antennas N_t is large enough and the law of large numbers becomes effective, the square norm $\check{p}_k$ can be approximated by (2.20). By substituting (2.20) into (2.26), we can ignore the dependence

Table 2.1: The distribution of $P_{|s_\ell|^2}(\delta)$ in the case of $N_t = 4$.

δ/E_t	probability
$3/5$	$1/64$
$7/5$	$3/32$
$11/5$	$15/64$
3	$5/16$
$19/5$	$15/64$
$23/5$	$3/32$
$27/5$	$1/64$
otherwise	0

of the conditional cdf of MF output on $\check{\mathrm{s}}_k$ and obtain (2.38), shown at the top of the next page.

$$F_{\hat{x}_k}(X|x_k = x) = \begin{cases} \left(\frac{1}{2} - \frac{x}{2\sqrt{x^2+(N_t-1)E_t+N_0}}\right)^{N_r} e^{\frac{2\sqrt{N_r}X}{\sqrt{x^2+(N_t-1)E_t+N_0}-x}} \\ \quad \times \sum_{i=0}^{N_r-1} \binom{N_r-1+i}{i} \left(\frac{1}{2} + \frac{x}{2\sqrt{x^2+(N_t-1)E_t+N_0}}\right)^i \\ \quad \times \sum_{l=0}^{N_r-i-1} \frac{1}{l!} \left(\frac{-2\sqrt{N_r}X}{\sqrt{x^2+(N_t-1)E_t+N_0}-x}\right)^l, \qquad \text{for } X \le 0, \\ 1 - \left(\frac{1}{2} + \frac{x}{2\sqrt{x^2+(N_t-1)E_t+N_0}}\right)^{N_r} e^{\frac{-2\sqrt{N_r}X}{\sqrt{x^2+(N_t-1)E_t+N_0}+x}} \\ \quad \times \sum_{i=0}^{N_r-1} \binom{N_r-1+i}{i} \left(\frac{1}{2} - \frac{x}{2\sqrt{x^2+(N_t-1)E_t+N_0}}\right)^i \\ \quad \times \sum_{l=0}^{N_r-i-1} \frac{1}{l!} \left(\frac{2\sqrt{N_r}X}{\sqrt{x^2+(N_t-1)E_t+N_0}+x}\right)^l, \qquad \text{for } X > 0, \end{cases} \tag{2.38}$$

Using (2.38) instead of the expressions involving (2.36) and (2.37), the *asymptotic* BER performance of M-QAM for a large value of N_t can be calculated by (2.36) without conditioning on $\check{p}_k$. For example, in the case of 16-QAM with Gray mapping, (2.35) reduces to

$$\begin{aligned} P_b = &\frac{1}{4}\left[1 + F_{\hat{x}_k}(0 \,|\, x_k = 3A) + F_{\hat{x}_k}(0 \,|\, x_k = A)\right. \\ &+ F_{\hat{x}_k}(\kappa \,|\, x_k = 3A) - F_{\hat{x}_k}(-\kappa A \,|\, x_k = 3A) \\ &\left.+ F_{\hat{x}_k}(-\kappa A \,|\, x_k = A) - F_{\hat{x}_k}(\kappa A \,|\, x_k = A)\right], \end{aligned} \tag{2.39}$$

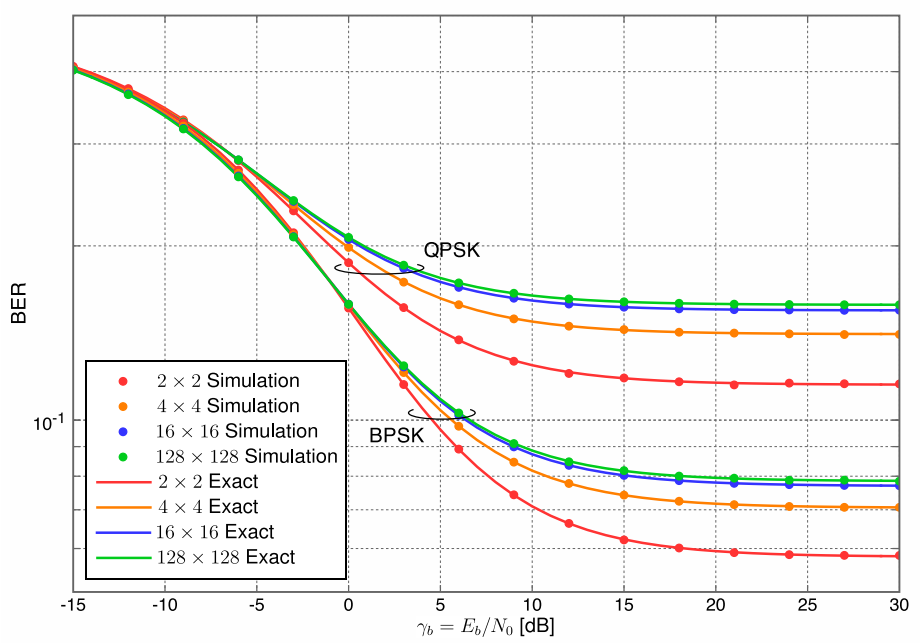

Figure 2.4: Comparison of theoretical expressions and simulation results for the uncoded BER in the case of $N_t \times N_r$ MIMO system (with $N_r = N_t$) and MF detector with BPSK and QPSK signaling.

with $A = \sqrt{E_t/10}$ and $\kappa = 2\sqrt{N_r}$. The above expression should become accurate as the number of transmit antennas N_t increases.

2.4.6 Numerical Results

To examine the correctness of the developed closed-form BER expressions, we compare the uncoded BER performances of BPSK and QPSK signaling based on (2.28) with (2.29) and (2.30) and those obtained by Monte-Carlo simulations. The results are given in Fig. 2.4 with the number of antennas at both sides set as $2, 4, 16$, and 128. From these results, it is apparent that our developed expressions agree well with all the simulation results.

We next compare the uncoded BER performances of 16-QAM signaling given by (2.36) using the exact expression based on (2.35) and (2.37) (only shown for the cases with $N_t = 2, 4$) as well as its asymptotic form (2.39) with (2.38) (shown for all the cases of N_t investigated), along with the results obtained by Monte-Carlo simulations. They are compared in Fig. 2.5, and the exact BER curves match perfectly with the simulation results even when the numbers of both antennas are either 2 or 4. On the other hand, the asymptotic BER based on (2.39) shows some discrepancy when the number of antennas is small. However, it tends to agree as the number of

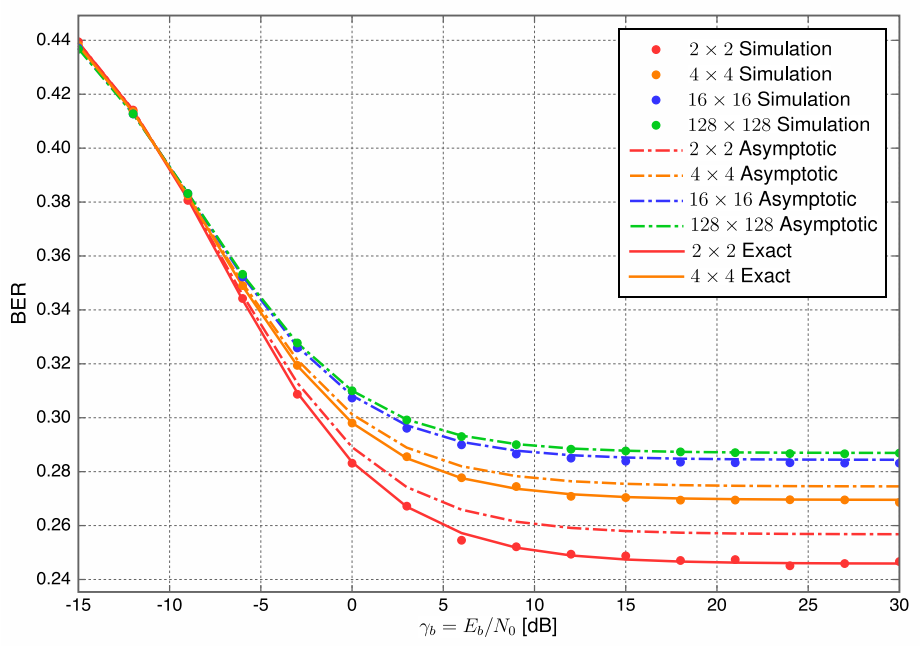

Figure 2.5: Comparison of theoretical expressions and simulation results for the uncoded BER in the case of $N_t \times N_r$ MIMO system (with $N_r = N_t$) and MF detector with Gray-mapped 16-QAM signaling. The exact BER curves are plotted only for the cases with $N_t = 2, 4$.

antennas increases as expected.

We investigate the BER limit of BPSK $\bar{P}_b$ in the case of $\gamma_b \to \infty$, i.e., (2.31), with respect to the number of receive antennas in Fig. 2.6. We observe that increasing N_t significantly degrades the achievable BER, but for given N_t, the error floor can be reduced by increasing N_r. These results demonstrate how the BER of MF detector can be mitigated by increasing N_r in high SNR regime, and they clearly indicate that N_r should be increased in order for the MF detector to become effective.

Finally, the theoretical BER expressions of MF and ZF detectors are compared in Fig. 2.7. We observe that MF detector outperforms ZF detector in the case of low SNR as discussed in Section 2.4.3, and the performance is not sensitive to the number of transmit antennas in this region. On the other hand, as the SNR increases, the BER of ZF improves without error floor due to the perfect cancellation of the symbols from other transmit antennas.

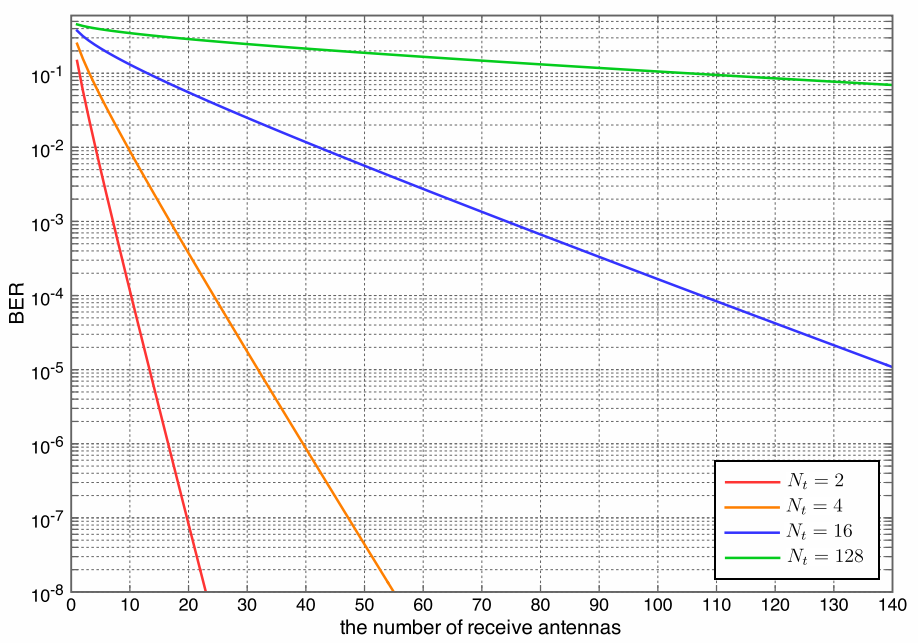

Figure 2.6: Asymptotic uncoded BER performance with $\gamma_b \to \infty$ of MIMO spatial multiplexing system with N_t transmit antennas and MF detection as a function of the number of receive antennas N_r (BPSK signaling).

2.5 Extension to Coded MIMO Systems

In practice, any MIMO system should be operated with channel coding for performance improvement with enhanced diversity effect. The use of channel coding especially plays a critical role for MF detector since it considerably suffers from the interference that leads to prohibitively high error floor, as we have observed in the previous section through our theoretical BER performance analysis.

In this section, we turn our attention to a more practical coded MIMO system with MF detector, and by exploiting the exact statistical model of the MF detector output developed in Section 2.3, we develop the *optimum* log-likelihood ratio (LLR) metric for low-complexity MF-detector based MIMO systems. In particular, we will observe that the optimal LLR expression agrees with the simple expression derived directly from the conditional Gaussian distribution.

We then investigate the performance limit of the coded MIMO system with MF detector in the framework of ideally interleaved Rayleigh fading channels by numerical calculation of the mutual information, followed by the corresponding simulation results based on a practical LDPC-coded MIMO system in terms of frame error rate (FER).

For the coded system in this chapter, we focus only on BPSK signaling for simplicity, but

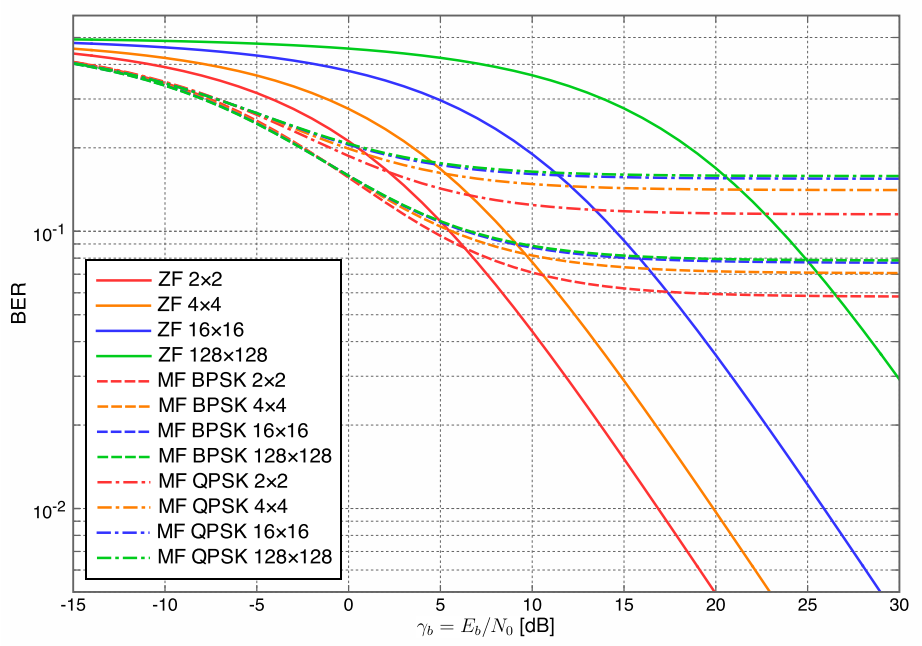

Figure 2.7: Comparison of the exact BER for MF and ZF detectors. In the case of ZF detector, the performance is the same for BPSK and QPSK, whereas degradation from BPSK is inevitable for MF detector when QPSK is applied.

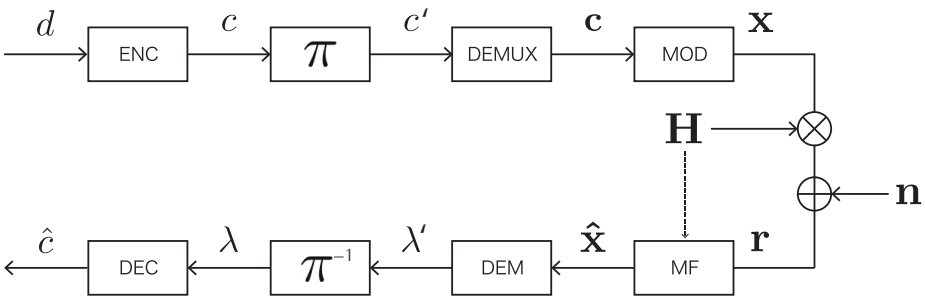

Figure 2.8: System model for coded MIMO systems.

its extension to QPSK and QAM is straightforward based on the conditional pdf expressions developed in Section 2.3.

2.5.1 System Model

The block diagram of the coded MIMO system considered in this section is shown in Fig. 2.8. At the transmitter, the binary information sequence d of length K_c is converted to the codeword c of N_c bits by the channel encoder of rate $R_c = K_c/N_c$. Each codeword is interleaved (denoted by π in Fig. 2.8) and then the resulting sequence c' is demultiplexed such that each N_t-tuple of

the output binary vector $\mathbf{c}$ is mapped onto a BPSK symbol vector $\mathbf{x} \in \mathcal{X}^{N_t \times 1}$, which will be transmitted over the $N_t \times N_r$ MIMO channel $\mathbf{H}$ described in Section 2.2.1.

At the receiver, the received symbol expressed by (2.1) is processed by MF detector as described in Section 2.2.3 to obtain the estimated BPSK symbol vector $\hat{\mathbf{x}}$. From each estimate BPSK symbol $\hat{x}_k$, the demodulator generates the LLR metric λ'_k, and a set of metrics is deinterleaved (denoted by π^{-1} in Fig. 2.8) to the original order of codeword and then the channel decoder performs decoding to generate the estimate codeword $\hat{c}$. In what follows, we focus on the FER, which is defined by

$$\text{FER} = \Pr\left(\hat{c} \neq c\right). \tag{2.40}$$

Due to the ideal channel interleaver, each BPSK symbol experiences statistically independent Rayleigh fading.

2.5.2 Optimum Metric Expression for MF Detector

The exact conditional pdf for the MF-based detector derived in (2.9) can be directly employed for the LLR derivation in the coded MIMO system. Specifically, for a given output $\hat{x}_k = \hat{x}$ from MF detector, the LLR corresponding to the kth coded bit, transmitted by the BPSK symbol x_k, is expressed in a closed form using (2.9) and (2.20) as

$$\begin{aligned}\lambda'_k &= \log \frac{p_{\hat{x}_k}\left(\hat{x}|x_k = \sqrt{E_t}\right)}{p_{\hat{x}_k}\left(\hat{x}|x_k = -\sqrt{E_t}\right)} = \log \frac{e^{-\frac{2\sqrt{N_r}\left(\sqrt{E_t+\check{p}_k+N_0}|\hat{x}|-\sqrt{E_t}\hat{x}\right)}{\check{p}_k+N_0}}}{e^{-\frac{2\sqrt{N_r}\left(\sqrt{E_t+\check{p}_k+N_0}|\hat{x}|+\sqrt{E_t}\hat{x}\right)}{\check{p}_k+N_0}}} \\ &= \frac{4\sqrt{N_r E_t}}{(N_t-1)E_t + N_0}\hat{x}. \end{aligned} \tag{2.41}$$

On the other hand, by directly employing the conditional Gaussian distribution of MF output from (2.16), the LLR may be also expressed as

$$\begin{aligned}\lambda'_k &= \log \frac{p_{\hat{x}_k}(\hat{x}|x_k = \sqrt{E_t}, \alpha_k)}{p_{\hat{x}_k}(\hat{x}|x_k = -\sqrt{E_t}, \alpha_k)} = \log \frac{e^{-\frac{1}{\alpha_k(\check{p}_k+N_0)}\left(\hat{x}-\sqrt{N_r}\alpha_k\sqrt{E_t}\right)^2}}{e^{-\frac{1}{\alpha_k(\check{p}_k+N_0)}\left(\hat{x}+\sqrt{N_r}\alpha_k\sqrt{E_t}\right)^2}} \\ &= \frac{4\sqrt{N_r E_t}}{(N_t-1)E_t + N_0}\hat{x}, \end{aligned} \tag{2.42}$$

which agrees with (2.41) and thus does not depend on α_k. Therefore, it is important to mention that the optimal metric derived from the exact pdf and that based on the conditional Gaussian dis-

tribution turn out to be identical, which justifies the use of the conventional Gaussian distribution in the case of coded system with MF detector.

2.5.3 Mutual Information

Based on the exact conditional pdf expressions developed in Section 2.3, we are able to calculate the mutual information of the MF-detector-based MIMO system with an arbitrary number of antennas.

The mutual information *per transmit antenna*, i.e., given in bit/sec/Hz/transmit antenna, is expressed as [55]

$$I = \log_2 |\mathcal{X}| - E\left\{ \log_2 \frac{\sum_{x' \in \mathcal{X}} p_{\hat{x}_k}(\hat{x}|x_k = x')}{p_{\hat{x}_k}(\hat{x}|x_k = x)} \right\}, \tag{2.43}$$

where $|\mathcal{X}|$ denotes the cardinality of the set $\mathcal{X}$ and the expectation should be taken over x and $\hat{x}$ (i.e., x_k and $\hat{x}_k$).

Figure 2.9 shows the *per-antenna* mutual information (2.43) over the ergodic Rayleigh fading channel for various antenna cases with $N_r = N_t$ and BPSK signaling as a function of SNR *per receive antenna*. Note that the expectation in (2.43) is performed by Monte-Carlo integration using the developed exact pdf. We observe that as the number of antennas increases, the mutual information *per antenna* decreases, and as $N_r \to \infty$, it converges to a constant value that is achieved by Gaussian distribution with $N_r \to \infty$. From Fig. 2.9, it is observed that the required SNR *per receive antenna* to achieve the *per-antenna* mutual information of 0.5 bits increases as the number of antennas increases under the condition of $N_t = N_r$, but it rapidly converges to the lower bound achieved by an infinite number of antennas. In other words, as long as the target information rate is properly chosen, the amount of the required SNR *per receive antenna* eventually reaches the upper limit. Thus, increasing the transmit and receive antennas simultaneously will simply increase the spectral efficiency without increasing the required SNR at each receive antenna.

2.5.4 Simulation Results over Ideally Interleaved Fading Channel

In order to verify the theoretical performance limit suggested by the mutual information through simulation with practical coding, we evaluate the frame error rate (FER) of LDPC-coded system assuming an ideal interleaver such that each coded symbol experiences statistically independent Rayleigh fading. The regular binary $(3, 6)$ LDPC code (with code rate $R_c = 1/2$) is

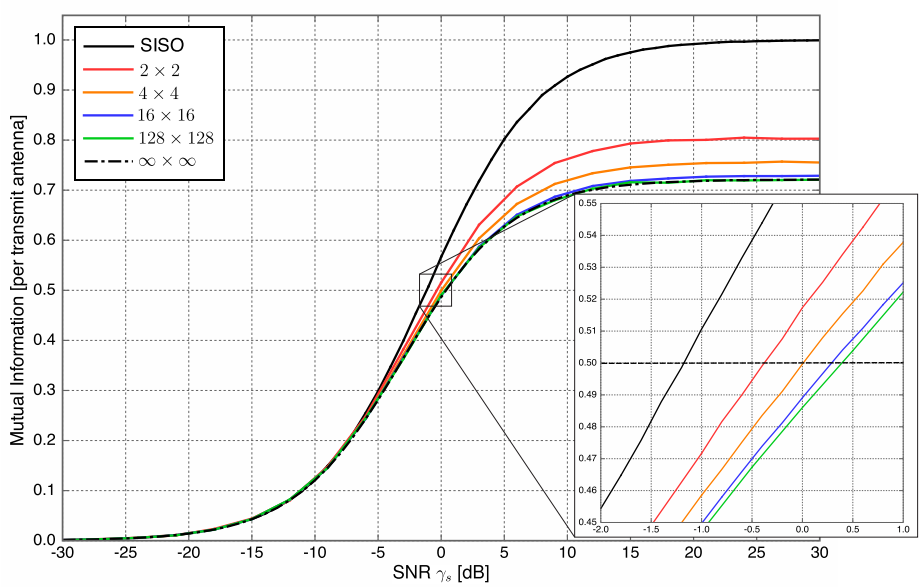

Figure 2.9: Mutual information *per transmit antenna* with BPSK signaling as a function of SNR *per receive antenna* in $N_t \times N_r$ MIMO system with MF detector and $N_t = N_r$. The region where the mutual information of each curve reaches 0.5 is enlarged for later reference.

chosen as our channel code with the codeword length $N_c = 4128$. For LDPC decoder, the sum-product algorithm is employed with the maximum number of iterations given by 100. The results are shown in Fig. 2.10. Note that the minimum required SNR to achieve an arbitrarily small FER provided that optimal channel coding is employed corresponds to the value where the resulting mutual information reaches $1/2$ in Fig. 2.9, and the corresponding values are also indicated in Fig. 2.10. From the results of FER using an actual LDPC code in Fig. 2.10, we observe a similar tendency that can be inferred from the behavior of mutual information: The required SNR per antenna to achieve the comparable FER performance should increase as the number of transmit antennas increases, but their SNR gap becomes smaller as is inferred from Fig. 2.9.

2.6 Effect of Imperfect Channel Estimation

In the preceding sections, we have analyzed the fundamental performance of the MF detector under the ideal assumption that the perfect CSI is available at the receiver. Such an assumption, however, may not be necessarily the case in practical MIMO systems. Therefore, in this section, we extend our analysis to the cases where the channel estimation error exists.

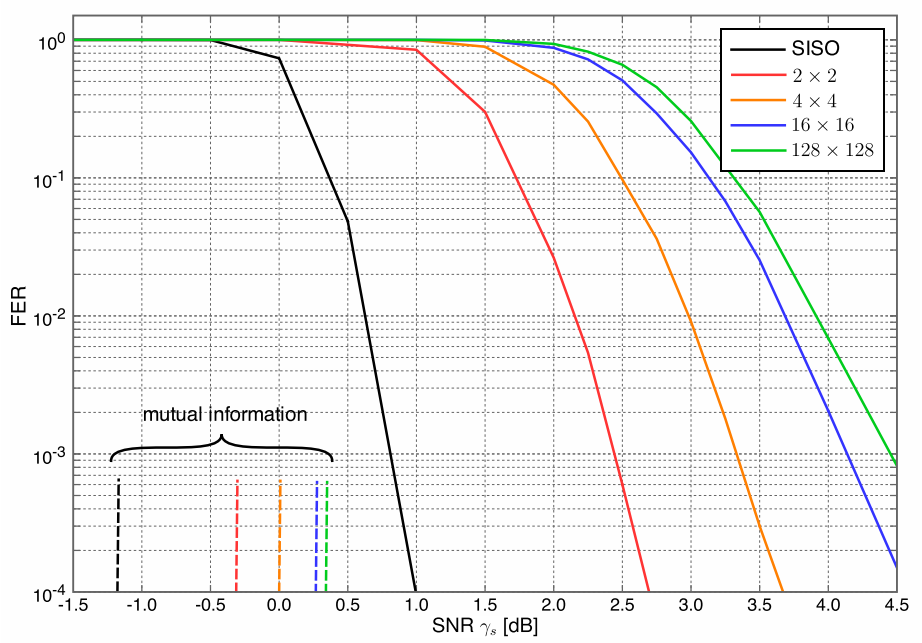

Figure 2.10: The coded FER performance in $N_t \times N_r$ MIMO system with MF detector (where $N_r = N_t$) over ideally interleaved Rayleigh fading channel. The vertical lines indicate the corresponding minimum SNR values suggested by the analysis of mutual information.

2.6.1 System Model with Channel Estimation Error

Assuming the use of maximum likelihood (ML) channel estimation at the receiver, the estimate channel can be expressed as [54, 56]

$$\hat{\mathbf{H}} = \mathbf{H} + \Delta\mathbf{H}, \tag{2.44}$$

where $\Delta\mathbf{H} = (\Delta\mathbf{h}_1\ \Delta\mathbf{h}_2\ \cdots\ \Delta\mathbf{h}_{N_t}) \in \mathbb{C}^{N_r \times N_t}$ is a complex channel estimation error matrix. Each column vector $\Delta\mathbf{h}_k = (\Delta h_{1,k}, \Delta h_{2,k}, \cdots, \Delta h_{N_r,k})^T$ represents the channel estimation error corresponding to the kth transmit antenna, and each entry $\Delta h_{i,k}$ is modeled as an i.i.d. random variable $\mathcal{CN}(0, \sigma_e^2)$, where $\sigma_e^2 = E\left\{|\Delta h_{i,k}|^2\right\}$. With the ML channel estimation, σ_e^2 can be given by [54, 56]

$$\sigma_e^2 = \frac{N_t N_0}{N_{\text{train}} E_{\text{train}}}, \tag{2.45}$$

where N_{train} is the length of the training sequence and E_{train} is the energy of the training symbols.

2.6.2 Exact MF Output

In the case of MF detector with channel estimation error, the weight matrix of (2.6) is replaced by

$$\mathbf{W}^{\mathrm{H}} = \hat{\mathbf{H}}^{\mathrm{H}}. \tag{2.46}$$

Consequently, the MF output with channel estimation error is expressed as

$$\hat{s}_k = \frac{1}{\sqrt{N_r}} \sum_{i=1}^{N_r} \left(h_{i,k}^* + \Delta h_{i,k}^*\right) \left(h_{i,k} s_k + \sum_{\ell=1,\ell\neq k}^{N_t} h_{i,\ell} s_\ell + n_i\right). \tag{2.47}$$

The real value of the MF output $\hat{x}_k = \Re\{\hat{s}_k\}$ is then given by

$$\begin{aligned}\hat{x}_k = &\sum_{i=1}^{N_r} \Re\left\{\frac{1}{\sqrt{N_r}}\left(h_{i,k}^* + \Delta h_{i,k}^*\right)\right\} \Re\left\{\left(h_{i,k} s_k + \sum_{\ell=1,\ell\neq k}^{N_t} h_{i,\ell} s_\ell + n_i\right)\right\} \\ &- \sum_{i=1}^{N_r} \Im\left\{\frac{1}{\sqrt{N_r}}\left(h_{i,k}^* + \Delta h_{i,k}^*\right)\right\} \Im\left\{\left(h_{i,k} s_k + \sum_{\ell=1,\ell\neq k}^{N_t} h_{i,\ell} s_\ell + n_i\right)\right\}. \end{aligned} \tag{2.48}$$

Noticing that real and imaginary parts of both $h_{i,k}$ and $\Delta h_{i,k}$ reserve symmetric statistical property, the MF output can be expressed by the following quadratic form:

$$\hat{x}_k = \sum_{i=1}^{2N_r} u_{i,k} v_{i,k}, \tag{2.49}$$

where $u_{i,k}$ and $v_{i,k}$ are *correlated* zero-mean real-valued Gaussian random variables with their variances given by

$$\sigma_{u_{i,k}}^2 = \frac{1+\sigma_e^2}{2N_r}, \tag{2.50}$$

$$\sigma_{v_{i,k}}^2 = \frac{x_k^2}{2} + \frac{1}{2}\sum_{\ell=1,\ell\neq k}^{N_t} |s_\ell|^2 + \frac{N_0}{2} = \frac{x_k^2 + \check{p}_k + N_0}{2}. \tag{2.51}$$

The correlation coefficient between $u_{i,k}$ and $v_{i,k}$ is given by

$$\rho_{i,k} = \frac{E\left\{\frac{\Re\{h_{i,k}\}^2}{\sqrt{N_r}}\right\} x_k}{\sigma_{u_{i,k}}\sigma_{v_{i,k}}} = \frac{x_k}{\sqrt{(1+\sigma_e^2)\left(x_k^2+\check{p}_k+N_0\right)}}. \tag{2.52}$$

Since $\hat{x}_k$ is the product of correlated real-valued Gaussian random variables, its pdf conditioned on the input x_k and the other transmitted symbols $\check{p}_k$ is expressed as

$$\begin{aligned} & p_{\hat{x}_k}\left(\hat{x}|x_k=x,\check{p}_k\right) \\ &= \frac{\sqrt{N_r}}{(N_r-1)!\sqrt{(1+\sigma_e^2)\left(x^2+\check{p}_k+N_0\right)}}\left[\frac{(1+\sigma_e^2)\left(\check{p}_k+N_0\right)+\sigma_e^2x^2}{2\left(1+\sigma_e^2\right)\left(x^2+\check{p}_k+N_0\right)}\right]^{N_r-1} \\ &\quad\times e^{-\frac{2\sqrt{N_r}\left(\sqrt{(1+\sigma_e^2)(x^2+\check{p}_k+N_0)}|\hat{x}|-x\hat{x}\right)}{(1+\sigma_e^2)(\check{p}_k+N_0)+\sigma_e^2x^2}} \\ &\quad\times\sum_{i=0}^{N_r-1}\frac{(N_r-1+i)!}{2^i\,i!\,(N_r-1-i)!}\left[\frac{2\sqrt{N_r\left(1+\sigma_e^2\right)\left(x^2+\check{p}_k+N_0\right)}\,|\hat{x}|}{(1+\sigma_e^2)\left(\check{p}_k+N_0\right)+\sigma_e^2x^2}\right]^{N_r-1-i} \end{aligned} \tag{2.53}$$

Note that by substituting $\sigma_e^2=0$, (2.53) agrees with (2.9) as expected.

2.6.3 Exact BER Expression

Since (2.53) is the exact general pdf expression of the MF output with channel estimation error, as in Section 2.4 the exact BER performance of MF detector with channel estimation error σ_e^2 can be derived as (2.28) where the SNR parameter μ for BPSK is replaced by

$$\mu_{\text{MF,BPSK}}(\sigma_e^2) = \frac{1}{\sqrt{(1+\sigma_e^2)\left(N_t+\frac{N_t}{\gamma_b}\right)}} = \frac{1}{\sqrt{(1+\sigma_e^2)}}\mu_{\text{MF,BPSK}}, \tag{2.54}$$

and for QPSK by

$$\mu_{\text{MF,QPSK}}(\sigma_e^2) = \frac{1}{\sqrt{(1+\sigma_e^2)\left((2N_t-1)+\frac{N_t}{\gamma_b}\right)}}\frac{1}{\sqrt{(1+\sigma_e^2)}}\mu_{\text{MF,QPSK}}, \tag{2.55}$$

with $\mu_{\text{MF,BPSK}}$ and $\mu_{\text{MF,QPSK}}$ given by (2.29) and (2.30), respectively. Therefore, we observe that the channel estimation error decreases the SNR parameter μ by a factor of $\sqrt{1+\sigma_e^2}$ and thus degrades the resulting achievable BER performance.

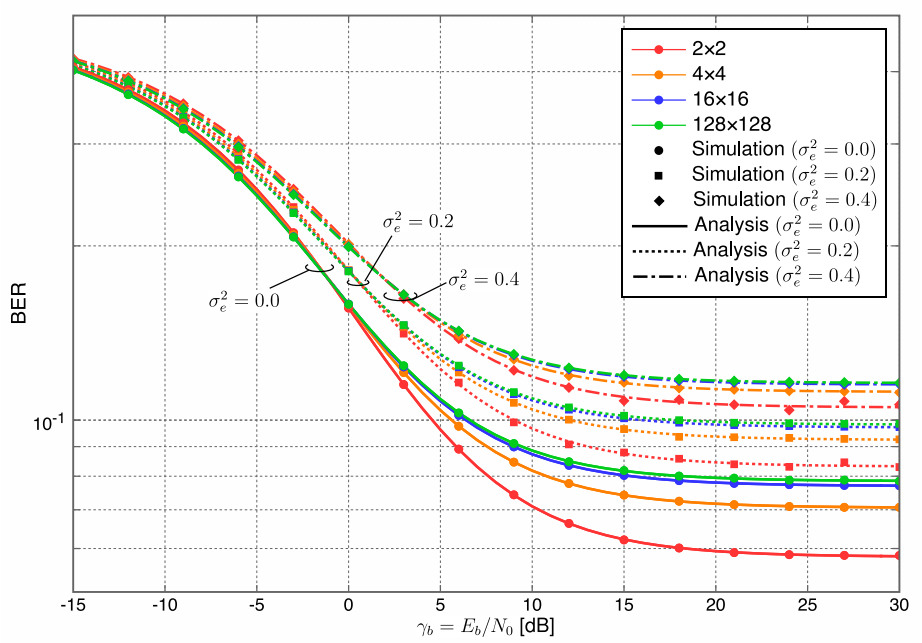

Figure 2.11: Comparison of theoretical expressions and simulation results for the uncoded BER in the case of $N_t \times N_r$ MIMO system and MF detector with BPSK signaling (with $N_r = N_t$) and several channel estimation error cases.

2.6.4 Numerical Results

In Fig. 2.11, we compare the exact theoretical BER performance and Monte-Carlo simulation with several estimation error cases. Perfect agreement between the two results is observed. We also observe that by increasing σ_e^2, the BER increases as expected. The analytical results may thus help us design the train sequences in order to maintain the desired BER. In the case of the coded MIMO system considered in Section 2.5, by employing (2.53) upon calculation of expectation in (2.43), we can also evaluate the mutual information of MF detector with arbitrary channel estimation error. The results with $\sigma_e^2 = 0.2, 0.4$, together with perfect CSI case are compared in Fig. 2.12. We observe that the achievable mutual information will be decreased as the channel estimation error increases.

2.7 Conclusion

In this chapter, we have theoretically analyzed the performance of MIMO spatial multiplexing systems with MF detector over uncorrelated Rayleigh fading channel. The main finding of this chapter is the exact closed-form distribution of the output of MF detector with an arbitrary

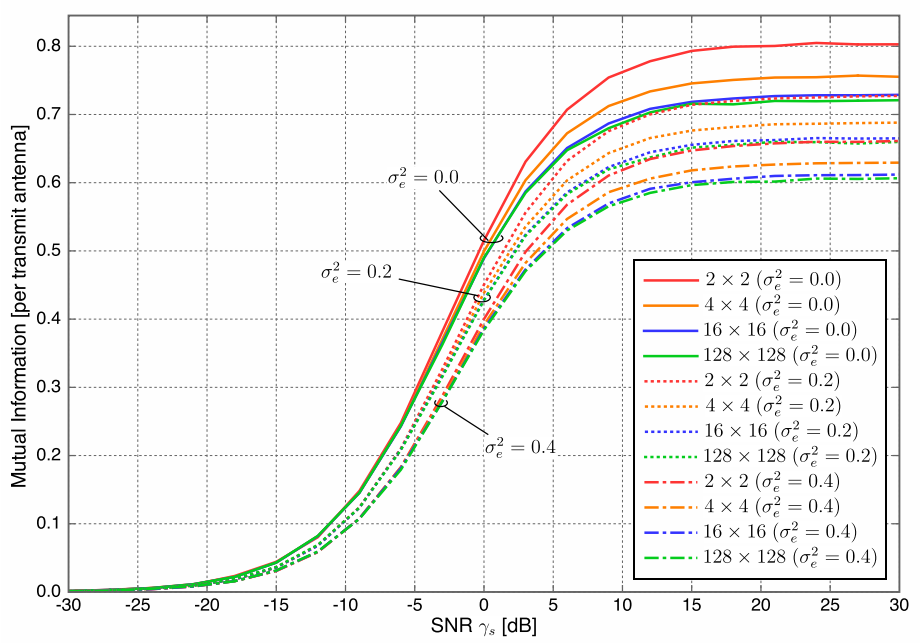

Figure 2.12: Mutual information *per transmit antenna* with BPSK signaling in $N_t \times N_r$ MIMO system (with $N_r = N_t$) based on MF detector with channel estimation errors $\sigma_e^2 = 0.2, 0.4$.

number of antennas. This has facilitated the derivation of the uncoded BER expressions in a closed form. In particular, comparison of MF and ZF in terms of the exact BER expressions for BPSK and QPSK cases has elucidated their behavioral difference in high and low SNR regions. Furthermore, for coded MIMO systems, it allows us to develop the exact closed-form LLR metric that is matched to the distribution of MF detector output. The results are justified by the analysis based on mutual information as well as simulations using practical channel codes. The effect of imperfect channel estimation on the performance of uncoded and coded MIMO systems has been also analyzed by deriving the exact BER expressions as well as mutual information. Throughout the theoretical analysis, we have derived the conditions of MIMO spatial multiplexing systems where the MF detector may work properly. These results may thus serve as a design guideline for developing MIMO systems operating with MF-based detector.

As future work, we shall investigate the MIMO system with channel correlation. Extension of our analysis to the system with interference cancellation should be also meaningful with notable practical importance.

Chapter 3

Matched-Filter Detector with Quadrature Interference Cancellation for Uplink MIMO Spatial Multiplexing

In this chapter, we propose a new interference cancellation technique designed for coded uplink multiuser MIMO systems, namely matched-filter detector with quadrature interference cancellation (MF-QIC).

Published as:

Y. Hama and H. Ochiai, "Matched-Filter Detector with Quadrature Interference Cancellation for Coded Uplink Multiuser MIMO Systems with Massive IoT Devices," *IEEE Trans. on Wireless Commun.,* early access.

3.1 Introduction

With the growth of emerging Internet-of-Things (IoT) applications, new physical-layer techniques should be developed that enable the connectivity of a massive number of devices with limited spectral resources. Supporting massive machine type communications (mMTC) was one of the major targets defined in the fifth generation mobile communications (5G). In future networks including the sixth generation (6G), it is redefined as *ultra-mMTC (umMTC)* or *massive ultra-reliable low-latency communications (mURLLC)*, which unifies the two challenging goals of URLLC and mMTC defined by 5G [4, 5].

In order to support reliable connections of massive IoT devices with limited bandwidth, the use of multiple-input multiple-output (MIMO) techniques should be essential [7, 22]. Furthermore, massive MIMO techniques have received significant recent attention, where a considerably large number of antennas are mounted at BS [16, 17]. Various approaches have been proposed for massive MIMO systems to enhance the system performance, and compared to beamforming, spatial multiplexing has a significant potential [20, 21] as it can enhance the channel capacity linearly with the number of antennas, provided that MIMO channels are subject to uncorrelated

fading. In multiuser massive MIMO systems, however, signal processing associated with signal separation of massive users should become a major challenge due to practical requirements on latency as well as power consumption. Therefore, careful selection of MIMO detectors [37, 57] becomes critical, especially as the number of devices (or transmitting antennas) becomes substantial. Furthermore, in order to perform precise channel estimation, orthogonal pilot sequences should be assigned to all the connecting users for each coherent time duration, which becomes infeasible as the number of users increases under the constraint on the total available bandwidth. As a consequence, the effect of channel state information (CSI) error should be carefully investigated for massive access networks, and developing a low complexity detector that has *strong robustness against imperfect CSI* should be of significant practical importance.

This chapter focuses on a physical-layer design for the uplink of a cellular network where a massive number of low-rate IoT devices in a single cell attempt to connect to a single base station (BS) equipped with the receiving antennas as much as that of the total IoT devices simultaneously connecting. A matched-filter (MF) detector [34, 35, 37] is known to be an effective low-complexity approach for massive MIMO systems since its *per user* complexity grows only linearly with the number of antennas. Several other reduced-complexity approaches have been proposed in the literature [57], and Neumann series (NS) as well as Gauss-Seidel (GS) methods are well-known approaches that approximate the channel inversion of linear detectors [58, 59]. Belief propagation (BP)-based detectors are also known to achieve near-optimal performance [60]. Nevertheless, these preceding studies have not considered the effect of channel estimation errors associated with massive access. On the other hand, the performance loss of MF detector associated with imperfect channel estimation has shown to be readily tractable [61].

Our target in this chapter is IoT networks where the transmitting devices are subject to significant power constraints. The transmit power is generally affected by the peak-to-average power ratio (PAPR) of the transmit signal, and thus each IoT device should transmit a signal with lower PAPR for higher power amplifier efficiency [62]. Thus, we focus on the network where each IoT device attempts to communicate with moderate information rate using QPSK signaling.

The major limitation of MF detector in the massive MIMO framework is its low *per antenna* spectral efficiency, which may not be an issue for an IoT network as long as the required *per user* spectral efficiency is significantly low (typically less than 1/2 bit *per user* per channel use), justifying the use of BPSK modulation with powerful channel coding. One of our primary goal in this chapter is to develop a MF-based system that can *even enhance* the resulting spectral efficiency by employing QPSK instead of BPSK. Since MF detector in general does not attempt to eliminate interfering signals transmitted from the other antennas, as the target spectral efficiency

increases using higher-order modulation, the resulting performance becomes significantly inferior to those based on the commonly adopted linear detectors such as zero-forcing (ZF) and minimum mean square error (MMSE) due to massive amount of residual interference. This performance degradation can be compensated for by the use of interference cancellation (IC).

In this chapter, we overcome the problem of low spectral efficiency of MF detector by introducing *quadrature interference cancellation*, which we refer to as *MF-QIC*, in coded uplink massive multiuser MIMO systems. As a channel coding example, we employ polar codes due to their flexibility in code rate design [15]. By employing QPSK instead of BPSK with judicious polar code design based on mutual information tailored for MF-QIC, we demonstrate that spectral efficiency of one bit per antenna per complex channel use can be achieved even under the challenging condition where the total numbers of IoT devices and receiving BS antennas are identical. Our proposed MF-QIC is a combination of multi-stage decoding (MSD) [63] and parallel interference cancellation with soft estimation.

The main contributions of this chapter are summarized as follows:

- We introduce a new IC approach based on parallel interference cancellation (PIC) with soft estimation and multi-stage decoding, referred to as *quadrature interference cancellation (QIC)*, which significantly enhances the error performance and spectral efficiency of MF detector.

- We develop a design guideline of polar codes associated with MF-QIC, based on the analysis of mutual information achieved by MF-QIC and Gaussian approximation (GA) construction.

- We demonstrate that the proposed MF-QIC system can enjoy both low complexity and improved error performance compared to the conventional approaches designed under the same spectral efficiency.

- The effect of channel estimation errors on the resulting error rate performance is analyzed, which demonstrates the robustness of the proposed MF-QIC approach against the CSI errors, a desirable property for the uplink of massive IoT networks.

This chapter is organized as follows. In the next section, we describe a basic system model considered throughout this chapter. Section 3.3 reviews the statistical properties of MF detector as well as its mutual information. Our proposed MF detector combined with quadrature interference cancellation is described in Section 3.4, where the PIC with soft estimation is also

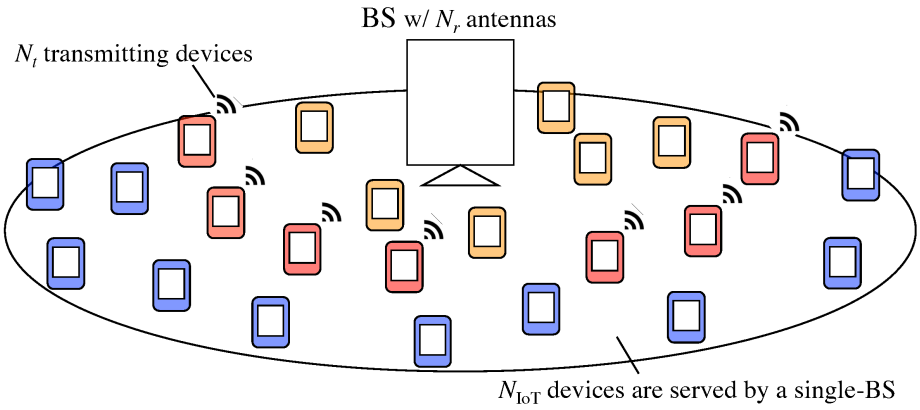

Figure 3.1: An uplink multiuser MIMO system supporting massive IoT devices with scheduling based on grouping according to their path loss.

introduced. Section 3.5 addresses the application of polar codes to the proposed MF-QIC system and describes their code rate design along with performance analysis. The extension of our proposed system to the case with imperfect channel estimation is discussed in Section 3.6. The performance comparisons based on the extensive simulations are provided in Section 3.7. Finally, Section 4.6 concludes this chapter.

3.2 Coded Uplink Multiuser MIMO System Model

In this chapter, we consider the uplink multiuser MIMO system as an extended framework of MIMO spatial multiplexing considered in Chapter 2. The detailed descriptions are summarized in this section.

3.2.1 Massive IoT Network with Scheduling

We consider the cellular network setting where a massive number of IoT devices attempt to connect a single BS equipped with N_r receiving antennas as shown in Fig. 3.1. Each user equipment (UE) is a low-cost low-power device with minimal transmission capabilities, and thus has a single antenna (i.e., single MIMO layer). Since the priority in terms of system requirements is given to higher power amplifier (PA) efficiency rather than achievable data rate, it will only transmit low PAPR symbols such as BPSK and QPSK. Let N_{IoT} denote the number of IoT devices that will be served by a single BS. Since $N_{\mathrm{IoT}} \gg N_r$ in general, we assume that an appropriate scheduling is performed such that for each time duration, the devices that experience a similar

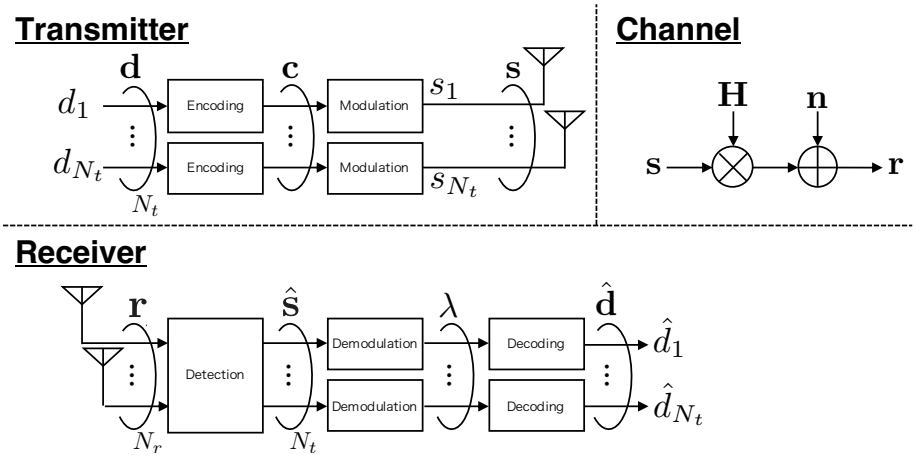

Figure 3.2: A block diagram of coded uplink multiuser MIMO system.

amount of path loss are selected as the same group. We further assume that the maximum number of devices in each group is less than or equal to N_r. Letting the number of transmitting devices in each group by N_t, we define the ratio of the total number of transmitting devices and receiving antennas as $\rho \triangleq N_r/N_t$. For simplicity in terms of mathematical modeling, we will assume that the scheduling is performed ideally such that each device in the same group experiences the same path loss, whereas the fading coefficient between each transmitting device and each receiving antenna at BS follows independent and identically distributed (i.i.d.) complex Gaussian distribution (i.e., Rayleigh fading). Furthermore, the fading coefficients remain constant during the transmission of each codeword (i.e., block fading). As such, each transmitting device in the same group employs the same coding parameters and modulation order, i.e., the same modulation and coding scheme (MCS). Under the additional assumption that all the users are synchronized in a symbol level, the entire network can be modeled as $N_r \times N_t$ MIMO system as described in Fig. 3.2.

3.2.2 System Description

Based on the assumptions in the previous subsection, we will formulate our system model. Let $\mathbf{d}_k = (d_{k,1}, d_{k,2}, \cdots, d_{k,K_c}) \in \{0,1\}^{K_c}$ denote the binary information sequence of length K_c sent by the kth device, where $k \in \{1, 2, \cdots, N_t\}$. This sequence is then encoded by a binary code $\mathcal{C}$ with rate $R_c = K_c/N_c$, where N_c denotes the codeword length. The resulting coded bit sequence is given by $\mathbf{c}_k = (c_{k,1}, c_{k,2}, \cdots, c_{k,N_c}) \in \{0,1\}^{N_c}$. Let M denote the modulation order and $m = \log_2 M$ denote the number of bits per transmitted symbol by each device. A set of m elements of $\mathbf{c}_k$ forms the lth transmitted symbol $s_k^{(l)} \in \mathcal{X} \subset \mathbb{C}$,

where $l \in \{1, 2, \cdots, N_s\}$ with $N_s = N_c/m$, and $\mathcal{X}$ represents a set of M-PSK constellation points. As a result, the modulated symbol sequence transmitted by the kth device is given by $\mathbf{s}_k = \left(s_k^{(1)}, s_k^{(2)}, \cdots, s_k^{(N_s)}\right)^T \in \mathcal{X}^{N_s}$. Let $\mathbf{S} = (\mathbf{s}_1 \ \cdots \ \mathbf{s}_k \ \cdots \ \mathbf{s}_{N_t})^T \in \mathbb{C}^{N_t \times N_s}$ denote the matrix composed of all the transmitted symbols from N_t devices. The corresponding received symbol matrix $\mathbf{R} = (\mathbf{r}_1 \ \cdots \ \mathbf{r}_k \ \cdots \ \mathbf{r}_{N_r})^T = \left(\mathbf{r}^{(1)} \ \cdots \ \mathbf{r}^{(l)} \ \cdots \ \mathbf{r}^{(N_s)}\right) \in \mathbb{C}^{N_r \times N_s}$ is given by

$$\mathbf{R} = \mathbf{HS} + \mathbf{N}, \tag{3.1}$$

where $\mathbf{N} = \left(\mathbf{n}^{(1)} \cdots \mathbf{n}^{(N_s)}\right) \in \mathbb{C}^{N_r \times N_s}$ denotes an additive white Gaussian noise (AWGN) matrix, and $\mathbf{H} = (\mathbf{h}_1 \ \mathbf{h}_2 \ \cdots \ \mathbf{h}_{N_t}) \in \mathbb{C}^{N_r \times N_t}$ is a complex channel matrix with each column vector $\mathbf{h}_k = (h_{1,k}, h_{2,k}, \cdots, h_{N_r,k})^T$ representing the channel corresponding to the kth device. The entries of $\mathbf{N}$ follow i.i.d. circularly symmetric complex Gaussian distribution with zero mean and variance $\sigma_n^2 = N_0$ *per complex dimension*, i.e., $n_i^{(l)} \sim \mathcal{CN}(0, N_0)$, where $i \in \{1, 2, \cdots, N_r\}$. Also, by assumption the entries of $\mathbf{H}$ are i.i.d. with $h_{i,k} \sim \mathcal{CN}(0, 1)$ and static over each codeword transmission. We initially assume that perfect channel state information (CSI) is available at the receiver side. The effect of imperfect CSI at the receiver will be analyzed in Section 3.6.

Let E_s denote the average received symbol energy at the BS and let E_t denote the average transmit symbol energy *per user*. Due to the ideal scheduling, without loss of generality the energy reduction caused by path loss and shadowing is normalized such that $E_s = N_t E_t$ and we define the average SNR *per receive antenna* as $\gamma_s = E_s/N_0$.

The block error rate (BLER) is often adopted for evaluating the performance of coded systems, and throughout this chapter, we define a *block* as the information sequence $\mathbf{d}_k$ of each user. In other words, the block error corresponds to the event with $\mathbf{d}_k \neq \hat{\mathbf{d}}_k$, where $\hat{\mathbf{d}}_k$ is the estimated information sequence of the kth user at the receiver, and BLER is evaluated by averaging the block errors over all N_t users.

3.2.3 Symbol Detection

Our primary interest in this chapter lies in low complexity receiver design and thus we mainly focus on the linear detection at BS. The estimated symbol matrix $\hat{\mathbf{S}}$ is then expressed as

$$\hat{\mathbf{S}} = \mathbf{W}^{\mathrm{H}}\mathbf{R}, \tag{3.2}$$

where $\mathbf{W} = (\mathbf{w}_1 \ \mathbf{w}_2 \ \cdots \ \mathbf{w}_{N_t}) \in \mathbb{C}^{N_r \times N_t}$ is the weight matrix and $\mathbf{w}_k \in \mathbb{C}^{N_r \times 1}$ is the weight vector applied to the received signal of the kth device, with $\mathbf{X}^{\mathrm{H}}$ representing the Hermitian trans-

pose of a matrix $\mathbf{X}$. The weight matrix of MMSE detector is given by

$$\mathbf{W}^{\mathrm{H}} = \left(\mathbf{H}^{\mathrm{H}}\mathbf{H} + \frac{1}{\gamma_s}\mathbf{I}_{N_t} \right)^{-1} \mathbf{H}^{\mathrm{H}}, \tag{3.3}$$

where $\mathbf{I}_N$ is the identity matrix of size N. Due to the inversion of the channel matrix of size $N_t \times N_t$, the resulting complexity order is $\mathcal{O}\left({N_t}^3\right)$, which becomes challenging for massive connectivity scenarios. On the other hand, the weight matrix of MF detector is simply

$$\mathbf{W}^{\mathrm{H}} = \mathbf{H}^{\mathrm{H}}, \tag{3.4}$$

and thus its complexity order is only $\mathcal{O}\left(N_t N_r\right)$ associated with the operation given by (3.2).

The channel decoder for $\mathcal{C}$ at BS requires a soft output from MIMO detector in the form of log-likelihood ratio (LLR), and the LLR corresponding to the tth coded bit in the lth symbol of the kth device is expressed for $t \in \{1, 2, \cdots, m\}$ as

$$\lambda_{k,t}^{(l)} = \log \frac{\sum_{s^0 \in \mathcal{S}_0^t} p_{\hat{s}}\left(\hat{s}_k^{(l)} | s^0\right)}{\sum_{s^1 \in \mathcal{S}_1^t} p_{\hat{s}}\left(\hat{s}_k^{(l)} | s^1\right)}, \tag{3.5}$$

where $p_{\hat{s}}(\cdot|\cdot)$ represents the conditional probability density function (pdf) of the detector output $\hat{s}$, and $\mathcal{S}_0^t$ and $\mathcal{S}_1^t$ are the constellation sets of PSK symbols with the tth bit labeled by 0 and 1, respectively.

3.3 MF Detector

In this section, we briefly review the statistical properties of MF detector with a given number of receiving antennas and associated LLR metric expression, which form the basis of our proposed MF-QIC design described in the next section. Throughout this section, we omit the symbol index l from the associated variables such as $s_k^{(l)}$ for simplicity.

3.3.1 Probability Distribution of MF Output

From (3.2) and (3.4), the complex-valued MF detector output for the kth user denoted by $\hat{s}_k = \hat{s}_k^{\mathrm{I}} + j\hat{s}_k^{\mathrm{Q}}$ is expressed as

$$\hat{s}_k = N_r \alpha_k s_k + \tilde{n}_k, \tag{3.6}$$

where α_k represents a channel coefficient and $\tilde{n}_k$ corresponds to the sum of the interference and noise, which are defined as

$$\alpha_k \triangleq \frac{1}{N_r}\sum_{i=1}^{N_r}|h_{i,k}|^2, \tag{3.7}$$

$$\tilde{n}_k \triangleq \sum_{i=1}^{N_r}\sum_{j=1,j\neq k}^{N_t} h_{i,k}^* h_{i,j} s_j + \sum_{i=1}^{N_r} h_{i,k}^* n_i, \tag{3.8}$$

respectively.

Let $\check{\mathbf{s}}_k$ denote a transmit symbol vector $\mathbf{s}$ with the kth symbol (transmitted from the kth antenna) excluded, i.e., $\check{\mathbf{s}}_k \triangleq (s_1, s_2, \cdots, s_{k-1}, s_{k+1}, \cdots, s_{N_t})^T$. Then, as shown in [61], conditioned on α_k and $\{s_k\}$, the MF detector output follows complex Gaussian distribution, i.e., $\hat{s}_k \sim \mathcal{CN}\left(\mu_{\text{MF}}\left(\alpha_k\right), \sigma^2_{\text{MF}}\left(\alpha_k\right)\right)$ with its mean and variance given by

$$\mu_{\text{MF}}\left(\alpha_k\right) = N_r \alpha_k s_k, \tag{3.9}$$

$$\sigma^2_{\text{MF}}\left(\alpha_k\right) = N_r \alpha_k \left(\check{p}_k + N_0\right), \tag{3.10}$$

where $\check{p}_k$ is the square norm of a vector $\check{\mathbf{s}}_k$, i.e., $\check{p}_k \triangleq \|\check{\mathbf{s}}_k\|^2$. Note that due to the assumption of PSK signaling, we have

$$\check{p}_k = \left(N_t - 1\right) E_t. \tag{3.11}$$

Consequently, the conditional pdf of the MF detector output $\hat{s}_k$ can be expressed as

$$p_{\hat{s}_k}\left(\hat{s}_k | s_k, \alpha_k, \check{p}_k\right) = \frac{1}{\pi N_r \alpha_k \left(\check{p}_k + N_0\right)} e^{-\frac{\left|\hat{s}_k - N_r \alpha_k s_k\right|^2}{N_r \alpha_k \left(\check{p}_k + N_0\right)}}. \tag{3.12}$$

3.3.2 Optimal Metric for Channel Decoding

In the case of BPSK with $s_k = \sqrt{E_t}(1 - 2c_k)$ for a given coded bit c_k, the corresponding LLR can be expressed using the exact distribution of the MF detector output (3.12) as

$$\begin{aligned}\lambda_k &\triangleq \log \frac{p_{\hat{s}_k}\left(\hat{s}_k | s_k = \sqrt{E_t}\right)}{p_{\hat{s}_k}\left(\hat{s}_k | s_k = -\sqrt{E_t}\right)} \\ &= \frac{4\sqrt{E_t}}{\check{p}_k + N_0}\hat{s}_k^{\text{I}} = \frac{4\sqrt{E_t}}{\left(N_t - 1\right)E_t + N_0}\hat{s}_k^{\text{I}}.\end{aligned} \tag{3.13}$$

As a reference, in the case of MMSE detector, the LLR is often approximated by resorting to Gaussian approximation of the conditional pdf as

$$\lambda_k \approx \frac{4\mu_{\text{MMSE}}}{\sigma^2_{\text{MMSE}}} \hat{s}^{\text{I}}_k, \tag{3.14}$$

where $\mu_{\text{MMSE}} = \mathbf{w}^{\text{H}}_k \mathbf{h}_k \in \mathbb{R}$ and $\sigma^2_{\text{MMSE}} = E_t \left(\mu_{\text{MMSE}} - {\mu_{\text{MMSE}}}^2\right)$ [64]. It may be worth emphasizing that the LLR expression of MF detector in (3.13) is exact, whereas the LLR of MMSE detector in (3.14) is not only an approximation but also difficult to be expressed in a simple closed form. It is also important to point out that the mean value μ_{MMSE} should be calculated every time the channel matrix is updated.

3.3.3 Achievable Rate with Limited Numbers of BS Antennas

In order to examine the limitation of the conventional MF detector when the number of receiving antennas is not significantly larger than the number of devices (i.e., $\rho \approx 1$), we study its achievable rate based on the mutual information assuming Gaussian codebook. The signal-to-interference plus noise ratio (SINR) observed at the MF detector output conditioned on γ_s and α_k can be expressed using (3.9)–(3.11) as

$$\begin{aligned} \gamma_{\text{MF}}\left(\gamma_s, \alpha_k\right) &= \frac{E\left\{\left|N_r \alpha_k s_k\right|^2\right\}}{E\left\{\left|\tilde{n}_k\right|^2\right\}} \\ &= \frac{\alpha_k N_r E_t}{\left(N_t - 1\right) E_t + N_0} = \frac{\alpha_k \rho}{1 - 1/N_t + 1/\gamma_s}. \end{aligned} \tag{3.15}$$

Therefore, the corresponding mutual information with two-dimensional Gaussian signaling over an ergodic fading channel, which we refer to as *MF capacity*, is given by

$$\begin{aligned} C_{\text{MF}}\left(\gamma_s\right) &= E\left[\log_2\left\{1 + \gamma_{\text{MF}}\left(\gamma_s, \alpha_k\right)\right\}\right] \\ &= \int_0^\infty \log_2\left\{1 + \gamma_{\text{MF}}\left(\gamma_s, \alpha_k\right)\right\} p_\alpha(\alpha_k) d\alpha_k, \end{aligned} \tag{3.16}$$

where $p_\alpha(x)$ represents the pdf of α_k [61]. On the other hand, under the assumptions of the perfect CSI at the receiver and no CSI at the transmitter, the conventional MIMO capacity is given by [22]

$$C_{\text{MIMO}}\left(\gamma_s\right) = E\left[\log_2 \det\left(\mathbf{I}_{N_t} + \frac{\gamma_s}{N_t} \mathbf{H}^{\text{H}} \mathbf{H}\right)\right], \tag{3.17}$$

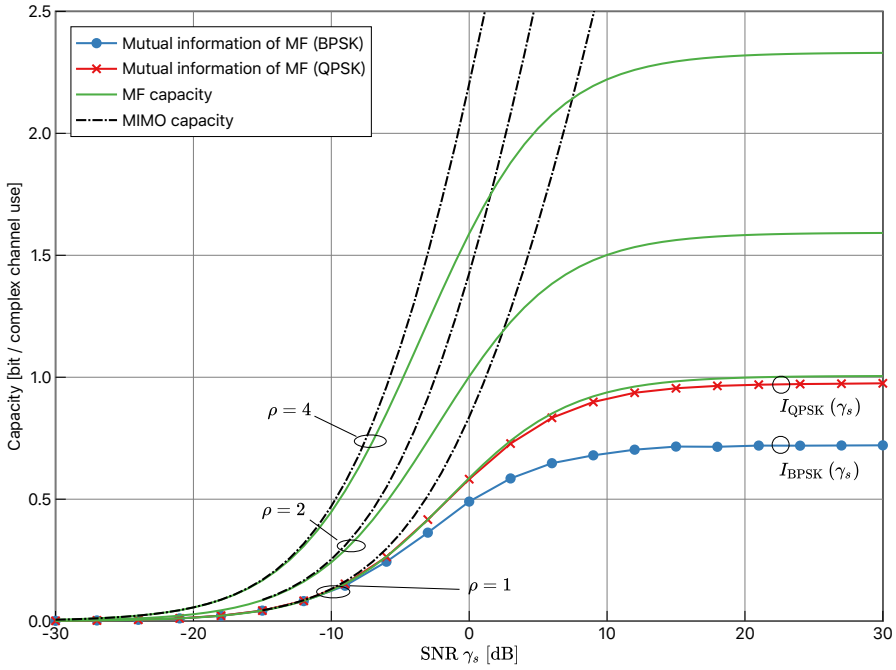

Figure 3.3: Comparison of *per user* mutual information achievable by MF detector as a function of SNR *per receive antenna* with $N_t = 128$ and $N_r = \rho N_t$, where $\rho = 1, 2$, and 4. The mutual information of MF detector with input constraint is also shown for BPSK and QPSK when $\rho = 1$.

which serves as an upper bound in terms of spectrum efficiency for MF detector, i.e., $C_{\mathrm{MF}}(\gamma_s) \leq C_{\mathrm{MIMO}}(\gamma_s)$.

Fig. 3.3 compares the MF capacity of (3.16) and MIMO capacity (3.17) with $N_t = 128$ and $\rho = 1$, 2, and 4, as a function of SNR *per receive antenna*. The mutual information curves achieved by MF detector with input constrained on BPSK and QPSK [61] are also plotted in the case of $\rho = 1$, designated by $I_{\mathrm{BPSK}}(\gamma_s)$ and $I_{\mathrm{QPSK}}(\gamma_s)$, respectively. We note that they are normalized with the number of transmitters and the resulting values thus correspond to the *per user* spectrum efficiency. Since MF detector cannot cancel the inter-channel interference, its spectral efficiency saturates at a certain limit. In addition, from the result of SINR-based capacity assuming Gaussian codebook with $N_r = 128$ (i.e., $\rho = 1$), the *per user* mutual information is bounded by around one bit per complex channel use and we observe that the mutual information of QPSK constellation is already close to this bound, suggesting that no further increase of constellation points may improve spectral efficiency. As the antenna ratio ρ increases, the relative SNR gap between (3.16) and (3.17) evaluated at a fixed spectral efficiency decreases. In other words, the performance of MF detector approaches that of the optimal detector as has been observed in [16].

BPSK versus QPSK

Let us compare BPSK and QPSK in the case of MF detector. For BPSK, all transmit power E_t is used for transmission of a single coded bit. Thus, the SINR *per coded bit* is expressed as

$$\gamma_b^{\text{BPSK}}(\gamma_s, \alpha_k) = \gamma_{\text{MF}}(\gamma_s, \alpha_k) = \frac{\alpha_k \rho}{1 - 1/N_t + 1/\gamma_s}. \tag{3.18}$$

On the other hand, since the transmit power per coded bit is $E_t/2$ in the case of QPSK, the corresponding SINR is expressed as

$$\gamma_b^{\text{QPSK}}(\gamma_s, \alpha_k) = \frac{\alpha_k \rho/2}{1 - 1/N_t + 1/\gamma_s}. \tag{3.19}$$

Comparing (3.19) with (3.18), we observe that the SINR *per coded bit* with QPSK signaling is half of that achieved by BPSK regardless of the channel SNR γ_s. This is due to the fact that in the case of MF detector, upon detecting the real part (I-component) of QPSK symbols, not only the real part but also the imaginary part (Q-component) of the QPSK symbols transmitted from the other $(N_t - 1)$ antennas will be observed as interference at the receiver. This fact also explains that in the case of MIMO spatial multiplexing systems, the amount of interference with QPSK signaling should be larger than that of BPSK by a factor of about 3 dB. Conversely, we still have room for performance improvement with MF detector by introducing suitable interference cancellation schemes.

3.4 Matched-Filter Detector with Quadrature Interference Cancellation

As observed in the previous section, if the numbers of transmitting devices and the receiving antennas are equal, low-complexity MF detector cannot achieve the spectral efficiency as high as one bit *per user* even with QPSK signaling. We will demonstrate that this problem can be overcome by MF-QIC proposed in this section.

3.4.1 Soft Parallel Interference Cancellation

We first describe a soft parallel interference cancellation (soft-PIC) scheme for a coded MIMO system with linear MIMO detector. The system block diagram for soft-PIC is shown in Fig. 3.4. Let us define a MIMO channel decoder for a binary code $\mathcal{C}$ that has a matrix of

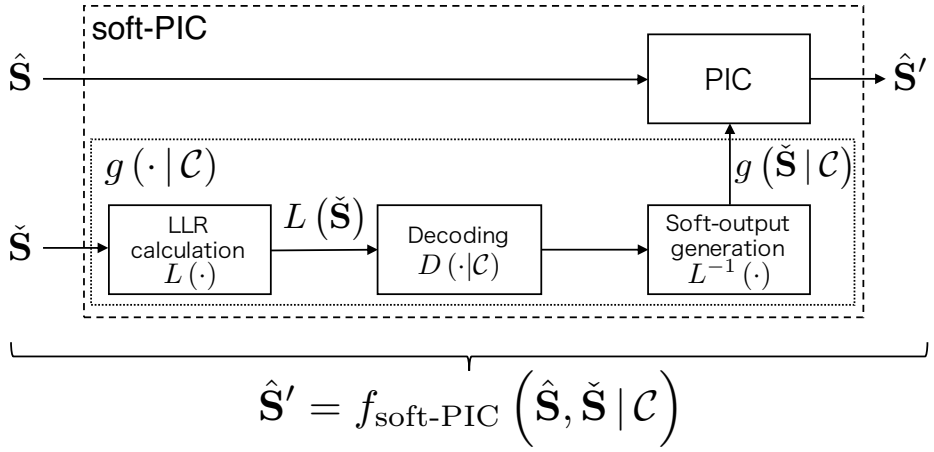

Figure 3.4: A block diagram of soft-PIC module.

LLR $\mathbf{\Lambda} \in \mathbb{R}^{N_t \times N_c}$ with its (k,t)th element corresponding to $\lambda_{k,t}$ as its input, and outputs the corresponding LLR $\mathbf{\Lambda}' \in \mathbb{R}^{N_t \times N_c}$:

$$\mathbf{\Lambda}' = D\left(\mathbf{\Lambda} \mid \mathcal{C}\right). \tag{3.20}$$

We also define the element-wise mapping function of a symbol matrix $\mathbf{S} \in \mathbb{C}^{N_t \times N_s}$ to its LLR matrix $\mathbf{\Lambda} \in \mathbb{R}^{N_t \times N_c}$ as $\mathbf{\Lambda} = L\left(\mathbf{S}\right)$ and its inverse as $\mathbf{S} = L^{-1}\left(\mathbf{\Lambda}\right)$, where each element $s \in \mathbf{S}$ is transformed to the corresponding m-tuples of $\lambda \in \mathbf{\Lambda}$ through (3.5). Furthermore, for a given specific binary code $\mathcal{C}$, we define the *soft-PIC module*, denoted by $f_{\text{soft-PIC}} : \mathbb{C}^{N_t \times N_s} \times \mathbb{C}^{N_t \times N_s} \rightarrow \mathbb{C}^{N_t \times N_s}$, which calculates the element-wise distance between the MIMO detector output matrix $\hat{\mathbf{S}} \in \mathbb{C}^{N_t \times N_s}$ and the corresponding soft output obtained from a complex-valued input matrix $\check{\mathbf{S}} = \check{\mathbf{S}}^{\mathrm{I}} + j\check{\mathbf{S}}^{\mathrm{Q}} \in \mathbb{C}^{N_t \times N_s}$ as follows:

$$f_{\text{soft-PIC}}\left(\hat{\mathbf{S}}, \check{\mathbf{S}} \mid \mathcal{C}\right) \triangleq \hat{\mathbf{S}} - \left[\mathbf{W}^{\mathrm{H}}\mathbf{H} - \left(\mathbf{W}^{\mathrm{H}}\mathbf{H}\right) \circ \mathbf{I}_{N_t}\right] g\left(\check{\mathbf{S}} \mid \mathcal{C}\right), \tag{3.21}$$

where $\mathbf{A} \circ \mathbf{B}$ denotes the Hadamard product of the matrices $\mathbf{A}$ and $\mathbf{B}$, i.e., $\left(\mathbf{W}^{\mathrm{H}}\mathbf{H}\right) \circ \mathbf{I}_{N_t}$ is a diagonal matrix in which its kth diagonal element is $w_{k,k}^{*} h_{k,k}$. In addition, $g : \mathbb{C}^{N_t \times N_s} \rightarrow \mathbb{C}^{N_t \times N_s}$ is a soft-output matrix generator defined depending on whether the input $\check{\mathbf{S}}$ is real, imaginary, or complex-valued as

$$g\left(\check{\mathbf{S}} \mid \mathcal{C}\right) \triangleq L^{-1}\left(D\left[L\left(\check{\mathbf{S}}^{\mathrm{I}}\right) \mid \mathcal{C}\right]\right) \mathbb{I}_{\check{\mathbf{S}}^{\mathrm{I}} \neq \mathbf{O}} + jL^{-1}\left(D\left[L\left(\check{\mathbf{S}}^{\mathrm{Q}}\right) \mid \mathcal{C}\right]\right) \mathbb{I}_{\check{\mathbf{S}}^{\mathrm{Q}} \neq \mathbf{O}}, \tag{3.22}$$

where $\mathbb{I}_{\mathsf{E}}$ is an indicator function that returns 1 if the event E is true and 0 otherwise, and $\mathbf{O}$ represents the all-zero matrix.

In the case of MF detector, the soft-PIC module (3.21) can be simplified as

$$f_{\text{MF-soft-PIC}}\left(\hat{\mathbf{S}}, \check{\mathbf{S}} \,|\, \mathcal{C}\right) = \hat{\mathbf{S}} - \mathbf{H}^{\mathrm{H}}\left(\mathbf{H} g\left(\check{\mathbf{S}} \,|\, \mathcal{C}\right)\right) + \left[\left(\mathbf{H}^{\mathrm{H}}\mathbf{H}\right) \circ \mathbf{I}_{N_t}\right] g\left(\check{\mathbf{S}} \,|\, \mathcal{C}\right), \tag{3.23}$$

where the kth diagonal element of $\left(\mathbf{H}^{\mathrm{H}}\mathbf{H}\right) \circ \mathbf{I}_{N_t}$ is equal to $N_r \alpha_k$.

Let $\hat{\mathbf{S}}'$ denote the output of the soft-PIC module according to (3.23) with the second input replaced by the first one through $\check{\mathbf{S}} \equiv \hat{\mathbf{S}}$, which we refer to as *MF-soft-PIC*:

$$\hat{\mathbf{S}}' = f_{\text{MF-soft-PIC}}\left(\hat{\mathbf{S}}, \hat{\mathbf{S}} \,|\, \mathcal{C}\right). \tag{3.24}$$

In what follows, we focus on a symbol level description and let $\tilde{\mathbf{s}}^{(l)} \in \mathbb{C}^{N_t \times 1}$ denote the lth column vector of the generator output $g\left(\check{\mathbf{S}} \,|\, \mathcal{C}\right)$. From (3.23), the soft-PIC module for MF detector corresponding to the lth symbol $\mathbf{s}'^{(l)} \in \mathbb{C}^{N_t \times 1}$ is performed as

$$\mathbf{s}'^{(l)} = \hat{\mathbf{s}}^{(l)} - \mathbf{H}^{\mathrm{H}}\left(\mathbf{H}\tilde{\mathbf{s}}^{(l)}\right) + \left[\left(\mathbf{H}^{\mathrm{H}}\mathbf{H}\right) \circ \mathbf{I}_{N_t}\right] \tilde{\mathbf{s}}^{(l)}, \tag{3.25}$$

and the kth element of (3.25) can be expressed as

$$\begin{aligned} \hat{s}_k'^{(l)} &= \hat{s}_k^{(l)} - \sum_{i=1}^{N_r} \sum_{j=1, j\neq k}^{N_t} h_{i,k}^* h_{i,j} \tilde{s}_j^{(l)} \\ &= N_r \alpha_k s_k^{(l)} + \sum_{i=1}^{N_r} \sum_{j=1, j\neq k}^{N_t} h_{i,k}^* h_{i,j} \left(s_j^{(l)} - \tilde{s}_j^{(l)}\right) + \sum_{i=1}^{N_r} h_{i,k}^* n_i^{(l)}, \end{aligned} \tag{3.26}$$

where $\tilde{s}_k^{(l)}$ is the kth element of $\tilde{\mathbf{s}}^{(l)}$.

BPSK Example

In the case of BPSK signaling, omitting the symbol index l for simplicity, the initial LLR λ_k of the kth BPSK symbol is calculated from the MF detector output $\hat{s}_k = \hat{s}_k^{\mathrm{I}} + j\hat{s}_k^{\mathrm{Q}}$ as

$$\lambda_k = L\left(\hat{s}_k^{\mathrm{I}}\right), \tag{3.27}$$

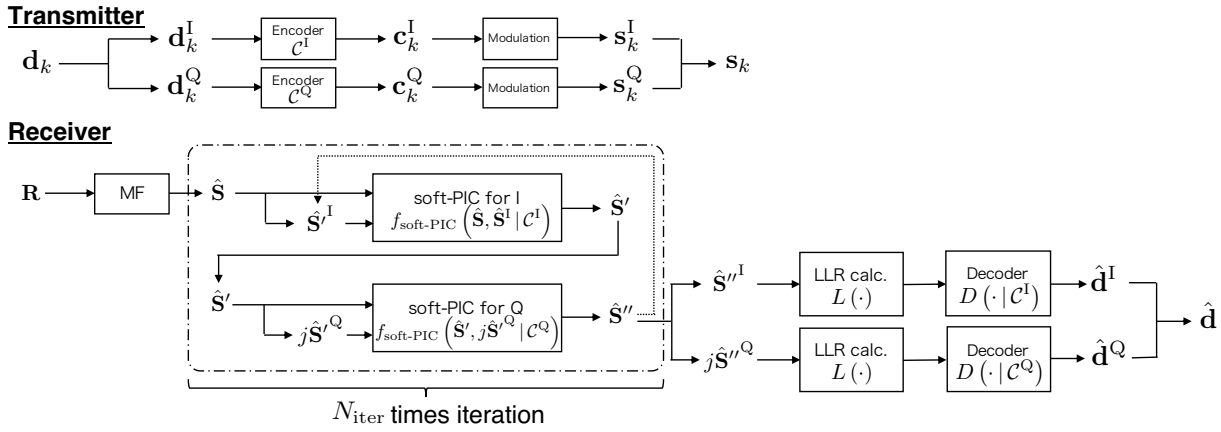

Figure 3.5: A block diagram of MF-QIC system.

which is given by (3.13). This is input to the channel decoder, and let λ'_k denote its corresponding output LLR. Then the kth symbol corresponding to the soft output, $\tilde{s}_k$ in (3.26), is expressed as

$$\tilde{s}_k = L^{-1}(\lambda'_k) = \sqrt{E_t}\tanh\left(\frac{\lambda'_k}{2}\right). \tag{3.28}$$

After soft-PIC according to (3.26), the channel decoding should be performed to its output $\hat{\mathbf{s}}'$ for making the final decision. Note that at this final decoding step, we calculate the LLR after soft-PIC from $\hat{s}'_k$ under the condition that all the interfering symbols are successfully canceled (i.e., $\check{p}_k \approx 0$) as

$$\hat{\lambda}'_k = \frac{4\sqrt{E_t}}{N_0}\hat{s}^{\mathrm{I}}_k, \tag{3.29}$$

which will be input to the final decoder.

3.4.2 QIC Signal Processing

The system block diagram of MF-QIC is shown in Fig. 3.5.

Transmitter

Similar to multilevel coded modulation (MLC) [65], in what follows we consider the modified transmitter where I-component and Q-component of the complex symbols are separately encoded with the binary encoder of different code rates. Specifically, let the binary information

sequence of the kth user, $\mathbf{d}_k$, be divided into two sub-sequences of lengths K_c^{I} and K_c^{Q}, denoted by $\mathbf{d}_k^{\mathrm{I}}$ and $\mathbf{d}_k^{\mathrm{Q}}$, respectively, where the former is encoded by the binary encoder $\mathcal{C}^{\mathrm{I}}$ of rate $R_c^{\mathrm{I}} = K_c^{\mathrm{I}}/N_c^{\mathrm{I}}$ into the codeword $\mathbf{c}_k^{\mathrm{I}}$ and the latter by the binary encoder $\mathcal{C}^{\mathrm{Q}}$ of rate $R_c^{\mathrm{Q}} = K_c^{\mathrm{Q}}/N_c^{\mathrm{Q}}$ into $\mathbf{c}_k^{\mathrm{Q}}$, under the condition that their codeword lengths N_c^{I} and N_c^{Q} are identical to $N_c/2$. Each set of $m/2$ elements of $\mathbf{c}_k^{\mathrm{I}}$ forms the lth transmitted symbol $s_k^{\mathrm{I}(l)} \in \mathcal{Z} \subset \mathbb{R}$, and that of $\mathbf{c}_k^{\mathrm{Q}}$ forms $s_k^{\mathrm{Q}(l)} \in \mathcal{Z} \subset \mathbb{R}$, where $\mathcal{Z}$ represents a set of one-dimensional constellation points. The resulting lth complex symbol of the kth user $s_k^{(l)} \in \mathcal{X}$ with $\mathcal{X} = \mathcal{Z}^2$ is generated by $s_k^{(l)} = s_k^{\mathrm{I}(l)} + j s_k^{\mathrm{Q}(l)}$. Note that the achievable error rate performance strongly depends on the design of the code rates R_c^{I} and R_c^{Q}, which will be discussed in Section 3.5.

Receiver

After conventional detection of symbols based on MF detector, MF-QIC process will be performed according to the following three steps: 1) soft-PIC for I-component, 2) soft-PIC for Q-component, and 3) final detection and decoding.

1) **Soft-PIC for I-component:** Let $\hat{\mathbf{S}} = \hat{\mathbf{S}}^{\mathrm{I}} + j\hat{\mathbf{S}}^{\mathrm{Q}}$ denote the output of MF detector. We decode $\hat{\mathbf{S}}^{\mathrm{I}}$ corresponding to $\mathcal{C}^{\mathrm{I}}$ and calculate the corresponding soft output. Then we apply the soft-PIC to only the I-component of $\hat{\mathbf{S}}$ as

$$\hat{\mathbf{S}}' = f_{\text{MF-soft-PIC}}\left(\hat{\mathbf{S}}, \hat{\mathbf{S}}^{\mathrm{I}} \,|\, \mathcal{C}^{\mathrm{I}}\right). \tag{3.30}$$

Let $\hat{\mathbf{S}}' = \hat{\mathbf{S}}'^{\mathrm{I}} + j\hat{\mathbf{S}}'^{\mathrm{Q}}$ denote the corresponding output.

2) **Soft-PIC for Q-component:** We decode $\hat{\mathbf{S}}'^{\mathrm{Q}}$ corresponding to $\mathcal{C}^{\mathrm{Q}}$ and calculate the corresponding soft output. The resulting symbol vector obtained by applying soft-PIC to only the Q-component of $\hat{\mathbf{S}}'$ is expressed as

$$\hat{\mathbf{S}}'' = f_{\text{MF-soft-PIC}}\left(\hat{\mathbf{S}}', j\hat{\mathbf{S}}'^{\mathrm{Q}} \,|\, \mathcal{C}^{\mathrm{Q}}\right). \tag{3.31}$$

3) **Final Detection and Decoding:** Decoding is performed again to make the final decision.

The above QIC processing of Steps 1) and 2) can be iteratively repeated before Step 3) so as to further improve its performance as illustrated in Fig. 3.5. The corresponding QIC algorithm at the receiver is summarized in Algorithm 1, where $N_{\mathrm{iter}} \geq 1$ represents the number of iterations.

QPSK Example

Upon calculating (3.30), the corresponding LLR input to the decoder of $\mathcal{C}^{\mathrm{I}}$ can be expressed, omitting the symbol index l for simplicity, as

$$\begin{aligned}\lambda_k^{\mathrm{I}} &= \log \frac{p_{\hat{s}_k}\left(\hat{s}_k | s_k = \sqrt{E_t/2}\right)}{p_{\hat{s}_k}\left(\hat{s}_k | s_k = -\sqrt{E_t/2}\right)} \\ &= \frac{2\sqrt{E_t}}{\check{p}_k + N_0}\hat{s}_k^{\mathrm{I}} = \frac{2\sqrt{E_t}}{\check{p}_k^{\mathrm{I}} + \check{p}_k^{\mathrm{Q}} + N_0}\hat{s}_k^{\mathrm{I}},\end{aligned} \tag{3.32}$$

where $\check{p}_k^{\mathrm{I}}$ and $\check{p}_k^{\mathrm{Q}}$ denote the interference power corresponding to I-component and Q-component, respectively. Since $\check{p}_k$ in (3.32) corresponds to the total power of residual interference, we substitute $\check{p}_k = 0$ from the second iteration when the iterative QIC is employed. We note that this is an accurate model when all the interfering symbols are successfully canceled at the first iteration. When calculating (3.31) after the cancellation of I-component at the first iteration, the LLR can be expressed as

$$\lambda'^{\mathrm{Q}}_k = \frac{2\sqrt{E_t}}{\check{p}_k^{\mathrm{Q}} + N_0}\hat{s'}^{\mathrm{Q}}_k = \frac{2\sqrt{E_t}}{(N_t - 1)\,E_t/2 + N_0}\hat{s'}^{\mathrm{Q}}_k, \tag{3.33}$$

where we have introduced the approximation as $\check{p}_k^{\mathrm{I}} \approx 0$ and $\check{p}_k^{\mathrm{Q}} \approx \check{p}_k/2 = (N_t - 1)\,E_t/2$, an accurate model when I-component is successfully canceled in the preceding step. At the step of the final decision, we calculate the LLR corresponding to the symbol $\hat{s}''_k$ after QIC as

$$\lambda''_k = \frac{2\sqrt{E_t}}{N_0}\hat{s}''_k, \tag{3.34}$$

which is an accurate model when all the interfering symbols are successfully canceled in the previous steps. Finally, the information bits assigned to I-component and Q-component of the transmitting symbols are decoded based on the real and imaginary parts of λ''_k, respectively.

3.4.3 Complexity

We briefly discuss the computational complexity of our proposed MF-based detectors combined with IC techniques. Here, we define a floating-point operation (FLOP) as the number of complex summations and multiplications to calculate the estimated symbol vector $\hat{\mathbf{s}}$, as widely accepted in the MIMO detection literature [67,68]. We note that it excludes all the signal process-

Algorithm 1 Quadrature interference cancellation

Initialization:

$\hat{\mathbf{S}} \leftarrow \mathbf{H}^{\mathrm{H}}\mathbf{R}$

$\hat{\mathbf{S}}_{\text{init}} \leftarrow \hat{\mathbf{S}}$

$i \leftarrow 0$

Recursion:

while $i < N_{\text{iter}}$ **do**

$\hat{\mathbf{S}}' = f_{\text{MF-soft-PIC}}\left(\hat{\mathbf{S}}_{\text{init}}, \hat{\mathbf{S}}^{\mathrm{I}} \,|\, \mathcal{C}^{\mathrm{I}}\right).$

$\hat{\mathbf{S}}'' = f_{\text{MF-soft-PIC}}\left(\hat{\mathbf{S}}', j\hat{\mathbf{S}}'^{\mathrm{Q}} \,|\, \mathcal{C}^{\mathrm{Q}}\right)$

$\hat{\mathbf{S}} \leftarrow \hat{\mathbf{S}}''$

$i \leftarrow i + 1$

end while

Final decision:

Decode $\hat{\mathbf{S}}^{\mathrm{I}}$ and $\hat{\mathbf{S}}^{\mathrm{Q}}$ for all the users to get $\hat{\mathbf{d}}_k^{\mathrm{I}}$ and $\hat{\mathbf{d}}_k^{\mathrm{Q}}$

Table 3.1: Computation complexity.

detector	order	FLOPs
MF	$\mathcal{O}\left(N_t N_r\right)$	$\left(2N_r - 1\right) N_t$
MF-soft-PIC	$\mathcal{O}\left(N_t N_r\right)$	MF + $\left(4N_r + 2\right) N_t - N_r - 1$
MF-QIC	$\mathcal{O}\left(N_{\text{iter}} N_t N_r\right)$	MF + $N_{\text{iter}}\left\{\left(4N_r + 2\right) N_t - N_r - 1\right\}$
MMSE	$\mathcal{O}\left({N_t}^3 + {N_t}^2 N_r\right)$	$2N_r {N_t}^2 + \left(2N_r - 1\right) N_t$ + [inverse matrix calc. of size N_t]
MMSE-soft-PIC	$\mathcal{O}\left({N_t}^3 + {N_t}^2 N_r\right)$	MMSE + $\left(N_r + \frac{3}{2}\right) {N_t}^2 + \left(N_r - \frac{3}{2}\right) N_t$
MMSE-GS	$\mathcal{O}\left(N_{\text{iter}} {N_t}^2 N_r\right)$	$\left(4N_r + 4N_{\text{iter}} - 2\right) {N_t}^2 + \left(N_r - 2N_{\text{iter}} + 1\right) N_t$ (only multiplications) [66]
BP	$\mathcal{O}\left(N_{\text{iter}} N_t N_r\right)$	$N_{\text{iter}}\left(5N_r - 1\right) N_t$

ing related to channel decoding and demodulation (LLR calculation and constellation mapping) since these operations commonly apply to all detectors and they increase only linearly with the number of users. Table 4.1 lists the computational complexity corresponding to each detector in terms of the order and the number of FLOPs, where N_{iter} is the number of iterations for each detector and its suitable value depends on a specific detector employed.

As a result, the computational complexity order of all our proposed MF-based detectors follows $\mathcal{O}\left(N_t N_r\right)$ as summarized in Table 4.1. MF detector without IC requires only the operation corresponding to (3.2), and thus, its required FLOPs become $\left(2N_t - 1\right) N_r$ due to $\left(N_t - 1\right) N_r$ summations and $N_t N_r$ multiplications. Even with soft-PIC, the complexity order does not increase since the additional complexity becomes $\left(4N_r + 2\right) N_t - N_r - 1$ according to (3.25). In the case of QIC, soft-PIC module is repeated N_{iter} times and each iteration includes two soft-PIC

modules. However, its complexity per iteration is almost the same as soft-PIC since the PIC operation of soft-PIC module in (3.26) with the complex signal input $\tilde{\mathrm{s}} = \hat{\mathrm{s}}$ can be replaced by two independent soft-PIC modules with the signal inputs according to $\tilde{\mathrm{s}} = \hat{\mathrm{s}}^{\mathrm{I}}$ and $\tilde{\mathrm{s}} = \hat{\mathrm{s}}^{\mathrm{Q}}$.

We also list the complexity of some other competing schemes in Table 4.1. As a reference, MMSE detector as well as that with the proposed soft-PIC are also compared. Since their complexity order is cubic with the number of access users due to the matrix inversion, the use of Gauss-Seidel method has been proposed to reduce its complexity [59]. Nevertheless, in addition to the performance degradation, its complexity order still remains $\mathcal{O}\left(N_{\text{iter}} {N_t}^2 N_r\right)$ due to the existence of matrix multiplication operation $\mathbf{H}^{\mathrm{H}}\mathbf{H}$. On the other hand, belief propagation (BP) based on Gaussian approximation has been proposed as an iterative approach to achieve the near-optimal performance with complexity order as low as $\mathcal{O}\left(N_{\text{iter}} N_t N_r\right)$ [60], which is the same as our proposed MF-based detector. Their performances will be compared in Section 3.7 based on simulation, revealing that the MF detector with the proposed IC techniques may outperform the others.

3.5 Polar Code Design for MF-QIC

This section presents design criteria of polar codes tailored for MF-QIC based on the mutual information derived in Section 3.3. The performance lower bounds based on GA construction are also developed. Since our proposed MF-QIC is a combination of soft-PIC and MSD, a flexible code rate design should be important similar to the design of MLC [65]. We thus adopt polar codes since they are capacity approaching and their code rate can be flexibly adjusted.

In order to perform soft-PIC, the decoder should be able to generate a soft output corresponding to the codeword. For this purpose, we employ belief propagation (BP) decoding instead of successive cancellation (SC) decoding [69]. At the final decoding stage, however, one can apply SC decoding without performance degradation.

3.5.1 Code Rate Design

The code rate design of the component codes R_c^{I} and R_c^{Q} plays an important role in QIC. In this chapter, we design them based on the mutual information illustrated in Fig. 3.3.

Let us first consider the case that the I-component is successfully canceled. Then the MF

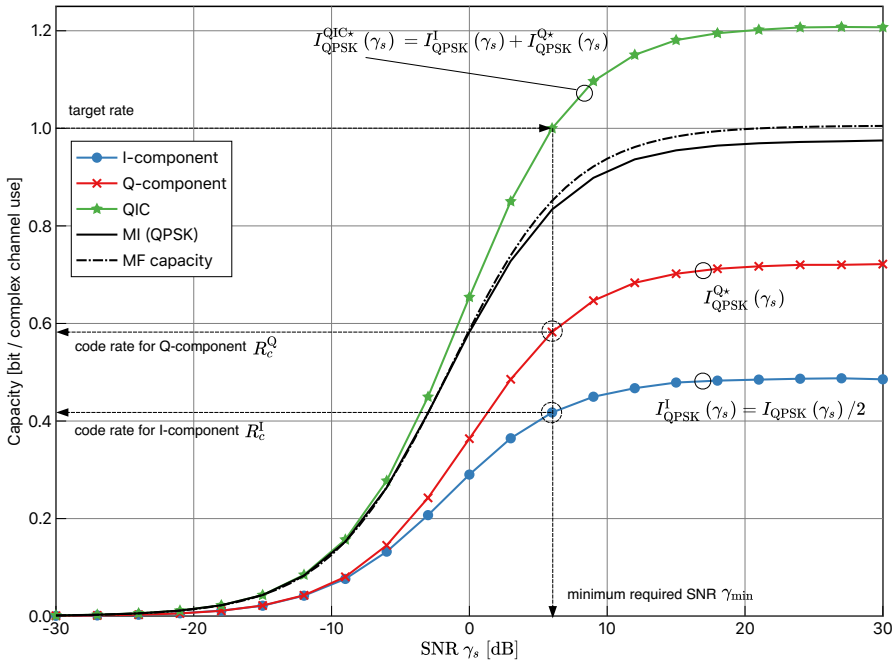

Figure 3.6: Mutual information and SINR-based capacity *per user* as a function of SNR *per receive antenna* in MIMO system with MF detector where $N_r = N_t = 128$. The corresponding mutual information for MF detector (with and without QPSK signal constraint) is also shown.

detector output for the l symbol of the kth user can be revised as

$$\hat{s}_k'^{(l)} = N_r \alpha_k s_k^{(l)} + j \sum_{i=1}^{N_r} \sum_{j=1, j\neq k}^{N_t} h_{i,k}^* h_{i,j} \hat{s}_j^{\mathrm{Q}(l)} + \sum_{i=1}^{N_r} h_{i,k}^* n_i^{(l)}. \tag{3.35}$$

In other words, the average power of interference observed at the MF detector output upon decoding of Q-component may be reduced by half compared to the case without QIC. Based on this observation, we plot the mutual information *per user* per complex channel use, associated with MF-QIC with $N_t = N_r = 128$ in Fig. 3.6, where that of Q-component represented by $I^{\mathrm{Q}\star}_{\mathrm{QPSK}}(\gamma_s)$ is calculated conditioned that the I-component has been successfully canceled. Let $I^{\mathrm{I}}_{\mathrm{QPSK}}(\gamma_s)$ be the mutual information for I-component with QPSK signaling defined as $I^{\mathrm{I}}_{\mathrm{QPSK}}(\gamma_s) = I_{\mathrm{QPSK}}(\gamma_s)/2$, where $I_{\mathrm{QPSK}}(\gamma_s)$ is the mutual information for MF detector in the case of QPSK initially shown in Fig. 3.3. The mutual information of MF-QIC denoted by $I^{\mathrm{QIC}\star}_{\mathrm{QPSK}}(\gamma_s)$ is calculated based on their sum. We observe that the mutual information of MF-QIC can achieve significantly higher value than that of the conventional MF detector (without IC). We initially set the target information rate $R^\star$ and determine the corresponding minimum

required SNR from the mutual information in MF-QIC as γ_{min}, i.e., $I_{\text{QPSK}}^{\text{QIC}\star}(\gamma_{\text{min}}) = R^{\star}$. Then, we determine the code rates for $\mathcal{C}^{\text{I}}$ and $\mathcal{C}^{\text{Q}}$ from the mutual information to be $R_c^{\text{I}} = I_{\text{QPSK}}^{\text{I}}(\gamma_{\text{min}})$ and $R_c^{\text{Q}} = I_{\text{QPSK}}^{\text{Q}\star}(\gamma_{\text{min}})$ as sketched in Fig. 3.6.

3.5.2 Gaussian Approximation Based Construction in QIC

The performance of polar codes depends on their construction (i.e., frozen bit selection). In this chapter, we focus on GA-based construction due to its simplicity. In this case, the *design SNR* plays a key role in generating an appropriate set of frozen bits [70].

Let us recall from Section 3.3.3 that the SINR at the MF detector output conditioned on the fading coefficient α_k is given by (3.15). Considering the fact that α_k approaches unity as the number of receive antennas increases due to the strong law of large numbers, we can define the average SINR of the MF detector output as

$$\Gamma_{\text{MF}}(\gamma_s) \triangleq E\{\gamma_{\text{MF}}(\gamma_s, \alpha_k)\} = \frac{\rho}{1 - 1/N_t + 1/\gamma_s}. \tag{3.36}$$

Note that the channel coefficient α_k can also be taken into account when the CSI is known at the transmitter side. For the design of I-component, we may use the SINR in the MF detector output with QPSK signaling directly since the symbols corresponding to I-component are initially detected and decoded prior to IC. Thus, the design SINR for I-component is expressed as a function of the minimum required SNR $\gamma_{\min}$ by

$$\Gamma_{\text{des}}^{\text{I}}(\gamma_{\min}) = \frac{\rho/2}{1 - 1/N_t + 1/\gamma_{\min}}. \tag{3.37}$$

On the other hand, the effect of interference is different for Q-component since it is detected and decoded after the cancellation of the symbols corresponding to I-component. Under the condition that all interfering symbols corresponding to I-component are canceled correctly, the power of the interference in Q-component will be reduced by half compared with that in I-component. Therefore, the design SINR for Q-component can be calculated as

$$\Gamma_{\text{des}}^{\text{Q}}(\gamma_{\text{min}}) = \frac{\rho}{1 - 1/N_t + 2/\gamma_{\text{min}}} = \Gamma_{\text{MF}}\left(\frac{\gamma_{\text{min}}}{2}\right). \tag{3.38}$$

Comparing (3.38) with (3.37), the average power of interference in decoding Q-component can be reduced by half, i.e., it is equivalent to that for BPSK signaling expressed by (3.36) with reduced channel SNR γ_s.

Example for Code Rate Design and Design SNR

As an example for polar code design with MF-QIC, we consider the case with the target rate $R^\star = 1.0$, which is achieved with QPSK signaling and code rate $R_c = 1/2$ in principle. From Fig. 3.6, MF-QIC can achieve the target rate when the channel SNR γ_s is higher than 6.0 dB, i.e., $\gamma_{\text{min}} = 6.0$ dB. Then, we observe that suitable code rates for I-component and Q-component are given by $R_c^{\text{I}} = 0.417$ and $R_c^{\text{Q}} = 0.583$, respectively. We may thus construct the polar code with design SNR given by (3.37) and (3.38) for $\mathcal{C}^{\text{I}}$ and $\mathcal{C}^{\text{Q}}$, respectively, with $\gamma_{\text{min}} = 6.0$ dB, which turns out that $\Gamma_{\text{des}}^{\text{I}}(\gamma_{\text{min}}) = -3.96$ dB and $\Gamma_{\text{des}}^{\text{Q}}(\gamma_{\text{min}}) = -1.75$ dB.

3.5.3 Performance Analysis of Polar Coded BLER Performance

We analyze the coded BLER performance of MF-QIC based on GA-based construction for polar codes [71]. We first derive that for MF detector without IC schemes.

Without loss of generality, we assume that the all zero codeword is transmitted from all the devices. We also assume for simplicity of description that the information bits $d_{k,1}, d_{k,2}, \cdots, d_{k,K_c}$ are sorted according to the order of successive cancellation decoding of polar codes designed by GA-based construction with the design SNR given by the minimum required SNR γ_{min}. Let B_i denote the event that all the preceding $(i-1)$ information bits are correctly decoded, i.e., B_i is the event that $\hat{d}_{k,1} = \cdots = \hat{d}_{k,i-1} = 0$, where $\hat{d}_{k,n}$ is the decoded bit for $d_{k,n}$. The bit error rate for the ith information bit conditioned with B_i is approximated as [70]

$$\begin{aligned} P_{b,i}(\gamma_s, \alpha_k) &= \Pr\left(\hat{d}_{k,i} \neq 0 | \mathsf{B}_i\right) \\ &\approx Q\left(\sqrt{\frac{\Lambda^{(i)}\left(\gamma_{\text{MF}}(\gamma_s, \alpha_k)\right)}{2}}\right), \end{aligned} \tag{3.39}$$

where $\Lambda^{(i)}(\beta)$ denotes the estimated output mean LLR corresponding to the ith information bit obtained by GA-based construction with β as its initial input SINR and the condition of B_i is excluded in the case of $i = 1$. The Q-function is defined as

$$Q(x) = \frac{1}{\sqrt{2\pi}} \int_x^\infty e^{-\frac{t^2}{2}} dt. \tag{3.40}$$

From (3.39), the estimated BLER can be approximately computed by [70]

$$\begin{aligned} P_{\text{BL}}\left(\gamma_s, \alpha_k\right) &\approx 1 - \prod_{i=1}^{K_c} \left\{1 - P_{b,i}\left(\gamma_s, \alpha_k\right)\right\} \\ &= 1 - \prod_{i=1}^{K_c} \left\{1 - Q\left(\sqrt{\frac{\Lambda^{(i)}\left(\gamma_{\text{MF}}\left(\gamma_s, \alpha_k\right)\right)}{2}}\right)\right\}. \end{aligned} \tag{3.41}$$

Since the MF output follows Gaussian distribution conditioned with the signal attenuation factor α_k, its SINR is also conditioned with α_k as (3.15). Therefore, the analytical BLER performance for MF detector is derived by averaging over α_k as

$$\begin{aligned} \bar{P}_{\text{BL}}\left(\gamma_s\right) &= \int_0^{\infty} P_{\text{BL}}\left(\gamma_s, \alpha_k\right) p_{\alpha}\left(\alpha_k\right) d\alpha_k \\ &= \int_0^{\infty} \left[1 - \prod_{i=1}^{K_c} \left\{1 - Q\left(\sqrt{\frac{\Lambda^{(i)}\left(\Gamma\left(\gamma_s, \alpha_k\right)\right)}{2}}\right)\right\}\right] p_{\alpha}\left(\alpha_k\right) d\alpha_k, \end{aligned} \tag{3.42}$$

where $p_{\alpha}\left(\alpha_k\right)$ is the pdf of α_k that follows a chi-square distribution with $2N_r$ degrees of freedom [61].

We now turn our attention to the proposed MF-QIC. Its performance depends on the interference power after QIC processing, which may not be precisely tractable. Thus, we model the SINR at the final decoding in MF-QIC as

$$\gamma_{\text{MF-QIC}}\left(\gamma_s, \alpha_k\right) = \frac{\alpha_k N_r E_t}{\check{p}_k^{\text{I}} + \check{p}_k^{\text{Q}} + N_0}, \tag{3.43}$$

where the residual interference power $\check{p}_k^{\text{I}}$ and $\check{p}_k^{\text{Q}}$ should depend on the number of bit errors observed in each codeword, and its average value should be proportional to the bit error probability. In this chapter, we approximate the corresponding power after QIC process by its mean value, which should become accurate as the codeword length increases due to the strong law of large numbers. Let $\bar{P}_b(\gamma_s)$ denote the average bit error rate (BER) over all the information bits in each codeword. It is expressed as

$$\begin{aligned} \bar{P}_b\left(\gamma_s\right) &= \frac{1}{K_c} \sum_{i=1}^{K_c} \text{Pr}\left(\hat{d}_{k,i} \neq d_{k,i}\right) \\ &\approx \frac{1}{K_c} \sum_{i=1}^{K_c} \left[P_{b,i}\left(\gamma_s\right) \text{Pr}\left(\mathsf{B}_i\right) + \frac{1}{2}\left(1 - \text{Pr}\left(\mathsf{B}_i\right)\right)\right], \end{aligned} \tag{3.44}$$

where we define $\Pr(\mathsf{B}_1) = 1$ and the bit error probability of the ith information bit is approximated as $1/2$ if the event B_i does not hold.

Thus, the residual interference power for each component is modeled as

$$\check{p}_k^{\mathrm{I}} = E_t \bar{P}_b^{\mathrm{I}}(\gamma_s)(N_t - 1) = \check{p}_k \bar{P}_b^{\mathrm{I}}(\gamma_s), \tag{3.45}$$

$$\check{p}_k^{\mathrm{Q}} = E_t \bar{P}_b^{\mathrm{Q}}(\gamma_s)(N_t - 1) = \check{p}_k \bar{P}_b^{\mathrm{Q}}(\gamma_s), \tag{3.46}$$

where $\bar{P}_b^{\mathrm{I}}$ and $\bar{P}_b^{\mathrm{Q}}$ are the average bit error rates corresponding to I-component and Q-component after soft-PIC in MF-QIC as shown in Fig. 3.5, respectively. They can be also estimated from (3.44) and (3.39) by substituting the SINR of (3.19) for I-component and that with the interference power replaced by $\check{p}_k \bar{P}_b^{\mathrm{I}} + \check{p}_k/2$ for Q-component.

The analytical BLER performance for each component in MF-QIC can be estimated from (3.42) as $P_{\mathrm{BL}}^{\mathrm{I}}(\gamma_s)$ and $P_{\mathrm{BL}}^{\mathrm{Q}}(\gamma_s)$ by substituting (3.43) based on (3.45) and (3.46), respectively. Finally, the resulting analytical BLER performance of MF-QIC is derived as

$$\bar{P}_{\mathrm{BL}}^{\text{MF-QIC}}(\gamma_s) = 1 - \left\{1 - \bar{P}_{\mathrm{BL}}^{\mathrm{I}}(\gamma_s)\right\}\left\{1 - \bar{P}_{\mathrm{BL}}^{\mathrm{Q}}(\gamma_s)\right\}. \tag{3.47}$$

3.5.4 Lower Bound of Polar Coded BLER Performance

Evaluation of the analytical BLER performance of MF-QIC described in Section 3.5.3 may involve unwieldy calculation. As an alternative analytical approach, we attempt to derive performance bounds for coded BLER with MF-QIC. In this chapter, we describe two kinds of lower bounds referred to as MF lower bound and QIC limit. The former is a valid model under the condition that both I- and Q-components are successfully canceled in the preceding process, whereas the latter is valid if the cancellation of I-component is successful. We also note that MF lower bound can be analytically derived, whereas QIC limit is derived making use of the simulation results, but it serves as a good reference for the convergence performance of QIC. More specifically, the MF lower bound is considered as the ideal performance limit of MF-based detector since all the interference is assumed to be canceled correctly, and thus is a loose lower bound for polar coded BLER performance of MF detector with IC. On the other hand, QIC limit is derived under the condition that I-component is successfully canceled in the preceding QIC step, yielding a reference BLER performance limit that can be approached by MF-QIC.

MF Lower Bound

MF lower bound is based on the fact that the gram matrix $\mathbf{H}^{\mathrm{H}}\mathbf{H}$ of the MIMO channel $\mathbf{H}$ approaches the identity matrix $N_r\mathbf{I}_{N_t}$ with the increase of BS antennas [72]. It can also be derived with under the condition that all the interfering symbols are successfully canceled (i.e., $\check{p}_{k,l} \approx 0$ in (3.8)) for the limited BS antennas as

$$\gamma_{\mathrm{MF}}^{\mathrm{low}}\left(\gamma_s, \alpha_k\right) = \gamma_{\mathrm{MF}}\left(\gamma_s, \alpha_k\right)\big|_{\check{p}_{k,l}=0} = \frac{\alpha_k N_r E_t}{N_0} = \alpha_k \rho \gamma_s. \tag{3.48}$$

Consequently, MF detector can improve its output SNR in proportion to the ratio of the number of antennas at both sides. It suggests that (3.48) corresponds to the maximum SINR (or SNR) achieved by MF detector such that all the interference is removed perfectly.

Thus, the MF limit in terms of the estimated BLER at a given minimum required SNR γ_{min} can be approximately computed according to Section 3.5.3 by replacing (3.43) with (3.48).

QIC Limit

In order to evaluate the performance limit of MF-QIC improved by iteration, we introduce a numerical lower limit referred to as QIC limit. It is based on an ideal model that I-component is successfully canceled at the first step in QIC as described in Section 3.4.2. In this manner, the remaining part of QIC is equivalent to MF with soft-PIC where only Q-component is encoded with the rate R_c^{Q}. With reference to (3.26) and the imaginary part of (3.35), we note that the average power of signal and interference for Q-component in MF-QIC after I-component cancellation is reduced by half from that of MF with soft-PIC for BPSK. In other words, the SINR per coded bit of MF-QIC after successful cancellation of I-component is expressed as

$$\Gamma_{\mathrm{QIC}}^{\mathrm{lim}}\left(\gamma_s\right) = \Gamma_{\mathrm{des}}^{\mathrm{Q}}\left(\gamma_s\right) = \frac{\rho}{1 - 1/N_t + 2/\gamma_s}. \tag{3.49}$$

Therefore, the lower bound of MF-QIC is easily obtained by the equivalent simulation of MF with soft-PIC encoded with rate R_c^{Q}, based on the model of (3.26) with the average power of AWGN in the third term replaced by $2N_0$.

3.6 Effect of Channel Estimation Error

So far, it has been assumed that perfect CSI is available at the receiver. Since precise CSI estimation in view of massive IoT devices under limited spectral resources is challenging, we

investigate the effect of CSI estimation error on the resulting performance.

3.6.1 System Model with Imperfect CSI

Let $\Delta\mathbf{H}$ denote a matrix representing the channel estimation error. For simplicity of analysis, we assume that each element $\Delta h_{i,k}$ in $\Delta\mathbf{H}$ follows an i.i.d. circularly symmetric complex Gaussian random variable with zero mean and variance σ_e^2 [56]. Assuming the use of maximum likelihood (ML) channel estimation [54, 73], the CSI at the receiver may be expressed as

$$\hat{\mathbf{H}} = \mathbf{H} + \Delta\mathbf{H}, \tag{3.50}$$

and its accuracy is determined by the variance of the estimation error expressed as [56, 74]

$$\sigma_e^2 = \frac{N_t N_0}{N_{\text{train}} E_{\text{train}}}, \tag{3.51}$$

where N_{train} and E_{train} represent the length and power of the training symbols, respectively.

In the case of MF detector with imperfect CSI, the weight matrix of (3.4) is replaced by

$$\hat{\mathbf{W}}^{\text{H}} = \hat{\mathbf{H}}^{\text{H}} = \mathbf{H}^{\text{H}} + \Delta\mathbf{H}^{\text{H}}. \tag{3.52}$$

3.6.2 Achievable Rate with Imperfect CSI

We may rewrite the MF detector output (3.6) considering the channel estimation error as

$$\hat{s}_k = N_r \alpha_k s_k + \sum_{i=1}^{N_r} \Delta h_{i,k}^* h_{i,k} s_k + \sum_{i=1}^{N_r} \sum_{j=1, j\neq k}^{N_t} \left(h_{i,k}^* + \Delta h_{i,k}^*\right) h_{i,j} s_j + \sum_{i=1}^{N_r} \left(h_{i,k}^* + \Delta h_{i,k}^*\right) n_i, \tag{3.53}$$

where its exact pdf is given in [61, eq.(53)]. The average SINR of the MF detector output (3.36) may be rewritten as

$$\hat{\Gamma}_{\text{MF}}\left(\gamma_s, \sigma_e^2\right) \triangleq \frac{N_r E_t}{\sigma_e^2 E_t + \left(1 + \sigma_e^2\right)\left(\check{p}_k + N_0\right)}. \tag{3.54}$$

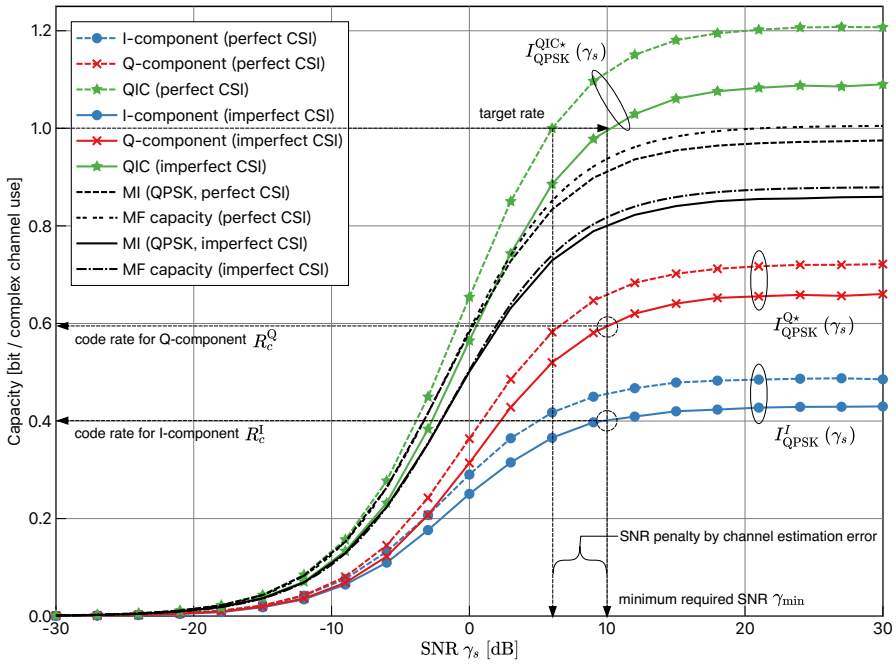

Figure 3.7: Mutual information and SINR-based capacity *per user* with channel estimation error as a function of SNR *per receive antenna* in MIMO system with MF detector where $N_r = N_t = 128$. The corresponding mutual information for MF detector (with and without QPSK signal constraint) is also shown.

In the case of massive access (i.e. $N_t \gg 1$), (3.54) can be approximated as

$$\begin{aligned}\hat{\Gamma}_{\mathrm{MF}}\left(\gamma_s, \sigma_e^2\right) &\approx \frac{N_r E_t}{\left(1+\sigma_e^2\right)\left(\check{p}_k + N_0\right)} \\ &= \frac{1}{1+\sigma_e^2}\frac{\rho}{1 - 1/N_t + 1/\gamma_s} = \frac{1}{1+\sigma_e^2}\Gamma_{\mathrm{MF}}\left(\gamma_s\right). \end{aligned} \tag{3.55}$$

As a consequence, the achievable SINR of MF detector is reduced by a factor of $1+\sigma_e^2$.

Fig. 3.7 shows the mutual information with the channel estimation error ($\sigma_e^2 = 0.2$) corresponding to each component of MF-QIC compared to the perfect CSI ($\sigma_e^2 = 0$) shown in Fig. 3.6. As expected, the imperfect CSI may increase the minimum required SNR $\gamma_{\min}$, and in the case of $R^\star = 1.0$, the SNR penalty becomes about 4 dB. In the next section, we will perform simulations assuming a practical scenario where the knowledge of CSI estimation error is available neither at the transmitter nor at the receiver. We thus design the polar code without considering the effect of σ_e^2, and the receiver employs the conventional MF detector assuming $\sigma_e^2 = 0$.

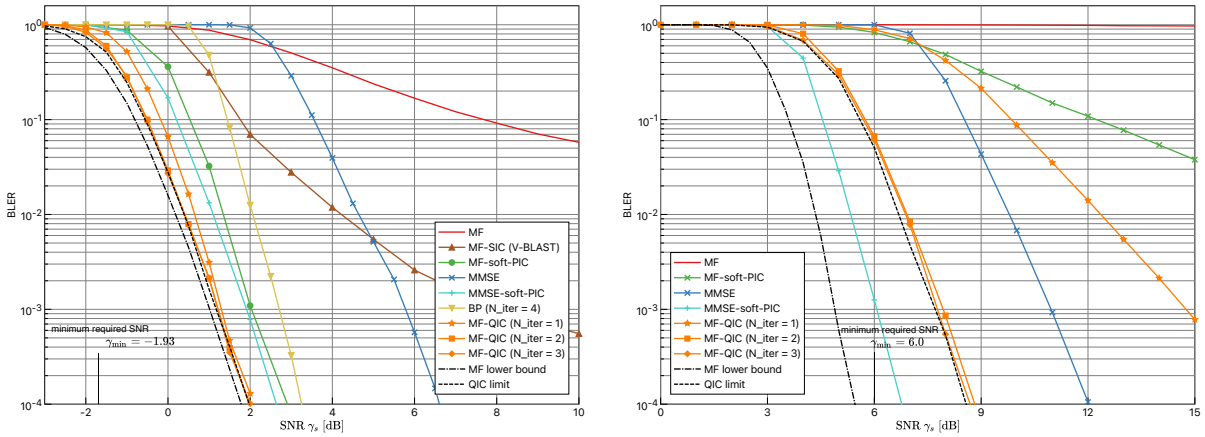

(a) Target rate $R^\star = 0.5$

(b) Target rate $R^\star = 1.0$

Figure 3.8: Polar coded BLER performance of MF-QIC in the uplink multiuser MIMO system with $N_r = N_t = 128$.

3.7 Simulation Results

We evaluate our proposed MF detector with QIC through computer simulation. To this end, we employ a non-systematic polar code with BP decoder for soft cancellation, and the number of iterations is set as 60. Throughout our simulation, we set the codeword length as $N_c = 1024$. We consider the uplink multiuser massive MIMO system with full loading ($\rho = 1$) as a severe case with $N_r = N_t = 128$. The channel is assumed to be i.i.d. block Rayleigh fading and thus it is static over the transmission of a single codeword.

In the case of the system with QIC, since the total codeword length N_c is given by the sum of two components, each codeword length is set as $N_c^{\mathrm{I}} = N_c^{\mathrm{Q}} = N_c/2 = 512$ bits. We evaluate and compare the performance of MF-QIC in terms of BLER, and the block is defined as the sum of two codewords. Therefore, we calculate the corresponding BLER as

$$\begin{aligned} P_{\mathrm{BL,QIC}} &= \Pr\left(\mathbf{d}_k \neq \hat{\mathbf{d}}_k\right) \\ &= 1 - \left\{1 - \Pr\left(\mathbf{d}_k^{\mathrm{I}} \neq \hat{\mathbf{d}}_k^{\mathrm{I}}\right)\right\}\left\{1 - \Pr\left(\mathbf{d}_k^{\mathrm{Q}} \neq \hat{\mathbf{d}}_k^{\mathrm{Q}}\right)\right\}. \end{aligned} \tag{3.56}$$

3.7.1 Polar Coded Performance of MF-QIC with Perfect CSI

First, we assume that perfect CSI is available at the receiver and evaluate the ideal performance with the target rate as $R^\star = 0.5$. The component code rate for QIC is set as $R_c^{\mathrm{I}} = 0.215$

and $R_c^{\mathrm{Q}} = 0.285$ based on the mutual information analysis as described in Section 3.5.1. We evaluate the polar coded BLER performance achieved by QIC in Fig. 3.8(a). We first compare the performance of MF detector employing soft-PIC (denoted by MF-soft-PIC) with the conventional MF, MMSE (without IC), and BP achieved by BPSK signaling and code rate $R_c = 1/2$. Throughout this chapter, BP-based detector is employed according to [60] based on Gaussian approximation of the inter-channel interference, where the number of iterations in BP is set as $N_{\mathrm{iter}}^{\mathrm{BP}} = 4$ so that the uncoded BER performance converges. Severe error floor is observed for MF detector, but MF-soft-PIC is able to cancel the interference and thus we observe no error floor, outperforming MMSE and BP. We also plot that of the conventional MF detector with SIC, which is inferior to MF-soft-PIC. The MMSE detector combined with soft-PIC (denoted by MMSE-soft-PIC) is also compared, which turns out to outperform MF-soft-PIC. On the other hand, MF-QIC shows the best performance among those evaluated here, and we observe that the corresponding BLER begins to decrease as the SNR γ_s exceeds the minimum required SNR γ_{min} even without iteration. The MF lower bound and QIC limit are also shown in Fig. 3.8(a). The gaps between the simulated value and its QIC limit are caused by the remaining interference and error propagation in I-component after MF-QIC, which becomes negligible by a few iterations of MF-QIC.

We now focus on the case with $R^\star = 1.0$, where we set the code rate to be $R_c^{\mathrm{I}} = 0.417$ and $R_c^{\mathrm{Q}} = 0.583$ based on the mutual information analysis in Fig. 3.6 with $K_c^{\mathrm{I}} = 214$ and $K_c^{\mathrm{Q}} = 298$. In this case, even MF-soft-PIC may only partially cancel the interference, and thus we still observe the error floor due to the residual interference. On the other hand, our proposed MF-QIC can achieve one bit per complex channel use without error floor. As in the case with $R^\star = 0.5$, the performance of MF-QIC achieves QIC limit by iterative QIC as expected, and $N_{\mathrm{iter}} = 2$ is sufficient even with $R^\star = 1.0$. Nevertheless, in the case of $R^\star = 1.0$, even MF-QIC may not outperform MMSE-soft-PIC, but it should be noted that the complexity of MF-QIC is much lower than that of MMSE-soft-PIC, and this complexity gap becomes significant as N_t and N_r increase.

We next compare the polar coded BLER performances given by the computer simulations and the analytical expressions developed in Section 3.5.3 and 3.5.4. We evaluate the case with the target rate as $R^\star = 0.5$ with the same parameter settings as in Fig. 3.8(a). Fig. 3.9 shows the polar coded BLER performance of MF as well as MF-QIC with up to two iterations, where all the results indicated by discrete marks are based on the computer simulation, whereas the solid lines (without marks) correspond to the analytical approximated BLER developed in Section 3.5.3. (The corresponding MF lower bound as well as QIC limit are also plotted as a reference.) The

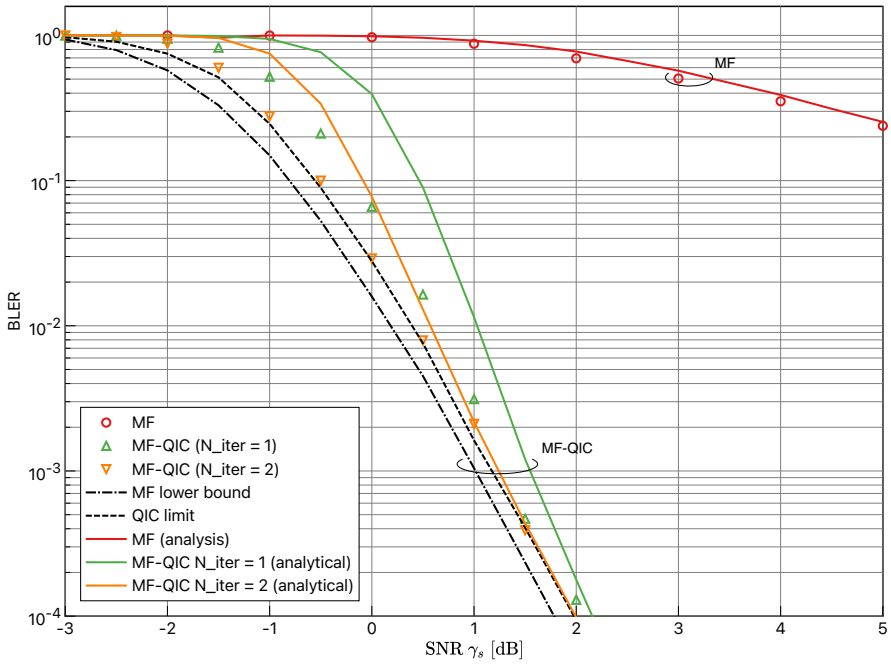

Figure 3.9: Polar coded BLER performance of MF-based detectors through the computer simulation and mathematical analysis with rate $R^\star = 0.5$ in the uplink multiuser MIMO system with $N_r = N_t = 128$.

analytical and simulation results for MF detector prior to QIC show good agreement. On the other hand, we observe some gap between analytical BLER and simulation results of MF-QIC, which is due to the approximations introduced in the derivation process. Nevertheless, our derived analytical BLER performance can well capture the behavior of the corresponding simulation results including the performance improvement offered by each iteration of QIC.

3.7.2 Polar Coded Performance of MF-QIC with Channel Estimation Error

We now turn our attention to the case with imperfect CSI at the receiver. We show the polar coded BLER performance of MF-QIC ($N_{\text{iter}} = 1$) with rate $R^\star = 0.5$ in Fig. 3.10(a), where the variance of CSI errors is set as $\sigma_e^2 = 0, 0.05, 0.2$, and 0.4. Here, we focus on the case where the receiver does not have any knowledge of CSI error and thus it is assumed that $\sigma_e^2 = 0$. As a reference, the performances of MMSE and BP with and without channel estimation error are plotted in Fig. 3.10(a). It is apparent that the resulting performance degrades with the increase of channel estimation error, since it decreases the channel SINR as observed in (3.54) and (3.55).

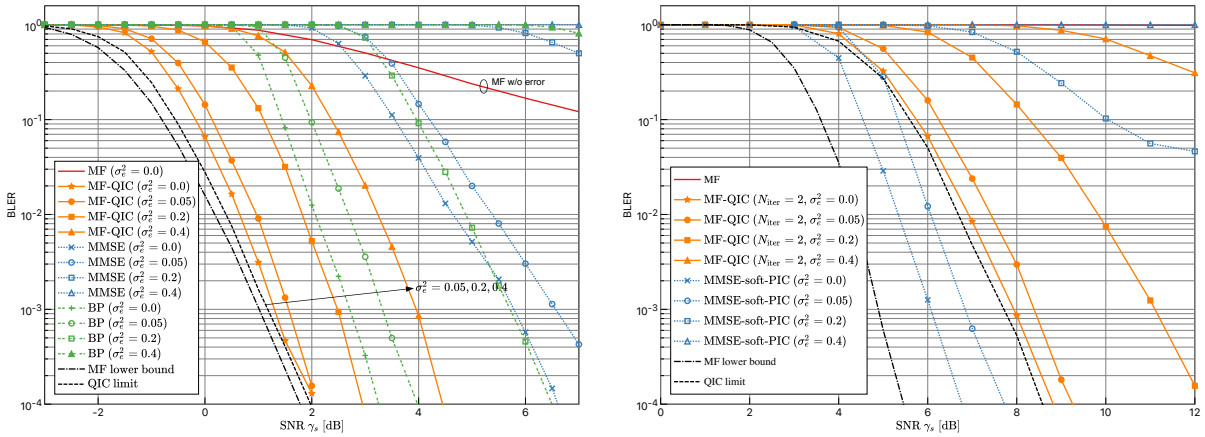

(a) Target rate $R^\star = 0.5$

(b) Target rate $R^\star = 1.0$

Figure 3.10: Polar coded BLER performance of MF-QIC in the uplink multiuser MIMO system with $N_r = N_t = 128$.

However, MF-QIC outperforms the other approaches compared here.

We finally examine the case with $R^\star = 1.0$ in the presence of CSI error in Fig. 3.10(b), where we compare the performances of MF-QIC at $N_{\text{iter}} = 2$ with those of MMSE-soft-PIC with reference to the results of perfect CSI shown in Fig. 3.8(b). As observed previously, MF-QIC fails to outperform MMSE-soft-PIC under the perfect CSI condition, and this is also the case with $\sigma_e^2 = 0.05$. However, when we compare the cases with larger estimation error, our proposed MF-QIC eventually outperforms MMSE-soft-PIC while retaining much lower detection complexity.

The overall simulation results suggest that our proposed MF-QIC works well and it can effectively cope with the complex-valued interference which limits the performance of MIMO spatial multiplexing with MF detector. Furthermore, since it is robust against channel estimation error, it is a suitable approach for massive IoT networks in view of the trade-off between the error rate performance and computational complexity.

3.8 Conclusion

In this chapter, we have proposed a low-complexity MF detector combined with quadrature interference cancellation (QIC) in coded uplink multiuser MIMO systems. We have developed a polar code design tailored for MF-QIC, and demonstrated that the proposed MF-QIC system

can significantly outperform the conventional MMSE detector with significantly lower *per user* complexity with strong robustness against CSI error. Our system relies on the ideal scheduling assumption that the average signal power received from simultaneously connecting IoT devices should be balanced. This assumption is critical as the average error rate performance is significantly affected by the worst-case user suffering from severe path loss. Therefore, a scheduling algorithm that forms each group of IoT devices with equivalent path loss should be established, which is left as future work.

Chapter 4
Scaling Matched-Filter Detector for MIMO Spatial Modulation

In this chapter, we propose a scaling MF detector optimized for coded MIMO spaital modulation systems.

Published as:
Y. Hama and H. Ochiai, " Performance of Coded MIMO Spatial Modulation with Scaling Matched-Filter Detector, " *IEEE GLOBECOM,* Taipei, Taiwan, Dec. 2020.

4.1 Introduction

Multiple-input multiple-output (MIMO) techniques play an essential role in current wireless communications systems due to their ability in increasing spectral efficiency as well as energy efficiency without exploiting additional frequency resources [22]. More recently, massive MIMO cellular systems where each base station (BS) is equipped with a large number of antennas have become major candidates for their potential in boosting their achievable capacity and reliability [16]. However, there are several practical issues associated with their implementation such as high computational complexity for signal processing as well as increasing hardware complexity associated with radio frequency (RF) components.

Spatial modulation (SM) introduced by Mesleh *et al.* [23] is an attractive transmission technique for MIMO systems due to its low inter-channel interference (ICI) as well as low hardware complexity. Therefore, SM has significant implementation advantages over the conventional MIMO schemes such as spatial multiplexing and beamforming systems, especially when the number of antenna elements is large. In recent work, a feasible SM system for massive MIMO is investigated [75]. Furthermore, many advanced SM schemes are proposed and their performances are compared in terms of capacity [24]. On the other hand, many challenges still remain for practical design of SM, among which is the design of SM systems combined with channel coding. In recent wireless communications systems, powerful capacity-approaching channel

codes are adopted, e.g., low-density parity-check (LDPC) code and polar code in 5G NR. They make use of a soft output from MIMO detector as their decoder input, and their performance depends on the accuracy of the soft output [76]. Therefore, in this chapter, we focus on a design of *coded* SM system where such powerful channel coding techniques are applicable.

Many theoretical studies on SM are based on the assumption of maximum likelihood (ML) detection [24, 77]. However, its main drawback is high computational complexity. In fact, practical MIMO systems often adopt low-complexity linear detection techniques such as minimum mean square error (MMSE). Sub-optimal detectors have also been proposed for SM but most of them still involve complex joint detection of active index and transmit symbols.

Motivated by the above background, we focus on the sub-optimal but low-complexity SM system based on MF detector, as was initially proposed in [23]. It first estimates the antenna index used by symbol transmission, and then demodulates the symbol on the estimated index. Since it detects the indices and symbols separately, it can be implemented with significantly lower complexity compared to ML detector. However, the detector proposed in [23] may not be directly applicable to the coded SM system. Hence, in this chapter, we focus on the *scaling* MF detector upon estimating the correct index [78, 79]. The original studies on the scaling MF detector were limited to uncoded SM systems. Therefore, in this chapter, based on mathematical analysis we derive soft-output metrics of scaling MF detector. The computer simulation results employing LDPC code verify the effectiveness of our proposed approach.

This chapter is organized as follows. Section 4.2 describes the system model of MIMO SM. The statistical properties of scaling MF detector output for SM are studied in Section 4.3, followed by its extension to coded system in Section 4.4. Extensive simulations are presented in Section 4.5, and Section 4.6 concludes this chapter.

4.2 System and Channel Models

In this chapter, we consider a single user $N_t \times N_r$ MIMO system with spatial modulation, where N_t and N_r denote the numbers of antennas at the transmitter and receiver, respectively. Note that we omit the symbol index l in (1.8) to focus on the lth transmit symbol through MIMO channel. For each symbol time slot, a single symbol is transmitted by selecting one antenna. Let $\mathbf{s} = (s_1, s_2, \cdots, s_{N_t})^T \in \mathbb{C}^{N_t \times 1}$ denote a transmit symbol vector. When the mth antenna is activated by the index modulation with $m \in \{1, 2, \cdots, N_t\}$, the resulting symbol vector is expressed as $\mathbf{s} = (0, \cdots, 0, s_m, 0, \cdots, 0)^T$.

Suppose that each symbol is modulated by M-ary PSK or QAM, and then transmitted over

one of N_t antennas. The total number of bits carried by one symbol transmission is expressed as $B = \log_2(N_t M) = B_{\text{id}} + B_{\text{sb}}$ where $B_{\text{id}} = \log_2 N_t$ is the number of bits carried by the index and $B_{\text{sb}} = \log_2 M$ is the number of bits carried by each modulated symbol, provided that N_t and M are integer powers of two. Let $(\mathbf{b}\,\mathbf{d}) \in \{0,1\}^B$ denote the binary symbol vector transmitted by this process, with $\mathbf{b} \in \{0,1\}^{B_{\text{id}}}$ representing the binary subvector that indicates the selected antenna index and $\mathbf{d} \in \{0,1\}^{B_{\text{sb}}}$ representing the binary subvector determined by the symbol transmitted on the selected antenna. Then the transmitted symbol is expressed as

$$\begin{cases} m = g(\mathbf{b}), \\ s_m = f(\mathbf{d}), \end{cases} \tag{4.1}$$

where $g : \{0,1\}^{B_{\text{id}}} \to \{1,2,\cdots,N_t\}$ is the mapping function corresponding to index modulation, and $f : \{0,1\}^{B_{\text{sb}}} \to \mathcal{X}$ is the symbol mapping function with $\mathcal{X}$ representing a set of PSK or QAM constellation points.

The received symbol vector, denoted by $\mathbf{r} \in \mathbb{C}^{N_r \times 1}$, is expressed as

$$\mathbf{r} = \mathbf{H}\mathbf{s} + \mathbf{n}, \tag{4.2}$$

where $\mathbf{n} = (n_1, n_2, \cdots, n_{N_r})^T \in \mathbb{C}^{N_r \times 1}$ is an additive white Gaussian noise (AWGN) vector and $\mathbf{H} = [\mathbf{h}_1\,\mathbf{h}_2\,\cdots\,\mathbf{h}_{N_t}] \in \mathbb{C}^{N_r \times N_t}$ is a channel matrix with its column vector $\mathbf{h}_k = (h_{1,k}, h_{2,k}, \cdots, h_{N_r,k})^T$ corresponding to the channel of the kth transmit antenna.

Throughout this chapter, we make the following assumptions for simplicity of analysis: The transmit symbol $\{s_m\}$ is modulated by M-PSK or M-QAM signaling, and each element n_i of the noise vector $\mathbf{n}$ follows an independent and identically distributed (i.i.d.) circularly symmetric complex Gaussian random variable with zero mean and variance $\sigma_n^2 = N_0$ *per complex* dimension, i.e., $n_i \sim \mathcal{CN}(0, N_0)$. Also, the channel is modeled as Rayleigh fading and thus each element of the channel matrix $\mathbf{H}$ is an i.i.d. circularly symmetric complex Gaussian random variable with zero mean and unit variance, i.e., $h_{i,k} \sim \mathcal{CN}(0,1)$. Therefore, $E\left\{|h_{i,k}|^2\right\} = 1$ for any pair of $i \in \{1,2,\cdots,N_r\}$ and $k \in \{1,2,\cdots,N_t\}$, where $E\{\cdot\}$ denotes expectation operation.

Let E_s denote the average energy *per receive antenna*, where the transmit energy is also equal to E_s, as we assume that the path loss is normalized to unity. Finally, the perfect channel state information (CSI) is available at the receiver, whereas the transmitter does not have any CSI.

4.3 MF Detector for Spatial Modulation

At the receiver, we adopt the matched-filter (MF) detector for MIMO symbol detection.

4.3.1 MF Detector

Let the vector $\hat{\mathbf{s}} = (\hat{s}_1, \hat{s}_2, \cdots, \hat{s}_{N_t})^T \in \mathbb{C}^{N_t \times 1}$ denote the output of a linear detector, which is in general given by

$$\hat{\mathbf{s}} = \mathbf{W}^{\mathrm{H}}\mathbf{r}, \tag{4.3}$$

where $\mathbf{W} = [\mathbf{w}_1, \mathbf{w}_2, \cdots, \mathbf{w}_{N_t}] \in \mathbb{C}^{N_r \times N_t}$ is the weight matrix and $\mathbf{w}_k = (w_{1,k}, w_{2,k}, \cdots, w_{N_r,k})^T$ is the weight vector corresponding to the kth transmit antenna, with $\mathbf{X}^{\mathrm{H}}$ representing the Hermitian transpose of a matrix $\mathbf{X}$. In the case of MF detector, the weight matrix is given by $\mathbf{W}^{\mathrm{H}} = \mathbf{H}^{\mathrm{H}}$, or equivalently, $\mathbf{w}_k = \mathbf{h}_k$ for all k.

Assuming that the mth transmit antenna is active, from (4.2) and (4.3), the estimated symbol vector based on MF detection is written by

$$\hat{\mathbf{s}} = \mathbf{W}^{\mathrm{H}}\left(\mathbf{h}_m s_m + \mathbf{n}\right) = \mathbf{H}^{\mathrm{H}}\mathbf{h}_m s_m + \mathbf{H}^{\mathrm{H}}\mathbf{n}, \tag{4.4}$$

or equivalently,

$$\begin{aligned} \hat{s}_k &= \mathbf{h}_k^{\mathrm{H}}\mathbf{h}_m s_m + \mathbf{h}_k^{\mathrm{H}}\mathbf{n} \\ &= \begin{cases} \alpha_m N_r s_m + \displaystyle\sum_{i=1}^{N_r} h_{i,m}^* n_i & (k = m), \\ \displaystyle\sum_{i=1}^{N_r} h_{i,k}^* \left(h_{i,m} s_m + n_i\right) & (k \neq m). \end{cases} \end{aligned} \tag{4.5}$$

The first term at the top of (4.5) is a scaled version of the transmit signal s_m, where the attenuation factor α_k corresponding to kth transmit antenna is defined as

$$\alpha_k \triangleq \frac{1}{N_r}\sum_{i=1}^{N_r} |h_{i,k}|^2 = \frac{1}{N_r}\left\|\mathbf{h}_k\right\|^2. \tag{4.6}$$

Note that α_k is a random variable that follows chi-square distribution with its expectation normalized as $E\{\alpha_k\} = 1$.

Conditioned on $\mathbf{h}_k$, the MF output $\hat{s}_k$ follows complex Gaussian distribution [61] with its mean and variance given by

$$E\left\{\hat{s}_k \,|\, \mathbf{h}_k\right\} = \begin{cases} \alpha_m N_r s_m & (k=m), \\ 0 & (k \neq m), \end{cases} \tag{4.7}$$

$$\text{VAR}\left(\hat{s}_k \,|\, \mathbf{h}_k\right) = \begin{cases} \alpha_m N_r N_0 & (k=m), \\ \alpha_k N_r \left(E_s + N_0\right) & (k \neq m). \end{cases} \tag{4.8}$$

In other words, $\hat{s}_k$ can be modeled as complex Gaussian, i.e., $\hat{s}_m \sim \mathcal{CN}\left(\alpha_m N_r s_m, \alpha_m N_r N_0\right)$ for active index m, and $\hat{s}_k \sim \mathcal{CN}\left(0, \alpha_k N_r (E_s + N_0)\right)$ for inactive index $k \neq m$. Therefore, conditioned on $x \triangleq s_k$ and α_k, the probability density function (pdf) of the complex-valued random variable $y \triangleq \hat{s}_k$ is given by

$$p_{\hat{s}_k|s_k}\left(y \,|\, x, \alpha_k\right) = \begin{cases} \dfrac{1}{\pi \alpha_m N_r N_0} e^{-\frac{|y-\alpha_m N_r x|^2}{\alpha_m N_r N_0}} & (k=m), \\ \dfrac{1}{\pi \alpha_k N_r \left(E_s + N_0\right)} e^{-\frac{|y|^2}{\alpha_k N_r (E_s+N_0)}} & (k \neq m). \end{cases} \tag{4.9}$$

4.3.2 Scaling MF Detector

We consider a low-complexity estimator of the active index m of transmit antenna from the MF output $\hat{s}_k$. Instead of working on the MF output $\hat{s}_k$ directly for index selection, it is convenient to define a *scaling* MF output as

$$\tilde{s}_k \triangleq \frac{\hat{s}_k}{\sqrt{\alpha_k}}. \tag{4.10}$$

Then, we have the following property:

Theorem 2. *For a given active index m and any inactive index ℓ (i.e., $\ell \neq m$), if the noise is negligible, the following inequality holds for any realization of channel matrix $\mathbf{H}$:*

$$\left|\tilde{s}_m\right| \geq \left|\tilde{s}_\ell\right|, \quad \textit{for any } \ell \neq m. \tag{4.11}$$

Proof. For any realization of the channel matrix $\mathbf{H}$, it is sufficient to show that

$$\left|\tilde{s}_m\right|^2 - \left|\tilde{s}_\ell\right|^2 \geq 0. \tag{4.12}$$

Under the assumption that the noise is negligible, i.e., $N_0 \to 0$, from (4.5), the squared value of the scaling MF output in (4.10) provided that the antenna m was selected, is expressed as

$$|\tilde{s}_m|^2 = \left(\frac{|\hat{s}_m|}{\sqrt{\alpha_m}}\right)^2 = \frac{{\alpha_m}^2 {N_r}^2}{\alpha_m} |s_m|^2 = \alpha_m {N_r}^2 |s_m|^2 , \tag{4.13}$$

$$|\tilde{s}_\ell|^2 = \left(\frac{|\hat{s}_\ell|}{\sqrt{\alpha_\ell}}\right)^2 = \frac{\left(\sum_{i=1}^{N_r} \left|h_{i,\ell}^*\right| |h_{i,m}|\right)^2}{\alpha_\ell} |s_m|^2 . \tag{4.14}$$

Substituting (4.13) and (4.14) into the left-hand side of (4.12) and noticing that $|h_{i,\ell}^*| = |h_{i,\ell}|$, we have

$$\begin{aligned} &\left\{ \alpha_\ell \alpha_m {N_r}^2 - \left(\sum_{i=1}^{N_r} |h_{i,\ell}| \, |h_{i,m}| \right)^2 \right\} \frac{|s_m|^2}{\alpha_\ell} \\ &= \left\{ \left(\sum_{i=1}^{N_r} |h_{i,\ell}|^2 \right) \left(\sum_{i=1}^{N_r} |h_{i,m}|^2 \right) - \left(\sum_{i=1}^{N_r} |h_{i,\ell}| \, |h_{i,m}| \right)^2 \right\} \frac{|s_m|^2}{\alpha_\ell} \\ &\geq 0, \end{aligned} \tag{4.15}$$

where the last inequality is due to Cauchy–Schwarz inequality. □

Note that without scaling [77], the relationship in Theorem 2 does not hold in general.

Theorem 2 allows us to determine the estimated index $\hat{m}$ according to

$$\hat{m} = \arg \max_{k \in \{1,2,\cdots,N_t\}} |\tilde{s}_k| . \tag{4.16}$$

By defining the inverse mapping of g as $g^{-1} : \{1, 2, \cdots, N_t\} \to \{0, 1\}^{B_{\mathrm{id}}}$ and the constellation demapping function as f^{-1}, the estimated binary subvectors are given by

$$\begin{cases} \hat{\mathbf{b}} = g^{-1}(\hat{m}) \\ \hat{\mathbf{d}} = f^{-1}(\tilde{s}_{\hat{m}}) . \end{cases} \tag{4.17}$$

The output of the scaling MF, $\tilde{s}_k$, also follows Gaussian distribution as $\tilde{s}_m \sim \mathcal{CN}\left(\sqrt{\alpha_m} N_r s_m, N_r N_0\right)$ for active index m, and $\tilde{s}_k \sim \mathcal{CN}(0, N_r(E_s + N_0))$ for inactive in-

Table 4.1: Complexity comparison of scaling MF and ML detector in parallel architecture.

detector	complex multiplication
scaling MF	$2N_r$
ML	$2N_rN_t + N_tM + M$

dex $k \neq m$, i.e.,

$$p_{\tilde{s}_k|s_k}(y \mid x, \alpha_m) = \begin{cases} \dfrac{1}{\pi N_r N_0} e^{-\frac{1}{N_r N_0}|y-\sqrt{\alpha_m}N_r x|^2} & (k = m), \\ \dfrac{1}{\pi N_r (E_s + N_0)} e^{-\frac{1}{N_r(E_s+N_0)}|y|^2} & (k \neq m). \end{cases} \tag{4.18}$$

Note that the pdf of the *scaling* MF output for inactive index is independent of α_k as shown in (4.18).

We briefly discuss the uncoded BER performance of scaling MF detector with M-PSK signaling based on the simulation results shown in Fig. 4.1, where the numbers of antennas are fixed as $N_t = N_r = 4$. For comparison, that of ML detector is shown with points in the same figure. For uncoded cases, the scaling MF detector can approach ML performance with the increase of modulation order M. The reason for this is that the error event of the index bits does not depend on the modulation order M. Thus, their performance matches well especially in high signal-to-noise ratio (SNR) region since MF detector is equivalent to ML detector when ICI is negligible [61].

In the case of BPSK, the performance can be improved when the real value of the scaling MF output in (4.16) is applied:

$$\hat{m} = \arg \max_{k \in \{1,2,\cdots,N_t\}} |\Re\{\tilde{s}_k\}|, \tag{4.19}$$

since the noise power is reduced by half. Note that we have focused only on PSK signaling in Fig. 4.1, as QAM signaling may not perform well as will be described in Section 4.5.

4.3.3 Complexity

We summarize the computational complexity of scaling MF detector compared with ML detector in Table 4.1 where MF detector is implemented in parallel. Note that ML detector should estimate two subvectors $\mathbf{b}$ and $\mathbf{d}$ jointly, i.e., they cannot be detected in parallel. On the other hand, the calculation of MF detector given in (4.3) can be implemented in parallel. Therefore,

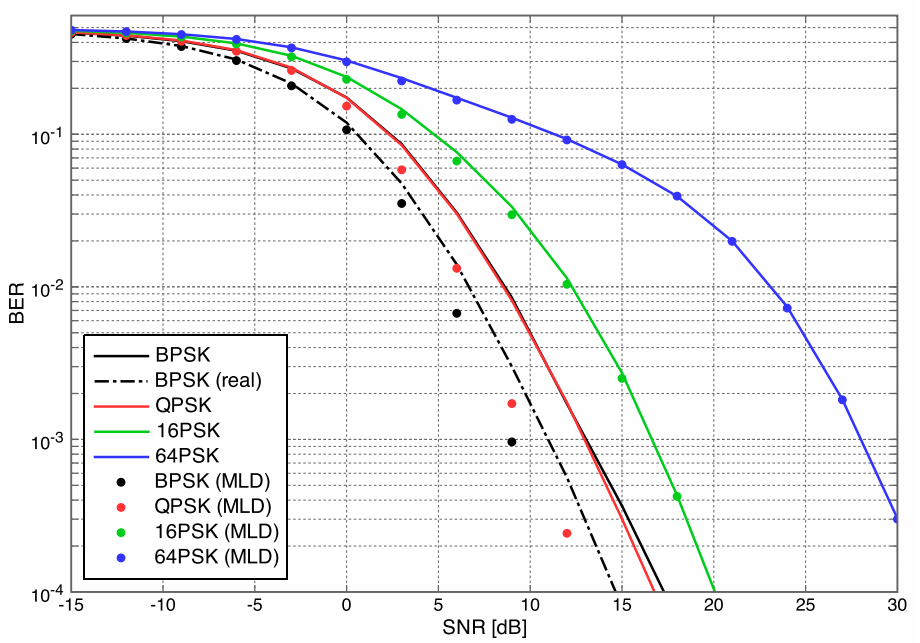

Figure 4.1: The comparison of BER performance with scaling MF and ML detectors in uncoded 4×4 MIMO system over i.i.d. Rayleigh fading channel as a function of SNR *per receive antenna*.

the required complex multiplication operation per single MF detector of (4.5) becomes $2N_r$ even with scaling, which is independent of the number of information bits $B = \log_2(N_t M)$. Nevertheless, its performance becomes comparable with ML detector with increasing B, as was observed in Fig. 4.1. This fact motivates us to employ scaling MF detector along with SM.

4.4 Extension to Coded System

In this section, we derive the optimal metric with PSK signaling based on the theoretical analysis of MF detector for channel coding. Our proposed system is sub-optimal due to the fact that we separately estimate coded bits corresponding to index part and symbol part. Therefore, the corresponding metrics are developed separately as well.

In order to apply modern error correcting codes such as LDPC codes, it is necessary to calculate the log-likelihood ratio (LLR) of coded bits. We first describe the LLR corresponding to the symbol part $\hat{\mathbf{d}}$ in (4.17). Let $\mathbf{d} = (d_1, d_2, \cdots, d_{B_{\mathrm{sb}}})$ denote the subvector of the transmitted symbol. It is calculated from the pdf of scaling MF output (4.18) corresponding to the estimated

index $\hat{m}$ as [61]

$$\begin{aligned}\lambda\left(d_\ell\right) &= \log \frac{P\left(d_\ell = 0|\tilde{s}_{\hat{m}}\right)}{P\left(d_\ell = 1|\tilde{s}_{\hat{m}}\right)} \\ &= \log \frac{\sum_{\mathcal{S}\in(d_\ell=0)} p_{\tilde{s}_m|s_m}\left(y = \tilde{s}_{\hat{m}} \,|\, x = \mathcal{S}, \alpha_m\right)}{\sum_{\mathcal{S}\in(d_\ell=1)} p_{\tilde{s}_m|s_m}\left(y = \tilde{s}_{\hat{m}} \,|\, x = \mathcal{S}, \alpha_m\right)}.\end{aligned} \tag{4.20}$$

In what follows, we derive the LLR expressions corresponding to the index part $\hat{\mathbf{b}}$ in (4.17). To this end, we introduce two types of metrics. One is based on the distribution of scaling MF output described in Section 4.3, and it is optimal for PSK signaling. The other is based on the use of the absolute value given by (4.16). This is sub-optimal but can be applied to multiple amplitude modulation schemes such as QAM signaling.

4.4.1 Distribution of the Absolute Value of Scaling MF Output

In order to derive the LLR corresponding to the index bits, the distribution of the absolute value of the scaling MF output $|\tilde{s}_k|$ from (4.16) is required. As discussed in Section 4.3, it follows Gaussian distribution given in (4.18). As a consequence, their absolute value corresponding to the active index follows Rice distribution, whereas that corresponding to the inactive index follows Rayleigh distribution. Therefore, their pdfs are expressed by [50]

$$p_{|\tilde{s}_m|}\left(x, \alpha_m\right) = \frac{2x}{N_r N_0} e^{-\frac{x^2 + \alpha_m {N_r}^2 E_s}{N_r N_0}} I_0\left(\frac{2\sqrt{\alpha_m E_s}x}{N_0}\right), \tag{4.21}$$

$$p_{|\tilde{s}_k|}\left(x\right) = \frac{2x}{N_r\left(E_s + N_0\right)} e^{-\frac{x^2}{N_r(E_s+N_0)}}, \tag{4.22}$$

where $I_0\left(x\right)$ is the modified Bessel function of the first kind with order 0.

In the case of BPSK signaling, the scaling output $\tilde{x}_k = \Re\{\tilde{s}_k\}$ follows folded Gaussian distribution, and its pdf is expressed as

$$\begin{aligned}p_{|\tilde{x}_m|}\left(x|\alpha_m\right) = &\frac{1}{\sqrt{\pi\alpha_m N_r N_0}} e^{-\frac{1}{\alpha_m N_r N_0}\left(x - \sqrt{\alpha_m} N_r \sqrt{E_s}\right)^2} \\ &+ \frac{1}{\sqrt{\pi\alpha_m N_r N_0}} e^{-\frac{1}{\alpha_m N_r N_0}\left(x + \sqrt{\alpha_m} N_r \sqrt{E_s}\right)^2},\end{aligned} \tag{4.23}$$

$$p_{|\tilde{x}_k|}\left(x\right) = \frac{2}{\sqrt{\pi N_r(E_s + N_0)}} e^{-\frac{1}{N_r(E_s+N_0)}x^2}. \tag{4.24}$$

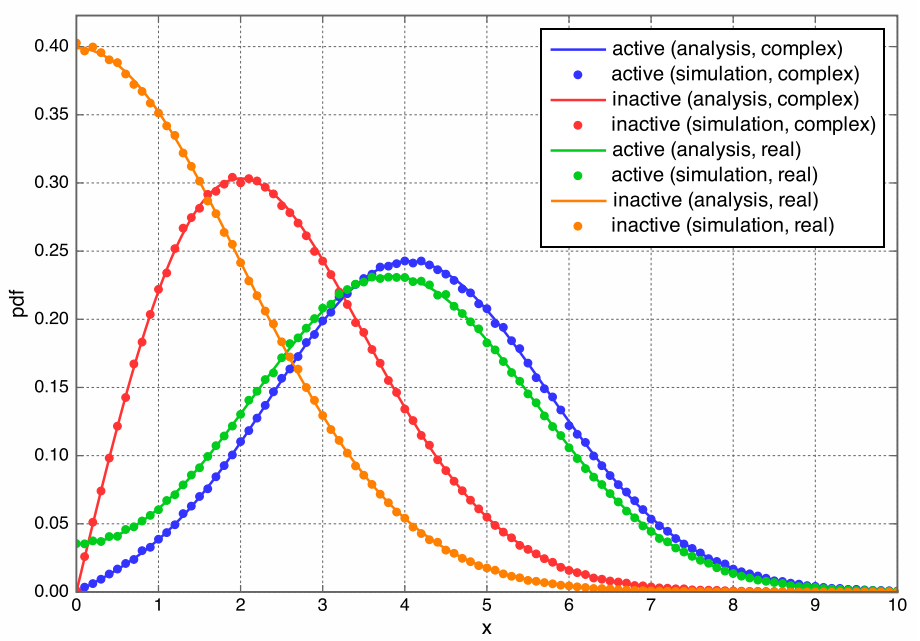

Figure 4.2: Comparison of pdfs of scaling MF detector output calculated by theoretical expressions as well as Monte-Carlo simulations with BPSK signaling ($E_s = 1$ and $\gamma_b = 0$ dB).

Example pdfs of the scaling MF output obtained by analysis and simulation are compared in Fig. 4.2, where we observe that the two results match perfectly.

Note that the above expressions may not be directly applicable to QAM signaling as their symbol amplitude is not constant.

4.4.2 Optimal LLR Metric for Index Bits (Type-1)

We derive the LLR corresponding to the index part as a metric input to the channel decoder. First, we propose a metric derived from (4.21) and (4.22), which will be referred to as type-1 in what follows.

Assuming that the selected antenna index is m, the posterior probability can be defined for a set of scaling MF outputs $\{\tilde{s}_k\}$ as

$$P_m \triangleq p_{|\tilde{s}_m|}\left(|\tilde{s}_m|, \alpha_m\right) \prod_{k=1, k\neq m}^{N_t} p_{|\tilde{s}_k|}(|\tilde{s}_k|). \tag{4.25}$$

Let $\mathbf{b} = (b_1, b_2, \cdots, b_{B_{\text{id}}})$ denote the subvector of the index and $\mathbf{b}(m) = g^{-1}(m) = (b_{m,1}, b_{m,2}, \cdots, b_{m,B_{\text{id}}})$ denote the specific subvector value corresponding to the antenna index

m. The LLR of the lth bit of $\mathbf{b}$ with $\ell \in \{1, 2, \cdots, B_{\text{id}}\}$ is expressed as

$$\lambda^{\text{Type-1}}(b_\ell) = \log \frac{\sum_{m=1, b_{m,\ell}=0}^{N_t} P_m}{\sum_{m=1, b_{m,\ell}=1}^{N_t} P_m}. \tag{4.26}$$

4.4.3 Sub-Optimal LLR Metric for Index Bits (Type-2)

The type-1 metric (4.26) calculates all the posterior probabilities corresponding to the transmit antennas. We also propose a simple metric using only the absolute value of the scaling MF output $\tilde{s}_k$, which we refer to as type-2. It is expressed as

$$\lambda^{\text{Type-2}}(b_\ell) = \log \frac{\sum_{m=1, b_{m,\ell}=0}^{N_t} |\tilde{s}_m|}{\sum_{m=1, b_{m,\ell}=1}^{N_t} |\tilde{s}_m|}. \tag{4.27}$$

Since (4.27) does not consider the distribution of the posterior probability, its performance is inferior to that of (4.26). Nevertheless, since (4.27) does not take modulation constraint into account, it is applicable to QAM.

4.5 Simulation Results

In this section, we demonstrate the uncoded and coded performance of the scaling MF detector with our derived metrics through computer simulation. The channel is assumed to be ideally interleaved Rayleigh fading in all the simulations for simplicity. The regular binary $(3, 6)$ LDPC code (with code rate $R_c = 1/2$) is chosen as our channel code with the codeword length $N_c = 1024$. For LDPC decoder, the sum-product algorithm is employed with the maximum number of iterations given by 100.

4.5.1 Comparison of Metrics

We examine the coded performance by using the two types of metrics based on Monte-Carlo simulations. The results are compared in Fig. 4.3 with 4×4 MIMO SM. For the 16-PSK signaling, the performance of type-1 metric outperforms that of type-2 due to its accuracy in the mathematical model. On the other hand, in the case of 16-QAM signaling, its symbol power depends on the constellation point and thus type-1 metric becomes inaccurate, resulting in significant performance degradation. As a reference, we also show the performance in the case of 64-PSK with type-1 and 64-QAM signaling with type-2 in Fig 4.3. With the increase of M,

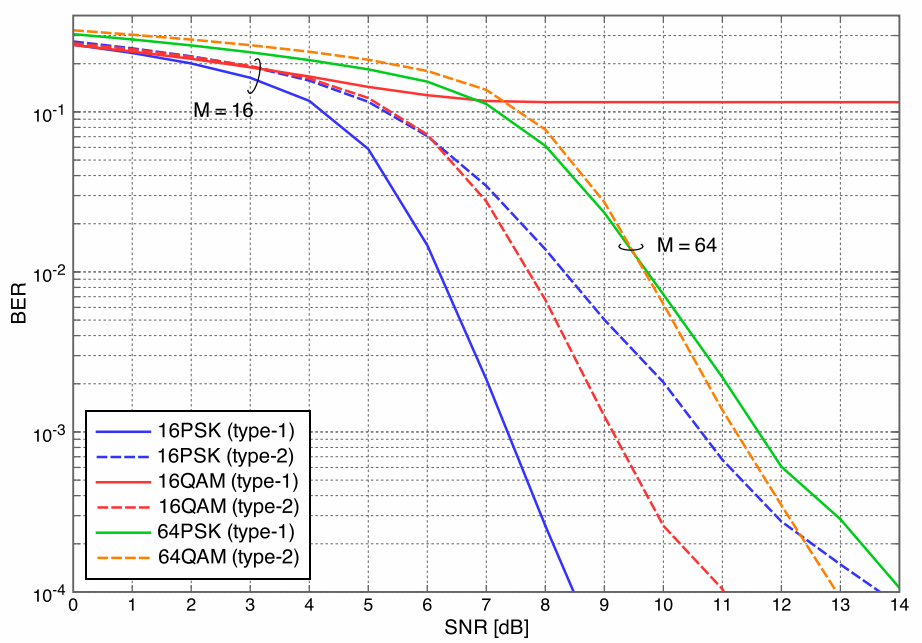

Figure 4.3: The coded BER performance of scaling MF detector in 4×4 MIMO SM system with PSK and QAM signaling over a Rayleigh fading channel.

the performance with PSK signaling becomes inferior due to the smaller minimum Euclidean distance of constellation points compared to that of QAM. However, when M is equal to 64 or less, the coded performance of M-PSK signaling shows good performance resulting from the advantage associated with optimality of type-1 metric.

For the rest of this chapter, we exclusively study the performance of M-PSK signaling. In Fig. 4.4, we compare the coded performance using the optimal metrics given by (4.20) and (4.26). We set M as $2, 4, 16$, and 64 so that the spectral efficiency becomes $3, 4, 6$, and 8 (when uncoded), respectively, in 4×4 MIMO spatial modulation systems. With BPSK signaling, we also show the performance by using real-valued metric given by (4.19). Due to the trade-off between the spectral efficiency and energy efficiency, the BER performance degrades as the modulation order M increases.

4.5.2 Performance Comparison under Fixed Spectral Efficiency

As an example, we compare the BER performance for a fixed spectral efficiency of $B = 8$ bits per SM symbol achieved by combination of a different number of transmit antennas N_t and modulation order M. The results without channel coding are shown in Fig. 4.5. From these results, we observe that the system with $N_t = 128$ and $M = 2$ achieves the best performance.

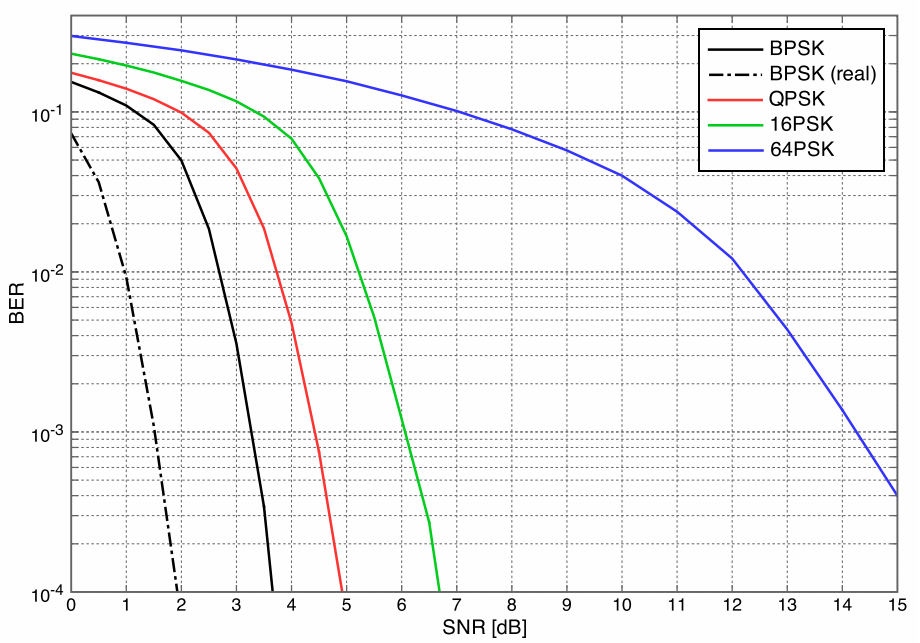

Figure 4.4: The coded BER performance of scaling MF detector in 4×4 MIMO system with M-PSK signaling over a Rayleigh fading channel.

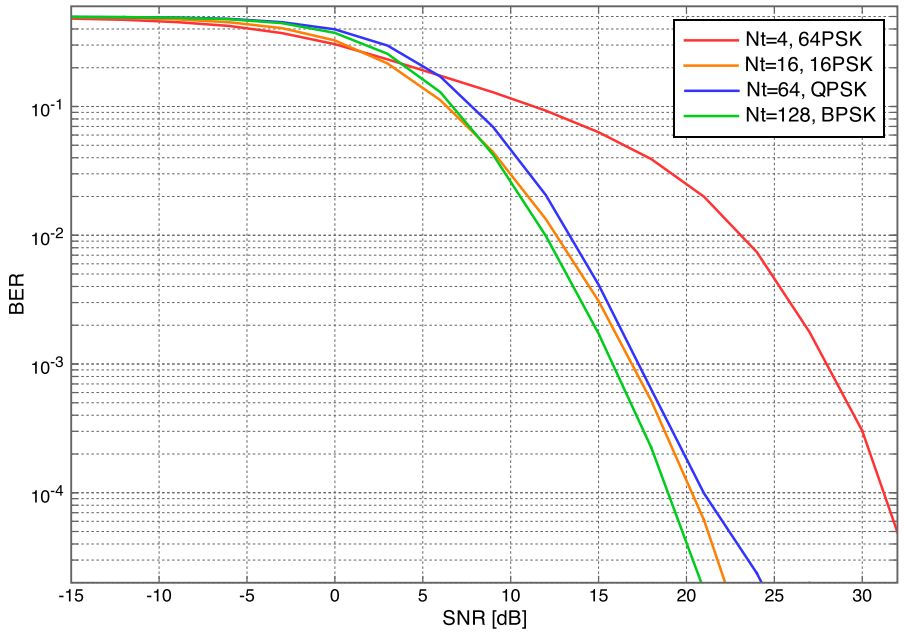

Figure 4.5: The uncoded BER performance of scaling MF detector in $N_t \times 4$ MIMO system with M-PSK signaling over a Rayleigh fading channel. (Spectral efficiency is 8 bit/SM symbol.)

This is because the noise power is successfully reduced by the proposed real-valued metric for index estimation.

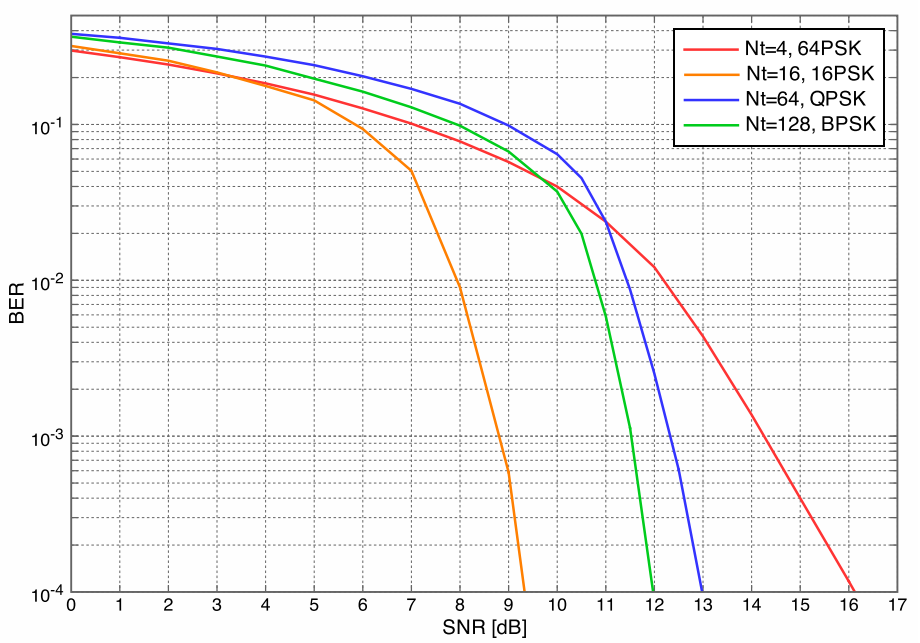

Figure 4.6: The coded BER performance of scaling MF detector in $N_t \times 4$ MIMO system with M-PSK signaling over a Rayleigh fading channel. (Spectral efficiency considering code rate $R_c = 1/2$ is 4 bit/SM symbol.)

The performance with channel coding is compared in Fig. 4.6. Since the channel coding reduces the operating SNR, the performance in low SNR region becomes of interest. In this case, however, due to the sub-optimality of our detector, the index error becomes dominant and thus the results are different from Fig. 4.5.

To further investigate the effect of index error, in Fig. 4.7 we separately plot the uncoded BER performance of index and symbol bits. The dot curves in the figure represent the ideal cases when the index is estimated correctly, and the lower modulation order M shows better performance in this respect. However, since lower modulation order M also leads to a larger number of transmit antennas N_t to achieve the target rate, it causes higher BER resulting from the index bit errors. In summary, there is a trade-off between the number of transmit antennas N_t and modulation order M, and the optimal parameter should be chosen based on the balance between the error events of index and symbol bits.

4.6 Conclusion

We have focused on the coded MIMO spatial modulation system with scaling MF detector, and proposed metrics for channel coding based on the mathematical analysis. Throughout

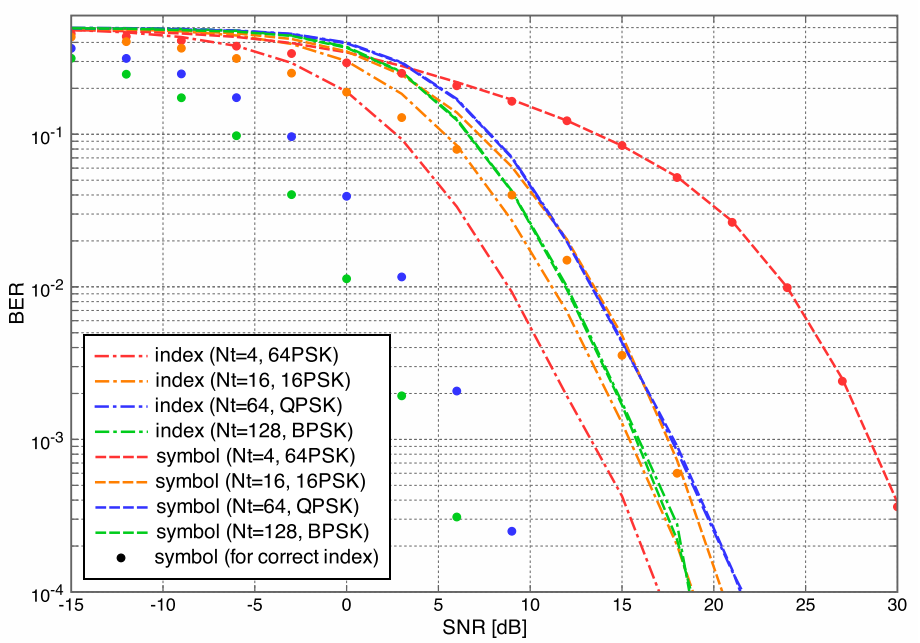

Figure 4.7: The uncoded BER performance of scaling MF detector in $N_t \times 4$ MIMO system corresponding to index and symbol bits with M-PSK signaling over a Rayleigh fading channel. (Spectral efficiency is 8 bit/SM symbol.)

computer simulations, we have demonstrated the trade-off relationship between the number of transmit antennas and modulation order.

Chapter 5

Conclusions

In this dissertation, we have analyzed the statistical property of MF detector over uncorrelated Rayleigh fading channel. Based on the obtained theoretical results, we have designed low-complexity detections based on MF detector for coded MIMO systems. The main focus of this dissertation has been on the two MIMO transmission schemes, spatial multiplexing and spatial modulation, which can be integrated by introducing generalized spatial modulation.

5.1 Summary and Contributions

Our proposal and contributions are summarized as follows:

Chapter 2

MF detector has recently been with much attention due to the advent and utilization of massive MIMO provoked by [16], where MF detector has been introduced as maximum ratio combining (MRC) for uplink transmission. The author of [16] has also derived the achievable performance of MRC with single cell massive MIMO systems, where the BS equips a large number of antennas. However, it has been limited to the case with the unlimited number of the receiving BS antennas. Furthermore, the resulting performances were derived only in the form of the capacity based on the average SINR. In other words, this analysis is insufficient since it does not consider the modulation constellation as well as the distribution of the SINR. Motivated by this fact, in Chapter 2, we have analyzed the exact distribution of the MF output corresponding to M-PSK and M-QAM signaling with an arbitrary number of antennas at both the transmitter and receiver. Based on this result, we have also derived the constellation constrained mutual information as an ideally achievable performance with the finite number of antennas and input alphabet. In addition, it enables the optimization of the decoding metric in terms of LLR and derivation of the exact BER performance for coded and uncoded MIMO spatial multiplexing systems, respectively.

Chapter 3

In spatial multiplexing systems, massive access by low-cost devices requires high power amplifier efficiency as well as high computational complexity at the receiver. Also, it may cause imperfect channel estimation due to the lack of orthogonal pilot sequences. Thus, it is necessary to be established a signal detection approach with high resistance for channel estimation errors. In order to tackle this problem, we have proposed a new IC technique, namely quadrature interference cancellation, optimized for MF detector. In practice, we have demonstrated the achievable performances of polar coded MF-QIC, where the code design criteria and approximated BLER performance for polar codes have also been introduced based on Gaussian approximation construction. The computer simulation has revealed that it outperforms other competing approaches such as MMSE and BP detectors even with lower complexity order.

Chapter 4

For spatial modulation, the optimal detection can be implemented with lower complexity compared to that in spatial multiplexing due to sparsely of the transmit symbol vector. In contrast, it is difficult to apply the sub-optimal detector based on the low-complexity linear detection, which is widely used in the practical MIMO systems adopted in LTE and 5G. Based on this observation, the sub-optimal detector that can be applied to coded spatial modulation systems is urgently required. Based on the exact distribution of the MF output derived in Chapter 2, we have first applied the appropriate scaling to MF detector so that it can estimate the active index correctly. For coded spatial modulation systems, we have also derived the optimal decoding metric in terms of LLR for scaling MF detector. Furthermore, we have developed the simplified LLR expression for further complexity reduction.

5.2 Future Works

The following remaining subjects should be investigated as our future works:

- Extension of our proposed approaches to the practical channel, such as correlated Rayleigh as well as Rician channels, should be investigated.
- Combining with the transmission algorithm such as MRT (or CB) is also meaningful work since the transmitter in the recent wireless system often employs some multiple-antenna transmission schemes such as beamforming and diversity techniques.

Bibliography

[1] W. Jiang, B. Han, M. A. Habibi, and H. D. Schotten, "The road towards 6g: A comprehensive survey," *IEEE Open Journal of the Communications Society*, vol. 2, pp. 334–366, 2021.

[2] S. Henry, A. Alsohaily, and E. S. Sousa, "5g is real: Evaluating the compliance of the 3gpp 5g new radio system with the itu imt-2020 requirements," *IEEE Access*, vol. 8, pp. 42 828–42 840, 2020.

[3] V. Raghavan and J. Li, "Evolution of physical-layer communications research in the post-5g era," *IEEE Access*, vol. 7, pp. 10 392–10 401, 2019.

[4] Z. Zhang *et al.*, "6G wireless networks: Vision, requirements, architecture, and key technologies," *IEEE Veh. Technol. Mag.*, vol. 14, no. 3, pp. 28–41, 2019.

[5] W. Saad, M. Bennis, and M. Chen, "A vision of 6G wireless systems: Applications, trends, technologies, and open research problems," *IEEE Netw.*, vol. 34, no. 3, pp. 134–142, 2019.

[6] Q. Qi, X. Chen, C. Zhong, and Z. Zhang, "Integration of energy, computation and communication in 6g cellular internet of things," *IEEE Communications Letters*, vol. 24, no. 6, pp. 1333–1337, 2020.

[7] G. J. Foschini, "Layered space-time architecture for wireless communications in a fading environment when using multi-element antennas," *Bell Labs Tech. J.*, vol. 1, no. 2, pp. 41–59, Oct. 1999.

[8] D. J. Costello and G. D. Forney, "Channel coding: The road to channel capacity," *Proceedings of the IEEE*, vol. 95, no. 6, pp. 1150–1177, 2007.

[9] C. E. Shannon, "A mathematical theory of communication," *The Bell system technical journal*, vol. 27, no. 3, pp. 379–423, 1948.

[10] C. Berrou, A. Glavieux, and P. Thitimajshima, "Near shannon limit error-correcting coding and decoding: Turbo-codes," in *Proc. IEEE ICC*, May 1993.

[11] L. Bahl, J. Cocke, F. Jelinek, and J. Raviv, "Optimal decoding of linear codes for minimizing symbol error rate (corresp.)," *IEEE Transactions on information theory*, vol. 20, no. 2, pp. 284–287, 1974.

[12] R. G. Gallager, *Low-Density Parity Check Codes*. Cambridge, MA: MIT Press, 1963.

[13] D. J. MacKay, "Good error-correcting codes based on very sparse matrices," *IEEE transactions on Information Theory*, vol. 45, no. 2, pp. 399–431, 1999.

[14] S.-Y. Chung, G. D. Forney, T. J. Richardson, and R. Urbanke, "On the design of low-density parity-check codes within 0.0045 db of the shannon limit," *IEEE Communications letters*, vol. 5, no. 2, pp. 58–60, 2001.

[15] E. Arikan, "Channel polarization: A method for constructing capacity-achieving codes for symmetric binary-input memoryless channels," *IEEE Trans. Inf. Theory*, vol. 55, no. 7, pp. 3051–3073, 2009.

[16] T. L. Marzetta, "Noncooperative cellular wireless with unlimited numbers of base station antennas," *IEEE Trans. Wireless Commun.*, vol. 9, no. 11, pp. 3590–3600, Oct. 2010.

[17] F. Rusek *et al.*, "Scaling up MIMO: Opportunities and challenges with very large arrays," *IEEE Signal Process. Mag.*, Jan. 2013.

[18] S. M. Alamouti, "A simple transmit diversity technique for wireless communications," *IEEE Journal on selected areas in communications*, vol. 16, no. 8, pp. 1451–1458, 1998.

[19] V. Tarokh, N. Seshadri, and A. R. Calderbank, "Space-time codes for high data rate wireless communication: Performance criterion and code construction," *IEEE transactions on information theory*, vol. 44, no. 2, pp. 744–765, 1998.

[20] P. W. Wolniansky, G. J. Foschini, G. D. Golden, and R. A. Valenzuela, "V-BLAST: An architecture for realizing very high data rates over the rich-scattering wireless channel," in *Proc. IEEE URSI Int. Symp. Signals, Systems and Electron. (ISSSE'98)*, Sep. 1998.

[21] G. D. Golden, G. J. Foschini, R. A. Valenzuela, and P. W. Wolniansky, "Detection algorithm and initial laboratory results using V-BLAST space-time communication architecture," *Electronics Letters*, vol. 35, no. 1, pp. 14–16, Jan. 1999.

[22] I. E. Telatar, "Capacity of multi-antenna Gaussian channels," *Euro. Trans. Telecomm.*, vol. 10, no. 6, pp. 585–595, Nov. 1999.

[23] R. Y. Mesleh, H. Haas, S. Sinanovic, C. W. Ahn, and S. Yun, "Spatial modulation," *IEEE Trans. Veh. Technol.*, vol. 57, no. 4, pp. 2228–2241, Jul. 2008.

[24] N. Ishikawa, S. Sugiura, and L. Hanzo, "50 years of permutation, spatial and index modulation: From classic RF to visible light communications and data storage," *IEEE Commun. Surveys Tuts.*, vol. 20, no. 3, pp. 1903–1938, 2018.

[25] A. Younis, N. Serafimovski, R. Mesleh, and H. Haas, "Generalised spatial modulation," in *2010 conference record of the forty fourth Asilomar conference on signals, systems and computers*. IEEE, 2010, pp. 1498–1502.

[26] H. Q. Ngo, A. Ashikhmin, H. Yang, E. G. Larsson, and T. L. Marzetta, "Cell-free massive mimo versus small cells," *IEEE Transactions on Wireless Communications*, vol. 16, no. 3, pp. 1834–1850, 2017.

[27] J. Zhang, S. Chen, Y. Lin, J. Zheng, B. Ai, and L. Hanzo, "Cell-free massive MIMO: A new next-generation paradigm," *IEEE Access*, vol. 7, pp. 99 878–99 888, 2019.

[28] W. V. Etten, "Maximum likelihood receiver for multiple channel transmission systems," *IEEE Trans. Commun.*, vol. 24, no. 2, pp. 276–283, Feb. 1976.

[29] X. Zhu and R. D. Murch, "Performance analysis of maximum likelihood detection in a MIMO antenna system," *IEEE Trans. Commun.*, vol. 50, no. 2, pp. 187–191, Feb. 2002.

[30] A. Younis, S. Sinanovic, M. Di Renzo, R. Mesleh, and H. Haas, "Generalised sphere decoding for spatial modulation," *IEEE Transactions on Communications*, vol. 61, no. 7, pp. 2805–2815, 2013.

[31] E. Viterbo and J. Boutros, "A universal lattice code decoder for fading channels," *IEEE Trans. Inf. Theory*, vol. 45, no. 5, pp. 1639–1642, Jul. 1999.

[32] D. Wubben, R. Bohnke, B. Kuhn, and K. D. Kammeyer, "MMSE extension of V-BLAST based on sorted QR decomposition," in *Proc. IEEE 58th Veh. Technol. Conf. (VTC'03-Fall)*, Oct. 2003.

[33] K. V. Vardhan, S. K. Mohammed, A. Chockalingam, and B. S. Rajan, "A low-complexity detector for large MIMO systems and multicarrier CDMA systems," *IEEE J. Sel. Areas Commun.*, vol. 26, no. 3, pp. 473–485, Apr. 2008.

[34] D. G. Brennan, "Linear diversity combining techniques," *Proc. IEEE*, vol. 47, no. 6, pp. 1075–1102, Jun. 1959.

[35] S. Verdú, *Multiuser Detection*. Cambridge Univ. Press, 1998.

[36] M. Joham, W. Utschick, and J. A. Nossek, "Linear transmit processing in MIMO communications systems," *IEEE Trans. Signal Process.*, vol. 53, no. 8, pp. 2700–2712, Jul. 2005.

[37] S. Yang and L. Hanzo, "Fifty years of MIMO detection: The road to large-scale MIMOs," *IEEE Commun. Surveys Tuts.*, vol. 17, no. 4, pp. 1941–1988, Sep. 2015.

[38] H. Q. Ngo, E. G. Larsson, and T. L. Marzetta, "Energy and spectral efficiency of very large multiuser MIMO systems," *IEEE Trans. Commun.*, vol. 61, no. 4, pp. 1436–1449, Apr. 2013.

[39] E. Larsson, O. Edfors, F. Tufvesson, and T. Marzetta, "Massive MIMO for next generation wireless systems," *IEEE Commun. Mag.*, vol. 52, no. 2, pp. 186–195, Feb. 2014.

[40] L. Lu, G. Li, A. Swindlehurst, A. Ashikhmin, and R. Zhang, "An overview of massive MIMO: Benefits and challenges," *IEEE J. Sel. Topics Signal Process.*, vol. 8, no. 5, Oct. 2014.

[41] T. K. Y. Lo, "Maximum ratio transmission," *IEEE Trans. Commun.*, vol. 47, no. 10, pp. 1458–1461, Oct. 1999.

[42] P. Suthisopapan, K. Kasai, A. Meesomboon, and V. Imtawil, "Achieving near capacity of non-binary LDPC coded large MIMO systems with a novel ultra low-complexity soft-output detector," *IEEE Trans. Wireless Commun.*, vol. 12, no. 10, pp. 5185–5199, Oct. 2013.

[43] H. V. Poor and S. Verdú, "Probability of error in MMSE multiuser detection," *IEEE Trans. Inf. Theory*, vol. 43, no. 3, pp. 858–871, May 1997.

[44] Y. Jiang, M. K. Varanasi, and J. Li, "Performance analysis of ZF and MMSE equalizers for MIMO systems: An in-depth study of the high SNR regime," *IEEE Trans. Inf. Theory*, vol. 57, no. 4, pp. 2008–2026, Apr. 2011.

[45] P. Li, D. Paul, R. Narasimhan, and J. Cioffi, "On the distribution of SINR for the MMSE MIMO receiver and performance analysis," *IEEE Trans. Inf. Theory*, vol. 58, no. 11, pp. 271–286, Jan. 2006.

[46] P. Liu and I.-M. Kim, "Exact and closed-form error performance analysis for hard MMSE-SIC detection in MIMO systems," *IEEE Trans. Commun.*, vol. 59, no. 9, pp. 2463–2477, Sep. 2011.

[47] A. J. Al-Askery, C. C. Tsimenidis, S. Boussakta, and J. A. Chambers, "Performance analysis of coded massive MIMO-OFDM systems using effective matrix inversion," *IEEE Trans. Commun.*, vol. 65, no. 12, pp. 5244–5256, Dec. 2017.

[48] C. Feng, Y. Jing, and S. Jin, "Interference and outage probability analysis for massive MIMO downlink with MF precoding," *IEEE Signal Process. Lett.*, vol. 23, no. 3, pp. 366–370, Feb. 2016.

[49] S. Atapattu, P. Dharmawansa, C. Tellambura, and J. Evans, "Exact outage analysis of multiple-user downlink with MIMO matched-filter precoding," *IEEE Commun. Lett.*, vol. 21, no. 12, pp. 2754–2757, Dec. 2017.

[50] J. Proakis and M. Salehi, *Digital Communications*, 5th ed. McGral-Hill, 2008.

[51] D. Tse and P. Viswanath, *Fundamentals of Wireless Communications*. Cambridge University Press, 2005.

[52] H. Q. Ngo, M. Matthaiou, T. Q. Duong, and E. G. Larsson, "Uplink performance analysis of multicell MU-SIMO systems with ZF receivers," *IEEE Trans. Veh. Technol.*, vol. 62, no. 9, pp. 4471–4483, Nov. 2013.

[53] S. Jacobsson, G. Durisi, M. Coldrey, U. Gustavsson, and C. Studer, "Throughput analysis of massive MIMO uplink with low-resolution adcs," *IEEE Trans. Wireless Commun.*, vol. 16, no. 6, pp. 4038–4051, Jun. 2017.

[54] F. Jiang, C. Li, and Z. Gong, "Accurate analytical BER performance for ZF receivers under imperfect channel in low-SNR region for large receiving antennas," *IEEE Signal Process. Lett.*, vol. 25, no. 8, pp. 1248–1250, Aug. 2018.

[55] E. Biglieri, *Coding for Wireless Channels*. Springer, 2006.

[56] C. Wang, E. K. S. Au, R. D. Murch, W. H. Mow, R. S. Cheng, and V. Lau, "On the performance of the MIMO zero-forcing receiver in the presence of channel estimation error," *IEEE Trans. Wireless Commun.*, vol. 6, no. 3, pp. 805–810, Mar. 2007.

[57] M. A. Albreem, M. Juntti, and S. Shahabuddin, "Massive MIMO detection techniques: A survey," *IEEE Commun. Surveys Tuts.*, vol. 21, no. 4, pp. 3109–3132, 2019.

[58] D. Zhu, B. Li, and P. Liang, "On the matrix inversion approximation based on Neumann series in massive MIMO systems," in *Proc. 2015 IEEE international conference on communications (ICC)*, Jun. 2015, pp. 1763–1769.

[59] L. Dai, X. Gao, X. Su, S. Han, I. Chih-Lin, and Z. Wang, "Low-complexity soft-output signal detection based on Gauss-Seidel method for uplink multiuser large-scale MIMO systems," *IEEE Trans. Veh. Technol.*, vol. 64, no. 10, pp. 4839–4845, 2014.

[60] W. Fukuda *et al.*, "Low-complexity detection based on belief propagation in a massive MIMO system," in *Proc. 2013 IEEE 77th Vehicular Technology Conference (VTC Spring)*, Jun. 2013.

[61] Y. Hama and H. Ochiai, "Performance analysis of matched-filter detector for MIMO spatial multiplexing over rayleigh fading channels with imperfect channel estimation," *IEEE Trans. Commun.*, vol. 67, no. 5, pp. 3220–3233, May 2019.

[62] H. Ochiai, "An analysis of band-limited communication systems from amplifier efficiency and distortion perspective," *IEEE Trans. Commun.*, vol. 61, no. 4, pp. 1460–1472, Apr. 2013.

[63] H. Imai and S. Hirakawa, "A new multilevel coding method using error-correcting codes," *IEEE Trans. Inf. Theory*, vol. 23, no. 3, pp. 371–377, 1977.

[64] N. Kim, Y. Lee, and H. Park, "Performance analysis of MIMO system with linear MMSE receiver," *IEEE Trans. Wireless Commun.*, vol. 7, no. 11, pp. 4474–4478, 2008.

[65] U. Wachsmann, R. F. Fischer, and J. B. Huber, "Multilevel codes: Theoretical concepts and practical design rules," *IEEE Trans. Inf. Theory*, vol. 45, no. 5, pp. 1361–1391, 1999.

[66] M. A. Albreem, "Approximate matrix inversion methods for massive MIMO detectors," in *Proc. 2019 IEEE 23rd International Symposium on Consumer Technologies (ISCT)*, Jun. 2019, pp. 87–92.

[67] Y. H. Gan, C. Ling, and W. H. Mow, "Complex lattice reduction algorithm for low-complexity full-diversity MIMO detection," *IEEE Trans. Signal Process.*, vol. 57, no. 7, pp. 2701–2710, 2009.

[68] S. Wu, L. Kuang, Z. Ni, J. Lu, D. Huang, and Q. Guo, "Low-complexity iterative detection for large-scale multiuser MIMO-OFDM systems using approximate message passing," *IEEE J. Sel. Topics Signal Process.*, vol. 8, no. 5, pp. 902–915, 2014.

[69] E. Arikan, "A performance comparison of polar codes and Reed-Muller codes," *IEEE Commun. Lett.*, vol. 12, no. 6, pp. 447–449, 2008.

[70] H. Ochiai, P. Mitran, and H. V. Poor, "Capacity-approaching polar codes with long codewords and successive cancellation decoding based on improved Gaussian approximation," *IEEE Trans. Commun.*, vol. 69, no. 1, Jan. 2021.

[71] D. Wu, Y. Li, and Y. Sun, "Construction and block error rate analysis of polar codes over AWGN channel based on Gaussian approximation," *IEEE Commun. Lett.*, vol. 18, no. 7, pp. 1099–1102, 2014.

[72] A. Chockalingam and B. S. Rajan, *Large MIMO Systems*. Cambridge University Press, 2014.

[73] E. Eraslan, B. Daneshrad, and C.-Y. Lou, "Performance indicator for MIMO MMSE receivers in the presence of channel estimation error," *IEEE Wireless Commun. Lett.*, vol. 2, no. 2, pp. 211–214, 2013.

[74] B. Hassibi and B. M. Hochwald, "How much training is needed in multiple-antenna wireless links?" *IEEE Trans. Inf. Theory*, vol. 49, no. 4, pp. 951–963, 2003.

[75] L. Xiao, P. Xiao, Z. Liu, W. Yu, H. Haas, and L. Hanzo, "A compressive sensing assisted massive SM-VBLAST system: Error probability and capacity analysis," *IEEE Trans. Wireless Commun.*, vol. 19, no. 3, pp. 1990–2005, Mar. 2020.

[76] D. Feng, H. Xu, J. Zheng, and B. Bai, "Nonbinary LDPC-coded spatial modulation," *IEEE Trans. Wireless Commun.*, vol. 17, no. 4, pp. 2786–2799, Apr. 2018.

[77] J. Jeganathan, A. Ghrayeb, and L. Szczecinski, "Spatial modulation: Optimal detection and performance analysis," *IEEE Communications Letters*, vol. 12, no. 8, pp. 545–547, Aug. 2008.

[78] G. Mingxi, J. Chong, and S. Yuehong, "Detection algorithm for spatial modulation system under unconstrained channel," in *Proc. IEEE International Conference on Communication Technology*, Nov. 2010, pp. 458–461.

[79] P. Yang, M. D. Renzo, Y. Xiao, S. Li, and L. Hanzo, "Design guidelines for spatial modulation," *IEEE Commun. Surveys Tuts.*, vol. 17, no. 1, pp. 6–26, 2015.

Publications

Journal Papers (2)

- Y. Hama and H. Ochiai, "Performance Analysis of Matched-Filter Dwetector for MIMO Spatial Multiplexing over Rayleigh Fading Channels with Imperfect Channel Estimaiton," *IEEE Transactions on Communications*, vol. 67, no. 4, pp. 3220-3233, May. 2019.

- Y. Hama and H. Ochiai, "Matched-Filter Detector with Quadrature Interference Cancellation for Coded Uplink Multiuser MIMO Systems with Massive IoT Devices," *IEEE Transactions on Wireless Communications*, early access.

Conference Papers (5)

- Y. Hama and H. Ochiai, "A Low-Complexity Matched Filter Detector with Parallel Interference Cancellation for Massive MIMO Systems," *IEEE 12th International Conference on Wireless and Mobile Computing, Network and Communications (WiMob2016),* New York, NY, Oct. 2016.

- Y. Hama and H. Ochiai, "Performance Analysis of Matched Filter Detector for MIMO Systems in Rayleigh Fading Channels," *IEEE Global Communications Conference (GLOBECOM2017),* Singapore, Dec. 2017.

- Y. Hama and H. Ochiai, "Performance Comparison of Low-Complexity MIMO System with Matched-Filter Detector and Interference Cancellation," *IEEE 25th International Conference on Telecommunications (ICT2018),* Saint-Malo, France, Jun. 2018.

- Y. Hama and H. Ochiai, "Performance of Polar Coded MIMO Systems with Matched-Filter Detector and Interference Cancellation," *IEEE Global Communications Conference (GLOBECOM2019),* Waikoloa, HI, USA, Dec. 2019.

- Y. Hama and H. Ochiai, "Performance of Coded MIMO Spatial Modulation with Scaling Matched-Filter Detector," *IEEE Global Communications Conference (GLOBECOM2020),* Taipei, Taiwan, Dec. 2020.

Related Journal Papers (1)

- D. Kitayama, Y. Hama, K. Goto, K. Miyachi, T Motegi, and O. Kagaya, "Transparent dynamic metasurface for a visually unaffected reconfigurable intelligent surface: controlling transmission/reflection and making a window into an RF lens," *Optics Express*, vol. 29, no. 18, pp. 29292-29307, Aug. 2021.

Related Conference Papers (1)

- Y. Hama, H. Ochiai, and S. Junji, "Performance Analysis of Wireless Steganography based on OFDM and DFT-s-OFDM Signals over Frequency-Selective Rayleigh Fading Channels," *IEEE 24th International Symposium on Wireless Personal Multimedia Communications (WPMC2021)*, Okayama, Japan, Dec. 2021.